

**ACSVL3 IS A NOVEL THERAPEUTIC TARGET IN GLIOBLASTOMA:
DRUG DISCOVERY AND ROLE IN PROTEIN LIPIDATION**

by
Emily M. Clay

A dissertation submitted to The Johns Hopkins University in conformity with the
requirements of the degree of Doctor of Philosophy

Baltimore, Maryland
October 2017

© Emily M. Clay 2017
All rights reserved

Abstract

Glioblastoma is an aggressive form of brain cancer with a five-year survival rate after diagnosis of less than 6%. More efficacious treatments are needed to improve patient prognosis. Very long-chain acyl-CoA synthetase (ACSVL3) is not detected in healthy glial cells, but is highly expressed in gliomas. Knockout of ACSVL3 in glioblastoma cells in culture decreases tumorigenicity and disrupts growth-factor induced cell signaling. However, the mechanism through which ACSVL3 promotes malignancy is not known. To address this question, lipid-based post-translational modifications were studied in wild-type and ACSVL3-knockout glioblastoma lines in cell culture. No significant differences were found in levels of protein palmitoylation or GPI anchors between wild-type and knockout cells. However, a global decrease in protein stearylation was observed with ACSVL3 knockout, and mass spectrometry revealed several individual proteins that exhibited increased or decreased stearylation with ACSVL3 knockout. From this we conclude that ACSVL3 is partially responsible for mediating stearylation in glioblastoma cells. Next, we searched for inhibitors of ACSVL3. Inhibitors are desired both as tools to study the mechanism of ACSVL3-promoted malignancy and as potential therapeutic agents in glioblastoma. Two methods were established to screen for inhibitors of ACSVL3. The first was a small screen of known inhibitors of the homologous enzyme ACSVL1. This screen determined whether these drugs and compounds inhibited the activation of the 18-carbon fatty acid stearate by glioblastoma cells. The second was development of a screen to evaluate the ability of an ACSVL3/ACSVL1 hybrid enzyme to uptake fluorescent fatty-acid analogs. In the first

screen, the small molecule CB5 was found to greatly inhibit activation of stearate. When glioblastoma cells in culture were treated with CB5, the compound slowed the rate of cell proliferation, induced differentiation, and decreased β -oxidation of long-chain fatty acids. Growth of subcutaneous xenografts produced from U87, but not Mayo-22, glioblastoma cells implanted subcutaneously in mice was significantly slowed by CB5 treatment. We conclude that the small molecule CB5 inhibits ACSVL3 activity in vitro and in vivo, and ACSVL3 is a promising novel therapeutic target in glioblastoma. The second screen shows high potential for conducting a high-throughput screen for additional inhibitors.

Thesis Advisor/Reader: Paul A. Watkins, M.D., Ph.D.

Thesis Reader: Daniel M. Raben, Ph.D.

Acknowledgments

I would like to acknowledge my committee members, who provided very valuable advice and direction over the course of my thesis research: Drs. Jun Liu, John Laterra, Jin Zhang, Paul Englund, and my committee chair Daniel Raben.

I would also like to thank all of the current and former members of the Watkins lab for all their help around the lab, advice, friendship, and camaraderie, especially Yanqiu Liu, Dr. Xiaohai Shi, and Dr. Liz Kolar. They made coming to work every day enjoyable, even when it was frustrating.

I was incredibly fortunate to work with the best advisor imaginable, Dr. Paul Watkins. Paul was unwaveringly supportive and always available to troubleshoot or just talk science. I thank him for instilling in me a love of lipids.

Finally, I thank my family, friends, and Lance for their encouragement throughout my time as a graduate student.

Table of Contents

Abstract	ii
Acknowledgments	iv
List of Tables	vi
List of Figures	vii
Background	1
Chapter 1: Identification and characterization of inhibitors of ACSVL3	
Introduction	14
Materials and methods	19
Results	33
Discussion	53
Chapter 2: GPI-anchored proteins in WT and ACSVL3-KO U87 cells	
Introduction	59
Materials and methods	62
Results	68
Discussion	77
Chapter 3: Protein acylation in WT and ACSVL3-KO U87 cells	
Introduction	80
Materials and methods	82
Results	90
Discussion	101
References	105
Curriculum Vitae	122

List of Tables

Table 1: Systematic names of drugs and compounds included in assays	20
Table 2: Primer sequences used to detect transcripts encoding for common GPI-anchored proteins	64
Table 3: Stearoylated proteins more abundant in WT U87 cells vs. ACSVL3-KO U87 cells	99
Table 4: Stearoylated proteins more abundant in ACSVL3-KO U87 cells vs. WT U87 cells	100

List of Figures

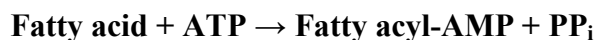
Figure 1: Phylogenetic tree of human ACS proteins	3
Figure 2: Sequence alignment of ACSVL3 and ACSVL1	16
Figure 3: Expression of ACSVL3 in WT and ACSVL3-KO U87 cells	33
Figure 4: Total activation of long- and very-long chain fatty acids in WT and ACSVL3-KO U87 cells.....	34
Figure 5: Inhibition of C18:0 activation by ACSVL1 inhibitors in WT and ACSVL3-KO U87 cells	37
Figure 6: Characterization of the ACSVL1/3 hybrid enzyme	39
Figure 7: Inhibition of ACSVL1/3 by ACSVL1 inhibitors	41
Figure 8: Inhibition of U87 proliferation by CB5.....	43
Figure 9: Morphology of U87 cells treated with CB5	44
Figure 10: Reversion of growth rate in U87 treated with CB5 after drug removal	45
Figure 11: Treatment of human fibroblasts with CB5.....	46
Figure 12: Scratch-wound assay of CB5-treated U87 cells.....	47
Figure 13: β -oxidation of long- and very long-chain fatty acids in U87 cells.....	48
Figure 14: Expression of GFAP in U87 cells	49
Figure 15: Treatment of mice bearing glioblastoma xenograft tumors with CB5	52
Figure 16: Diagram of a human GPI-anchored protein	60
Figure 17: Expression of GPI-anchored proteins in WT and ACSVL3-KO U87 cells	69
Figure 18: Expression and purification of PI-PLC from <i>E. coli</i>	71

Figure 19: Assessment of purified PI-PLC activity using the Ellman assay	74
Figure 20: Detection of GPI-anchored proteins in WT and ACSVL3-KO U87 cells	76
Figure 21: Detection of acylated proteins in WT and ACSVL3-KO U87 cells	92
Figure 22: Activation of Akt by EGF in U87 cells	93
Figure 23: Comparison of activation of Akt by EGF in WT and ACSVL3-KO U87 cells	94
Figure 24: Stearoylation of proteins in WT and ACSVL3-KO U87 cells stimulated with EGF	95

Background

Acyl-CoA Synthetases

Acyl-CoA synthetases (ACSSs) are a class of enzymes that catalyze the conversion of fatty acids to fatty acyl-CoA. The first step of this two-step reaction links the carboxylic acid group of the fatty acid to the α -phosphate of ATP, forming fatty acyl-AMP and releasing pyrophosphate. The second step is the formation of a thioester bond between the fatty acyl group and the thiol group of coenzyme A, forming fatty acyl-CoA and releasing AMP (Berg, 1956). This reaction, referred to as "activation", is outlined in the following equation:



Activation of fatty acids is required for fatty acids to participate in nearly all downstream metabolic processes, including energy production via β -oxidation, remodeling of the fatty acid such as elongation, incorporation into complex lipids for energy storage or membrane synthesis, and post- or cotranslational covalent attachment to proteins (Watkins, 1997).

ACSSs are conserved throughout all living organisms. In humans, a search of genomic data using highly conserved amino acid sequence motifs has revealed 26 ACS enzymes (Watkins et al., 2007). These enzymes are grouped into phylogenetic "families" that roughly represent the chain length of fatty acids that the family of ACSs is capable of activating (Figure 1). The families are short-chain (ACSS), medium-chain (ACSM), long-chain (ACSL), very long-chain (ACSVL), and "bubblegum" (ACSBG). These

families contain 22 of the 26 human ACSs, and there are four orphan ACSs (ACSF1-4). The family names represent the length of fatty acids that they are capable of activating rather than their preferred substrate length, and there is overlap in substrates between families. For example, members of the ACSVL family activate long-chain fatty acids at a higher rate than very long-chain fatty acids (Steinberg *et al.*, 1999). Similarly to the ACSVL family, the ACSBG family is capable of activating both long- and very-long chain fatty acids (Steinberg *et al.*, 2000; Pei *et al.*, 2003). ACSs differ from one another in not only their substrate specificity, but also in their tissue expression and subcellular location, providing each with a unique role.

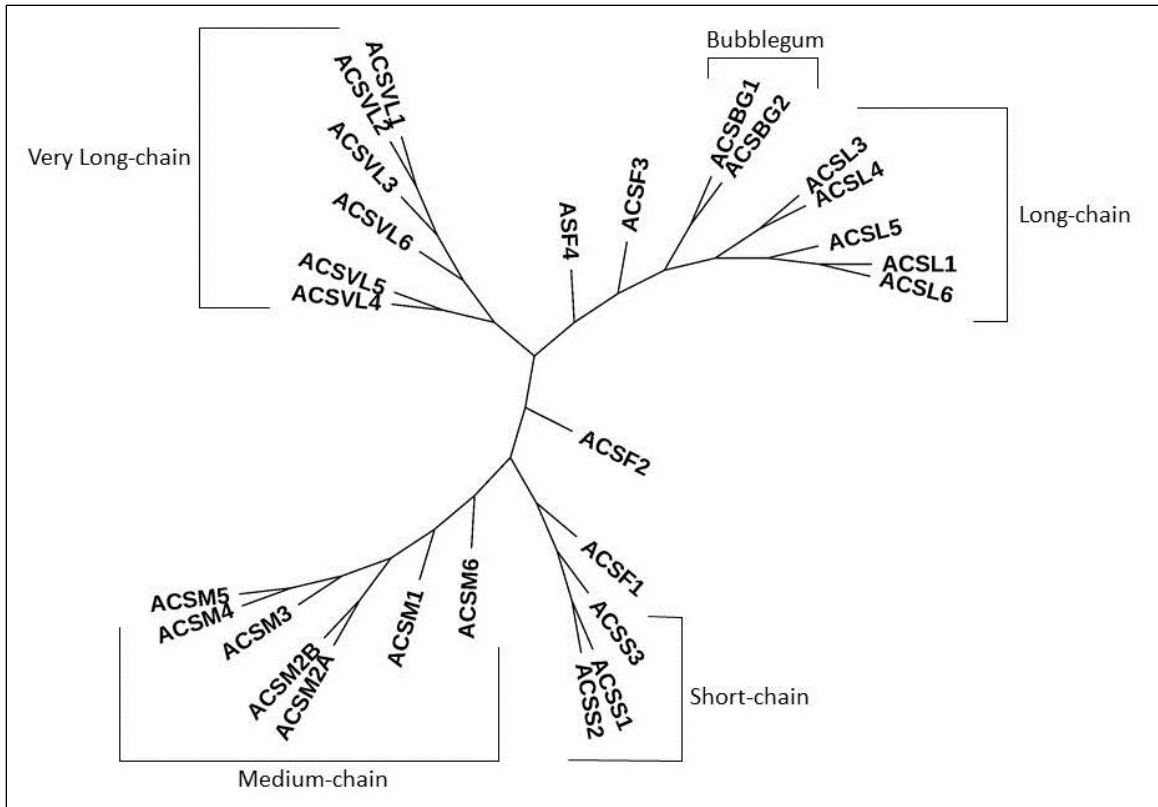


Figure 1: Phylogenetic tree of human ACS proteins

Full-length amino acid sequences of the longest isoform of each protein were used in phylogenetic analysis. ACS families are identified in brackets. Newick tree format was determined with European Bioinformatics Institute online tools (McWilliam *et al.*, 2013) and the tree was rendered using Interactive Tree Of Life (Letunic and Bork, 2016).

Each ACS has an N-terminal and C-terminal domain with a flexible linker region connecting the two domains. There are two conserved motifs within the C-terminal domain of each ACS in all species, called Motifs I and II (Watkins *et al.*, 2007). Motif I is a 10-residue AMP-binding domain that is conserved within many AMP-binding enzymes. Motif II is a 35-residue motif containing the proposed fatty acid binding “signature motif” described by Black *et al.* (1997). In the center Motif II is an arginine residue that is especially invariant, and is found in all known ACSs in all species except

for human ACSBG2, where it is replaced with a histidine residue (Pei *et al.*, 2006). Mutation of this arginine (or histidine in the case of ACBG2) renders the enzyme catalytically dead (Black *et al.*, 1997).

Very long-chain acyl-CoA synthetase 3 (ACSVL3) and its role in cancer

The six human ACSVL enzymes share 37–59% sequence identity (Watkins *et al.*, 2007). The last member of the ACSVL family to be characterized was ACSVL3 (gene name: SLC27A3). Historically, the ACSVL family has also been called fatty acid transporter proteins (FATP) because they were initially discovered due to their ability to transport the long-chain fatty acid analogue C₁-BODIPY-C₁₂ into cells (Schaffer and Lodish, 1994). In mammals, each enzyme has an ACSVL and a FATP designation. It is not yet known whether they aid in the physical transport of fatty acids through the cell membrane, or “trap” fatty acids that diffuse across the membrane in the cell by converting them to their CoA derivatives. ACSVL3 is also known as FATP3, but although it has demonstrable ACS enzyme activity, there is no evidence that it functions as a fatty acid transport protein (Pei *et al.*, 2004).

ACSVL3 is highly expressed in the adrenal gland, ovaries, and testes, and is expressed in lower levels in the brain, spinal cord, and lungs in adult mice (Pei *et al.*, 2004). However, ACSVL3 is expressed highly in embryonic mouse brain tissue, and expression decreases continuously from embryonic day 14 to postnatal day 15. ACSVL3 has also been found in human neural stem cells, indicating that the enzyme may play a role in the development of the central nervous system (Maekawa *et al.*, 2015). In adult mouse and human brain tissue, ACSVL3 is expressed in neurons but not glial cells (Pei *et*

al., 2004; Pei *et al.*, 2009). In humans, ACSVL3 is also expressed in pancreas, stomach, aorta, and spleen tissue (Pei *et al.*, 2013). Its expression along the digestive tract may reflect a role metabolizing fatty acids taken up during digestion. Within cells, ACSVL3 is localized to small punctate vesicles; the exact nature of these vesicles remains unknown (Pei *et al.*, 2004; Pei *et al.*, 2013). Like other members of the ACSVL family, ACSVL3 preferentially activates long- and very-long chain fatty acids (Pei *et al.*, 2013).

While ACSVL3 is undetectable in healthy adult glial cells, histochemical analysis showed that it is abundant in malignant gliomas (Pei *et al.*, 2009). To investigate the relevance of this observation, our laboratory began investigating cell culture models of glioma. When ACSVL3 was knocked down using RNA interference (RNAi) in the highly tumorigenic U87 human glioblastoma cell line and tumor cells derived from Mayo 22 glioblastoma xenografts, the rate of cell proliferation slowed dramatically, and fewer colonies formed in soft agar (a measure of tumorigenicity). Knockdown of ACSVL3 also disrupted Akt signaling, an important signaling pathway supporting tumorigenicity in glioma (Kapoor and O'Rourke, 2003) and in U87 cells (Pei *et al.*, 2009). ACSVL3 is also increased in glioblastoma stem cell neurosphere cultures and its expression decreased after differentiation of these cells into astrocytes or neurons (Sun *et al.*, 2014). Conversely, ACSVL3 knockdown led to an increase in markers of differentiation, indicating that ACSVL3 supports a cancer stem cell phenotype in glioma. When xenografts formed from U87 cells by implantation in immunocompromised mice, fewer and smaller tumors grow from U87 cells if ACSVL3 has been knocked out (Kolar, 2016).

There is evidence that ACSVL3 plays a similar role in lung cancer (Pei *et al.*, 2013). As was seen in glioma, ACSVL3 is highly expressed in many different types of

lung tumors, while it is only moderately expressed in bronchial epithelial cells in healthy lung tissue. RNAi knockdown of ACSVL3 also led to decreased cell proliferation and colony formation in soft agar in cell lines derived from lung tumors. Treatment of xenograft tumors derived from epithelial lung carcinoma with the anti-cancer agent fenretinide resulted in lower expression of *Acsvl3* mRNA (Durante *et al.*, 2014).

Lipid metabolism alterations observed in cancer

As ACSs are central to most aspects of lipid metabolism, it is unsurprising that other ACSs have been implicated in various cancers. Many of these are long-chain ACSs. A tumor suppressor microRNA called miR-205 that targets ACSL1 is downregulated in hepatocellular carcinoma, leading to increased ACSL1 (Cui *et al.*, 2014). ACSL4 (a.k.a. Fatty acid-CoA ligase 4 [FACL4]) is upregulated in hepatocarcinoma and sometimes in certain breast cancers, and in both cases its expression is correlated with cell proliferation and survival (Hu *et al.*, 2008; Wu *et al.*, 2013). ACSL5 (a.k.a. acyl-CoA synthetase 5 [ACS5]) is downregulated in epithelial cells in small intestinal adenomas and adenocarcinomas (Gassler *et al.*, 2013), but upregulated in some malignant gliomas, where it is also linked to proliferation (Yamashita *et al.*, 2000). The short-chain ACS protein ACSS2 (a.k.a. acetyl-CoA synthetase 2) is upregulated in some tumors. ACSS2 activates acetate that is used for energetic consumption and lipid synthesis, promoting cell survival in hypoxia and metabolically stressed, low-lipid environments (Yoshii *et al.*, 2009, Schug *et al.*, 2015).

Downstream of activation by ACSs, nearly all uses of fatty acids within cells are known to be disrupted in some way in tumor cells. In general, the production of many

types of lipids is upregulated, allowing tumor cells to proliferate rapidly and adapt to various conditions. Much of this increased production can be traced back to dysregulation of the sterol regulatory element binding proteins (SREBPs). These transcription factors control most fatty acid metabolic processes within the cell, activating transcription of the necessary enzymes only when lipid synthesis is required to maintain homeostasis.

SREBP1 (isoforms 1a and 1c) mainly regulates fatty acid, phospholipid, and triacylglycerol (TAG) synthesis, and SREBP2 regulates cholesterol synthesis (Eberlé *et al.*, 2014). The SREBPs are overexpressed in many cancers and overactivated in others, leading to increased expression of enzymes involved in lipid synthesis (Menendez and Lupu, 2007; Shao and Espenshade, 2012).

De novo synthesis of fatty acids is activated in many tumors formed from tissues that do not typically synthesize fatty acids (Menendez and Lupu, 2007). The expression of ATP citrate lyase, acetyl-CoA carboxylase, and fatty acid synthase, the main enzymes in fatty acid synthesis, are upregulated in these tumors. Expression of the elongase ELOVL7 is also overexpressed in prostate cancer, creating an abundance of long-chain fatty acids (Tamura *et al.*, 2009). Newly synthesized fatty acids can be activated and incorporated into TAG and stored in lipid droplets, which are found in increased numbers in cancer cells (Murphy, 2001). Other activated fatty acids are incorporated into phospholipids and become cell or organelle membranes. The upregulation of enzymes involved in the synthesis of phosphatidylcholine (PC), such as choline kinase, and phosphatidylethanolamine (PE), the two major lipids found in cell membranes, indicates that this process is also increased in tumors (Janardhan *et al.*, 2006; Cheng *et al.*, 2016).

Some complex lipids are upregulated in cancer, while others are downregulated. Activated fatty acids can also be incorporated into sphingosine and ceramide (an acylated sphingosine). Ceramide has been identified as a tumor suppressor, and the enzymes required for its synthesis are often lowered in tumors (Morad and Cabot, 2013). Conversely, sphingosine kinases 1 and 2 and their product sphingosine-1-phosphate is commonly upregulated in cancer (Pyne *et al.*, 2014). Acetyl-CoA, originating from either the citric acid cycle or the breakdown of fatty acids, can be incorporated into cholesterol, another lipid that has been shown to be accumulated in many types of cancer (Kuzu *et al.*, 2016). Cholesterol synthesis is upregulated in tumor cells (Kuzu *et al.*, 2016), and statins (drugs blocking cholesterol synthesis) decrease tumorigenesis in many cancerous cell lines (Pisanti *et al.*, 2014).

Another fate of activated fatty acids is post-translational modification of proteins. There is an increase in N-myristoyltransferase activity, the enzyme that catalyzes myristoylation (the attachment of a 14-carbon fatty acid) in human colorectal cancer, gallbladder carcinoma and brain tumors (Selvakumar *et al.*, 2007). Many palmitoyl acyltransferases, the enzymes that attach the 16-carbon fatty acid, palmitate, to proteins, function as either tumor suppressors or oncogenes in various cancers (Resh, 2016). A number of enzymes that undergo farnesylation, the covalent attachment the cholesterol intermediate farnesyl, have been found to be upregulated or mutated in cancer as well (Novelli and D'Apice, 2012).

Finally, activated fatty acids can be degraded by β -oxidation to produce energy. Prostate tumors exhibit overexpression of enzymes used in β -oxidation (Zha *et al.* 2005), and β -oxidation has been found to aid cell survival in cancers originating from tissue

types that do not typically perform β -oxidation, such as leukemia, breast cancer, and ovarian cancer (Samudio *et al.*, 2010; Camarda *et al.*, 2016; Nieman *et al.*, 2011).

Changes in lipid metabolism promote cancer phenotypes

These aberrancies in lipid metabolism contribute in many ways to cancerous phenotypes. First, the abundance of phospholipids and cholesterol can be used for membrane synthesis. Because of the rapid cell proliferation that is the hallmark of cancer, large amounts of lipids are needed to synthesize the nascent cell membranes, especially the phospholipids PC and PE. Often, membrane composition is higher in saturated fatty acids and cholesterol in tumor cells, reflecting the increased availability of these lipids (Rysman *et al.*, 2010). This leads to a reduction of membrane fluidity since saturated lipids pack more tightly (Ollila *et al.*, 2007). The changes in membrane dynamics also appear to promote survival by protecting cancer cells from both peroxidative stress and chemotherapeutic agents (Rysman *et al.*, 2010).

The increased lipid droplets and β -oxidation seen in many tumor cells can provide the cells with energy in times of metabolic stress. Lipid droplets aid survival in hypoxia and nutrient deficiency due to hypovascularization (Koizumi and Miyagi, 2016). Also, there is evidence that the upregulation of β -oxidation in intra-abdominal tumors allows the cancer cells to use lipids from neighboring adipocytes as a fuel source. This was observed *in vitro* when ovarian cancer cells were cultured with adipocytes, which induced lipolysis in adipocytes and β -oxidation in cancer cells (Nieman *et al.*, 2011).

Many signaling pathways activated in cancer involve lipids. The increased cholesterol in the plasma membrane leads to increased lipid raft domains that act as

signaling platforms. Lipid rafts harbor many receptor tyrosine kinases, such as growth factor receptors, and thus increased lipid rafts results in increased signaling through survival pathways such as the Akt signaling pathway. (Mollinedo and Gajate, 2015) Also critical to Akt signaling is another lipid, phosphatidylinositol (PI). In cancer, the conversion of PI to phosphatidylinositol-3,4,5-trisphosphate (PI(3,4,5)P₃) is increased (Fresno Vara et al., 2004). PI(3,4,5)P₃ recruits Akt to the inner leaflet of the plasma membrane, allowing Akt to be activated by phosphorylation. Sphingosine-1-phosphate promotes cell proliferation and tumor growth by deregulating the cell cycle and promoting inflammation (Pyne *et al.*, 2014). Finally, the lipid-based post-translational modifications of proteins act as signals that contribute to cancer phenotypes. For example, palmitoylation of human integrin β 4, a transmembrane receptor that aids extracellular matrix adhesion, correlates with invasiveness in breast cancer cells (Coleman *et al.*, 2015). Finally, farnesylation of Ras is required for its association with the inner leaflet of the plasma membrane, where it is further modified to its biologically active form and promotes proliferation in response to growth factors. Ras is often mutated in cancers to an always-active state, which allows uncontrolled cell growth and proliferation (Rowinsky *et al.*, 1999).

Inhibitors of many lipid-metabolizing enzymes have been demonstrated to slow proliferation or induce apoptosis of cancer cells *in vitro* and in mouse models. Triacsin C, a nonspecific inhibitor of many long-chain acyl-CoA synthetases, induces apoptosis in glioma cells and improves the prognosis of mice bearing xenografts in conjunction with chemotherapy (Mashima *et al.*, 2009). The fatty acid synthase inhibitor cerulenin induces apoptosis in murine colorectal cancer cell lines and reduces the number and sizes of liver

metastatic colorectal tumors in mice (Merata *et al.*, 2010). Inhibition of carnitine palmitoyl transferase 1 with etoximir, which prevents fatty acids from shuttling into mitochondria for β -oxidation, reduces viability in human glioblastoma cells in culture (Pike *et al.*, 2011). The farnesyl transferase inhibitor Lonafarnib, as well as statins, have been examined in clinical settings as cancer therapeutics. Some tumors responded well to Lonafarnib in Phase I and II clinical trials, although no improvement in survival was found in Phase III trials (Morgillo and Lee, 2006). A meta-analysis of 41 studies studying revealed that statin use decreased mortality in cancer patients, including those suffering from colorectal, prostate, breast, and other cancers (Zhong *et al.*, 2015).

Currently, cancer treatments do not target lipid metabolism pathways directly. Targeting the many upregulated and overactive enzymes that promote cancer phenotypes is a promising therapeutic strategy.

Glioblastoma

The most common primary CNS tumors are gliomas, accounting for 78% of malignant CNS tumors (Ostrom *et al.*, 2016). Gliomas include tumors originating from all glial cells, but are named after the type of cell with which they share histological features rather than the cell of origin. Gliomas include astrocytomas, oligodendrogliomas, ependymomas, and mixed gliomas. Instead of staging, gliomas and other CNS tumors are categorized by grades I-IV defined by the World Health Organization (Louis *et al.*, 2016). Low grade gliomas (grades I and II) are more differentiated and have higher survival rates, while high grade gliomas (III and IV) are undifferentiated, grow rapidly, are invasive, and have lower survival rates. Glioblastomas (GBM; a.k.a glioblastoma

multiforme) are grade IV astrocytomas. They are the most common form of glioma, accounting for 55.4% of glioma cases, and 46.6% of all primary malignant brain tumors (Ostrom *et al.*, 2016). Prognosis for patients is very low, with a 5-year survival rate of only 5.5%. There were 12,150 new cases of GBM diagnosed in the United States in 2016, with 12,390 expected diagnoses in 2017.

An important tool in GBM research is the U87MG (U87) cell line. This cell line has been mentioned in over 2,000 publications since it became available in 1966. Originally, this cell line was isolated from a 44-year-old Caucasian male with a grade IV astrocytoma. However, recent genetic analysis shows that the current cell line used is different from the purported tumor of origin (Allen *et al.*, 2016). Fortunately, modern U87 cells are most likely still glioblastoma. The characterization of ACSVL3 in cancer was performed largely in U87 cells (Pei *et al.*, 2009; Sun *et al.*, 2014). Our lab has generated both ACSVL3 knockout and stable knockdown U87 cells in order to further study its role in tumorigenesis.

Thesis Aims

As discussed earlier, the acyl-CoA synthetase ACSVL3 is aberrantly expressed in human gliomas. Knockdown of ACSVL3 decreases cell proliferation and tumorigenicity in glioblastoma cells in culture and xenografts. While ACSVL3 appears to be critical to the cancer phenotype of glioma cells, it is not known how the enzyme acts to promote tumorigenesis. Since acyl-CoA synthetases are central to lipid metabolism, there are many pathways that ACSVL3 might affect. One of the major roles of lipids that requires activation by an ACS is post-translational modifications of proteins. In this thesis, I

discuss the role of ACSVL3 in two types of post-translational modifications: acylation of proteins with the long-chain fatty acids palmitate and stearate, and the attachment of glycosylphosphatidylinositol (GPI) anchors to proteins.

The prognosis of patients diagnosed with GBM is very poor even with aggressive treatment. New, more efficacious treatments are needed, and targeting lipid metabolism is a promising new direction. Since ACSVL3 is not expressed in healthy glial cells but is abundant in glioma cells, it is an attractive therapeutic target. In this thesis, I discuss two screening mechanisms used to identify inhibitors of ACSVL3 activity. I also show the effects of one robust inhibitor of ACSVL3 on U87 cells in culture and in mice bearing xenografts originating from glioblastoma.

Chapter 1: Identification and characterization of inhibitors of ACSVL3

Introduction

ACSVL3 is an attractive therapeutic target for glioma. ACSVL3 is not expressed in healthy glial cells, but it is highly expressed in glioblastomas (Pei *et al.*, 2009). Knockdown of ACSVL3 in glioblastoma cells led to slower growth rate, decreased tumorigenicity *in vitro* and in xenograft models, and disrupted Akt signaling. We hypothesized that inhibition of ACSVL3 activity with a drug or chemical inhibitor would have a similar anti-tumorigenic effect. We developed a two-prong approach to identify ACSVL3 inhibitors. First, inhibitors of the homologous enzyme ACSVL1 were screened for inhibition of ACSVL3. Second, a fluorescence-based high-throughput screen was developed to screen chemical libraries for inhibition of ACSVL3.

A homologue of ACSVL3 is another very long-chain acyl-CoA synthetase, ACSVL1 (a.k.a. fatty acid transport protein 2 [FATP2]). Like ACSVL3, ACSVL1 converts both long- and very long chain fatty acids to their CoA derivatives. ACSVL1 is expressed highly in liver and kidney tissue and localizes to peroxisomes and the endoplasmic reticulum (Steinberg *et al.*, 1999). In addition to its enzyme activity, ACSVL1 facilitates the transport of fluorescent or radiolabeled fatty acids across the plasma membrane and into the cell matrix. Although it is not known for certain whether ACSVL1 physically transports the fatty acids or simply traps them in the cell by

converting them to their CoA derivatives, it is assumed that catalytic activity is required for fatty acid uptake (Jia *et al.*, 2007; Falcon *et al.* 2010). In addition to being stored in cells, uses for long- and very long-chain fatty acids activated and/or transported by ACSVL1 include phosphatidylinositol synthesis (Melton *et al.*, 2011) and sphingosine 1-phosphate metabolism (Ohkuni *et al.*, 2013).

The C-terminal catalytic domains of ACSVL1 and ACSVL3 are highly homologous (Figure 2). These domains bind both fatty acids and ATP, and thus are responsible for the conversion of long- and very-long chain fatty acids to their acyl-CoA derivatives. However, the smaller, N-terminal domains of ACSVL1 and ACSVL3 are significantly different. While the exact purpose of the N-terminal domains is not known, it is assumed to be a regulatory domain, possibly involved in subcellular location determination or membrane association.

Black and DiRusso exploited the fatty acid transport property of ACSVL1 to develop a high-throughput screen for inhibitors of this enzyme (U.S. Patent No. 7,070,944, 2006). They produced a strain of yeast deficient in both fatty acid uptake and acyl-CoA synthetase activity, and exogenously expressed human ACSVL1. ACSVL1-overexpressing cells took up C₁-BODIPY-C₁₂, a fluorescent long chain fatty acid analog, while the deficient cells did not. Using fatty acid uptake as a surrogate for acyl-CoA synthetase activity, over 100,000 drugs and compounds were screened (Li *et al.*, 2008; Sandoval *et al.*, 2010). Yeast cells were treated with compounds from three libraries: the SpectrumPlus library from MicroSource Discovery Systems Inc., the NCI Diversity Set Compound Library and the ChemBridge Corporation compound library. The yeast cells were treated with C₁-BODIPY-C₁₂ and trypan blue after incubation with compounds. Trypan blue quenched extracellular fluorescence, so only fluorescence from C₁-BODIPY-C₁₂ taken up by the cells was measured. The screen identified several compounds that inhibited the uptake of C₁-BODIPY-C₁₂. Secondary screening eliminated autofluorescent compounds, compounds that quenched C₁-BODIPY-C₁₂ fluorescence, and compounds that permeabilized the cell membrane. The SpectrumPlus screen revealed 28 ACSVL1 inhibitors, many of which were tricyclic, phenothiazine-derived antipsychotic drugs. The Diversity Set/Chembridge screen revealed 216 ACSVL1 inhibitors, which were clustered into 5 structural classes. Inhibition of uptake of fatty acids in human cell lines was characterized using a compound representative of each structural class.

Since ACSVL1 is homologous to ACSVL3 throughout the catalytic domain, we expected that the identified inhibitors of ACSVL1 might also inhibit the acyl-CoA

synthetase activity of ACSVL3. Due to the aberrant expression of ACSVL3 in gliomas, we hypothesized that an inhibitor could act as a therapeutic agent. We assessed several of the identified drugs from the SpectrumPlus screen (triflupromazine, phenazopyridine, chlorpromazine, emodin, and perphenazine) and four of the compounds characterized following the Diversity Set/Chembridge screen (referred to as CB2, CB5, CB6, and CB16.2) for their effect on the acyl-CoA synthetase activity of ACSVL3 *in vitro*. We found that many of these drugs and compounds inhibited ACSVL3 activity.

The most potent inhibitor of ACSVL3 activity was a compound from ChemBridge Corporation compound library, 2-benzyl-3-(4-chlorophenyl)-5-(4-nitrophenyl)pyrazolo[1,5-a]pyrimidin-7(4H)-one, referred to here as CB5 (a.k.a. Grassofermata). CB5 was also one of the most potent ACSVL1 inhibitors and was found to robustly inhibit the uptake of oleic acid in Caco-2 cells (Sandoval *et al.*, 2010). CB5 has been recently found to prevent palmitate-induced lipotoxicity and apoptosis in cells in culture and inhibit fatty acid uptake across the intestinal epithelium in mice (Saini *et al.*, 2015).

We treated U87 human glioblastoma cells with CB5, and found that it decreased β -oxidation of long-chain and very long chain fatty acids. CB5 also dramatically slowed the growth rate of U87 cells, decreased invasiveness, and induced a unique morphology and the expression of a marker of differentiation. When given to mice bearing xenograft tumors, CB5 slowed growth and eventually reduced the size of tumors formed from U87 cells, although it did not have a significant effect on another human glioma xenograft model, Mayo-22. Based on our results, CB5 appears to be both a useful tool for

understanding the role of ACSVL3 in tumorigenesis and a potential therapeutic drug for some glioblastomas.

In this study we also introduce a new fluorescence-based screen to identify other inhibitors of ACSVL3. Based on the screen described by Li *et al.* (2008), this screen assesses the uptake of C₁-BODIPY-C₁₂ in Cos-1 cells expressing a hybrid enzyme called ACSVL1/3. This enzyme is a domain-swapped chimera comprised of the regulatory domain of ACSVL1 and the catalytic domain of ACSVL3. This domain swap couples the ability to uptake C₁-BODIPY-C₁₂ (which wild-type ACSVL3 cannot do) with the acyl-CoA synthetase activity of ACSVL3. Here we use this screening method as a method to compare the effects of identified ACSVL1 inhibitors on the uptake of C₁-BODIPY-C₁₂ on the hybrid ACSVL1/3.

Materials and Methods

Cell culture

U87MG and Cos-1 cells were obtained from American Type Culture Collection. Both lines were cultured in Dulbecco's Modified Eagle's Medium (DMEM) with 10% fetal bovine serum (FBS). GM9503 skin fibroblasts (healthy 10 year old male) were obtained from the Coriell Institute (Camden, NJ). They were cultured in Minimum Essential Medium (MEM) with 10% FBS. All cell lines were maintained at 37°C and 5% CO₂ atmosphere.

Drugs and compounds

Table 1 lists the formula of the drugs and compounds added to various assays, listed by the name they are referred to throughout this chapter.

Table 1: Systematic names of drugs and compounds included in assays

Common Name	Systematic Name
Triflupromazine	10-[3-(Dimethylamino)propyl]-2-trifluoromethylphenothiazine
Phenazopyridine	3-[(E)-Phenyldiazenyl]-2,6-pyridinediamine
Chlorpromazine	[3-(2-Chloro-phenothiazin-10-yl)-propyl]-dimethyl-amine
Emodin	1,3,8-Trihydroxy-6-methyl-9,10-anthraquinone
Perphenazine	2-{4-[3-(2-Chloro-10H-phenothiazin-10-yl)propyl]-1-piperazinyl} ethanol
CB2	(5E)-5-[(3-bromo-4-hydroxy-5-methoxyphenyl)methylene]-3-(3-chlorophenyl)-2-thioxothiazolidin-4-one
CB5	2-benzyl-3-(4-chlorophenyl)-5-(4-nitrophenyl)-1H-pyrazolo[5,1-b]pyrimidin-7-one
CB6	2-[7-(trifluoromethyl)-2,3-dihydro-1H-1,4-diazepin-5-yl]naphthalen-1-ol
CB16.2	5'-bromo-5-phenyl-spiro[3H-1,3,4-thiadiazole-2,3'-indoline]-2'-one

Generation of ACSVL3-KO U87 cell line

The ACSVL3-knockout (KO) U87 was produced with the CompoZr Knockout Zinc Finger Nuclease plasmids designed and created by Millipore Sigma. The forward and reverse sequences target genomic DNA before and after the second exon in the ACSVL3 sequence. (Forward: 5'-TGTGCTTTCCCACCCTTCTA-3', reverse: 5'-AGGTGAGGAGACTGGGAGT-3'.) Plasmids were transfected into WT U87 cells via

Fugene (Promega) and harvested using trypsin after 48 hours. Cells were counted with a hemocytometer and plated into 96-well plates at an average density of 0.9 cells/well with the goal of creating clones generated from a single cell. Clones were selected with hygromycin and expanded. ACSVL3 knockout was previously verified with PCR of both genomic DNA and cDNA generated from mRNA and mass spectrometry (Kolar, 2016). Immunofluorescence and western blotting as described below were used to assess ACSVL3 knockout. A 1:10 dilution of culture media from hybridoma cells producing monoclonal α -ACSVL3 antibody was used as the primary antibody source for both methods. Secondary antibodies used were goat α -mouse IgG-HRP (1:8,000 dilution in milk solution, Santa Cruz Biotechnology) for Western blotting, and goat- α -mouse Cy3 (1:150 dilution in PBS/BSA, Jackson ImmunoResearch).

Acyl-CoA Synthetase Activity Assays

To harvest cells, 10 cm plates of cells in culture were treated with 1 mL of 0.25% trypsin to release cells from the plates. The suspension of cells was pelleted by centrifugation and then washed twice with phosphate-buffered saline (PBS) containing a protease inhibitor cocktail. The pellets were resuspended in buffer containing 0.25 M sucrose, 1 mM Tris-HCl pH 7.5, and 1 mM EDTA (STE buffer). Protein concentration was measured using the assay described by Lowry *et al.* (1951).

Acyl-CoA synthetase assays were adapted from the protocol described by (Watkins *et al.*, 1991). A working solution was made containing 1 nmol of radiolabeled [1-¹⁴C]palmitic, stearic, behenic, or lignoceric acid (Moravek) and 4 nmol unlabeled corresponding fatty acid (Millipore Sigma) per 50 μ L in benzene. For each drug in both

WT and ACSVL3-KO U87 cell lines, duplicate samples were assayed. 50 μL of the working solution was added to 13x100 mm glass test tubes and dried down under nitrogen gas. The fatty acids were solubilized in 50 μL 10 mg/mL α -cyclodextrin in 10 mM Tris (pH 8.0). The tubes were sonicated in a water-bath sonicator for 2 minutes at 37°C and then incubated in a 37°C water bath shaker for 30 minutes to fully solubilize the fatty acids. Next, cell suspensions containing 30 μg of total protein in 50 μL (or 48 μL for assays containing drugs or compounds) of STE were added to each tube. For synthetase assays containing drugs or compounds, 2 μL drug or compound was then dissolved in DMSO (final assay concentration of 80, 10, 1 or 0.1 μM) and mixed into the suspension. Finally, 150 μL of a reaction mix was added to each tube, leading to final assay concentrations of 40 mM Tris-CL (pH 8.0), 10 mM ATP, 1 mM MgCl_2 , 0.2 mM CoA, and 0.2 mM dithiothreitol (DTT). The tubes were vortexed and incubated in a 37°C water bath shaker for 20 minutes. The reaction was stopped with 1.25 mL modified Dole's solution (40:10:1 Isopropanol: Heptane: 2N H_2SO_4). The tubes sat at 20°C for at least 20 minutes, and then centrifuged at 831g at 20°C for 10 minutes to pellet debris. Supernatants were removed for work-up.

Next, fatty acyl-CoA derivatives were extracted from unreacted fatty acids via Dole's method (Dole, 1956). 0.75 mL heptane and 0.5 mL H_2O were added to each sample. Samples were vortexed, and the upper organic phase was aspirated. 0.75 mL heptane was added again, followed by another vortex and aspiration of the upper organic phase. A third 0.75 mL heptane was added. Samples were vortexed and then centrifuged at 831g at 20°C for 1 minute prior to aspiration of the upper organic phase. The lower aqueous phase from each sample was transferred to a scintillation vial and 5 mL of

Budget-Solve HFP was added. Radioactivity of samples was measured by liquid scintillation counting.

The output from the counter was in disintegrations per minute (DPM). The DPMs from duplicate samples were averaged and the average DPMs of the blank sample were subtracted. An aliquot of the stearic acid working solution was counted to determine DPMs/nmol (specific activity), and results were converted to nmol stearic acid activated per 20 minutes per mg protein.

Generation and characterization of a domain-swapped ACSVL1/3 hybrid

The N-terminal domain of ACSVL1 and the enzymatic C-terminal domain of ACSVL3 were cloned together to form a hybrid enzyme. Sequence and ligation independent cloning (SLIC) was used as described by Li and Elledge (2012) to produce chimeric cDNA from the sequence of ACSVL3. The nucleotides coding for amino acids 1-210 of ACSVL3 were replaced with those coding for amino acids 1-100 of ACSVL1. The sequence was cloned into the mammalian expression vector pcDNA3 (Invitrogen) and transfected into COS-1 cells with FuGENE6 (Promega). Transfected colonies resistant to G418 were selected. The resulting hybrid enzyme is referred to as ACSVL1/3.

pcDNA3 containing the sequences of ACSVL3 and ACSVL1 as well as the empty vector were all transfected into COS-1 cells for comparison and characterization of ACSVL1/3. COS-1 cells stably expressing each construct were plated onto glass coverslips and allowed to attach in normal media. The media was aspirated and replaced with serum-free media for 30 minutes, and then incubated with 2 μ M 4,4-difluoro-5-

methyl-4-bora-3a,4a-diaza-s-indacene-3-dodecanoic acid (C₁-BODIPY-C₁₂; Thermo Fisher Scientific) for 20 minutes. Coverslips were washed with PBS and visualized via fluorescence microscopy to assess C₁-BODIPY-C₁₂ uptake.

To quantify C₁-BODIPY-C₁₂ uptake, COS-1 cells stably expressing ACSVL3, ACSVL1, ACSVL1/3, and the empty vector pcDNA3 were plated into opaque-walled 96-well plates and allowed to grow to confluence under normal conditions. The culture media was removed and replaced with serum-free DMEM for serum starvation. After 1 hour, the serum-free media was replaced with DMEM containing 5 μM C₁-BODIPY-C₁₂, 5 μM bovine serum albumin (BSA), and 1.97 mM trypan blue. The plates were incubated for 20 minutes at 37°C and 5% CO₂. The trypan blue quenches fluorescence of extracellular C₁-BODIPY-C₁₂ that is not uptaken by cells. Fluorescence of uptaken C₁-BODIPY-C₁₂ was quantitated using a SpectraMax M5 microplate reader.

C₁-BODIPY-C₁₂ uptake inhibition in Cos-1 cells expressing ACSVL1/3

Cos-1 cells expressing the ACSVL1/3 hybrid were plated into opaque-walled 96-well plates and grown and serum-starved as described above. The serum-free media was removed and replaced with DMEM containing 5 μM C₁-BODIPY-C₁₂, 5 μM BSA, 1.97 mM trypan blue, and either an ACSVL1 inhibitor or the equivalent volume of DMSO. Duplicate wells were set up, and each of the following concentrations of each inhibitor was tested: 0.1, 0.5, 1, 5, and 10 μM (dissolved in DMSO and diluted 1:1000 in the assay). The plates were incubated for 20 minutes. Fluorescence was quantitated using a SpectraMax M5 microplate reader.

Cell growth studies with CB5

Growth curves of U87 cells treated with 3 μ M CB5: 5000 WT or ACSVL3-KO

U87 cells were seeded into wells of 6-well plates containing DMEM + 10% FBS (U87 cell culture media) on day 0. On day 1, media was aspirated and replaced with cell culture media containing either 3 μ M CB5 (1:1000 dilution of 3 mM stock concentration in DMSO) or equivalent DMSO only (control). Triplicate wells of each condition were harvested via trypsin and counted by hemocytometer on days 3, 6, 9, 12, and 15. Cell media and drug/DMSO were refreshed every 3 days.

Growth response of U87 cells to varying doses of CB5: 5000 WT U87 cells were

seeded into wells of 6-well plates on day 0. On day 1, triplicate wells were aspirated and treated with varying concentrations of CB5 in U87 cell culture media. Concentrations used were 1, 1.5, 2 2.5, 3, 3.5, 4, 4.5, 5, 7.5, and 10 μ M CB5. CB5 was dissolved into DMSO for stock solutions, which were diluted 1:1000 in culture media. Media and CB5 were refreshed every 3 days. On day 12, all wells were harvested via trypsin and counted by hemocytometer.

Reversion of growth in U87 cells previously treated with CB5: 5000 WT U87

cells were seeded into 6-well plates on day 0. Three groups were set up: CB5 treatment throughout the experiment, CB5 treatment through day 9 followed by DMSO treatment, and DMSO treatment throughout the experiment. Cells were treated with 3 μ M CB5 or DMSO as described above on day 1. On day 9, media from half of the cells treated with CB5 was aspirated and replaced with media containing equivalent DMSO for the remainder of the experiment. Triplicate wells were harvested via trypsin and counted by

hemocytometer on days 9, 12, 15, 18, 21, and 23. Cell media and drug/DMSO were refreshed every 3 days.

Imaging U87 cells grown in 3 μ M CB5

5000 WT or ACSVL3-KO U87 cells were seeded onto 3.5 cm plates on day 0. On day 1, half were treated with 3 μ M CB5 as described earlier and half were treated with equivalent DMSO. To assess changes in morphology induced by CB5, cells were imaged with using light microscopy with an Axiovert 100 TV microscope (Carl Zeiss) on days 3, 6, 9, and 12. Cell media and drug/DMSO were refreshed every 3 days.

Fatty acid β -oxidation assay

WT U87 cells were seeded into 6-well plates and allowed to grow to near confluence. For each fatty acid, duplicate blank wells (media only, no cells) were set up to serve as extraction controls. Approximately 1.5 hour before the assay, media was removed and replaced with 540 μ L serum-free DMEM containing 2.2 mM carnitine and 3 μ M CB5 (3 mM stock in DMSO diluted 1:1000 in media) or equivalent DMSO for control and blank wells. Replicate wells were set up to determine protein concentration.

For the assay, fatty acid working solutions were made containing 20 μ M radiolabeled [$1-^{14}$ C]fatty acid and 80 μ M unlabeled fatty acid in benzene. Fatty acids assayed were palmitic, stearic, oleic (radiolabeled from Moravek, unlabeled from Millipore Sigma), behenic, and lignoceric acid. Working solutions were warmed to 37°C in a water bath for 5 minutes, sonicated in a water bath type sonicator for 2 minutes, and briefly vortexed. The total working solution needed of each fatty acid was added to a

glass test tube and dried down under nitrogen gas. The fatty acids were resolubilized in an equivalent volume of 10 mg/mL α -cyclodextrin in 10 mM Tris (pH 8.0). The tubes were incubated for 40 min at 37°C in a water bath type sonicator with occasional vortexing to optimize solubilization. 60 μ L of each solubilized fatty acid was added to duplicate wells containing U87 cells treated with CB5, U87 cells treated with DMSO, and blank, cell-free wells. Plates were manually shaken gently to mix and incubated at 37°C for 2 hours. The incubation was stopped by adding 120 μ L of ice-cold 18% HClO₄ to each well. Plates were kept at 4°C for 40 minutes. The contents of each well were moved to 12x75 mm glass test tubes.

Water-soluble products of β -oxidation were extracted from unreacted fatty acids using a Folch extraction (Folch *et al.*, 1957). 3.75 mL of 1:1 CHCl₃:Methanol was added to 16x125 mm screw-top test tubes (one per sample). 450 μ L of sample was added to these tubes which were then vortexed. 1.9 mL CHCl₃ was added to the tubes, which were again vortexed. 1.2 mL H₂O was added to each tube and the samples were vortexed. Tubes were centrifuged at 831g for 5 minutes to separate the phases. The upper, aqueous phase of each sample was transferred to a scintillation vial. 10 mL of Budget-Solve HFP (Research Products International) was added to each vial. The vials were agitated to mix contents, and radioactivity was determined by liquid scintillation counting.

Media from replicate wells that were set up to determine protein concentration was aspirated. Wells were washed with PBS and then treated with 400 μ L lysis buffer comprised of 0.1 M sodium phosphate pH 7.5, 0.15 M NaCl, and X% NP40. The Pierce 660 nm Protein Assay was used to determine concentration.

The output from the counter was in disintegrations per minute (DPM). The DPMs from duplicate samples were averaged and the average DPMs of the blank sample were subtracted. An aliquot of the stearic acid working solution was counted to determine DPMs/nmol (specific activity), and results were converted to nmol stearic acid activated per 20 minutes per mg protein.

Immunofluorescence

Cells were seeded into plates containing glass coverslips. The next day, media containing 3 μ M CB5 or equivalent DMSO was added. Cells were treated for 9 days. Media and drug/DMSO was refreshed every 3 days.

Coverslips were removed from culture plates and washed 3 times with Dulbecco's phosphate-buffered saline (DPBS) containing calcium and magnesium. Cells were fixed by incubating the coverslips for 20 minutes in PBS with 3% formaldehyde. Coverslips were again washed 3 times with PBS. Cells were permeabilized by incubating for 5 minutes in 40 μ g/mL digitonin in PBS. Coverslips were washed 3 times in PBS again, then incubated for 40 minutes in α -GFAP antibody (Dako) diluted 1:5000 in 0.01% BSA in PBS. Coverslips were washed 7 times in PBS, then incubated for 40 minutes in Cy3-linked goat- α -rabbit secondary antibody (Jackson ImmunoResearch) diluted 1:150 in 0.01% BSA in PBS. Coverslips were again washed 7 times. Coverslips were mounted to glass microscope slides (mount solution: 1 mg/mL phenylenediamine and 0.1 M Tris pH 8.7 in 90% glycerol) and sealed. Cells were visualized by fluorescence microscopy using an Axio Imager M2 with ApoTome attachment (Carl Zeiss).

Western blotting

Sodium dodecyl sulfate-polyacrylamide gel electrophoresis (SDS-PAGE) was used to separate proteins. Protein samples were boiled in sample loading buffer (5X stock, final 1X concentrations of 2% SDS, 50 mM Tris, 0.2 mg/mL bromophenol blue, 5% 2-mercaptoethanol, 12.5 mM EDTA, and 10% glycerol). 20 µg of protein was added to each lane of a 10% acrylamide gel prepared by the method of Laemmli (1970). Proteins were separated at 100 V, then transferred from the gel to PVDF membrane for 2 hours in tris-glycine buffer with 20% methanol at 100 V. The PVDF membrane was blocked with 10% milk (w/v) in TBST (0.15 M NaCl, 0.05% Tween-20, and 0.01 M Tris, pH 7.4) for at least 1 hour. Next, the membrane was incubated in a diluted primary antibody solution in 10% milk in TBST for 1 hour, then washed 3 times with TBST. The membrane was then incubated in a diluted secondary antibody solution in 10% milk in TBST for 1 hour, then again washed 3 times with TBST. The membrane was incubated in SuperSignal West Pico Chemiluminescent Substrate (Thermo Fisher Scientific) according to the reagent manual's instructions and exposed to film to detect signal. The primary antibody used was α -GFAP (1:500 dilution in milk solution; Dako). Due to unequal loading, β -actin was also detected as a loading control using α - β -actin antibody (1:800 dilution in milk solution; Santa Cruz Biotechnology). The secondary antibody used was goat α -rabbit IgG-HRP (1:8000 dilution in milk solution; Santa Cruz Biotechnology).

Treatment of fibroblasts with CB5

To examine the effect of CB5 on a non-cancerous cell line, human primary fibroblast GM9503 cells were treated with the drug for several days. Cells were seeded into wells in a 12-well plate at approximately 80% confluency. The next day, duplicate wells of cells were treated with the following concentrations of CB5: 1 μM , 3 μM , 6.5 μM , 10 μM , and DMSO only. Stock solutions of CB5 in DMSO were made for each concentration so the dilution into culture media was 1:1000 in each condition. Cells were allowed to grow for 5 days and then imaged with an EVOS XL Core Imaging System (Thermo Fisher Scientific). Media and drug was refreshed on the 3rd day.

Scratch-wound assay

Cells were seeded into 6-well plates and allowed to grow to about 80% confluence. A 1000 μL pipet tip was used to scratch the cell layer in each well. Scratches were imaged immediately after the scratch, 24 hours post-scratch and 48 hours post-scratch to assess cell growth over the scratch wound. Imaging was performed with an EVOS XL Core Imaging System (Thermo Fisher Scientific).

Treatment of mice bearing xenografts with CB5

All mice were obtained from were obtained from the Johns Hopkins University Sidney Kimmel Comprehensive Cancer Center Office of Research Services Animal Resources.

Toxicity of CB5 in mice: CB5 was dissolved at a concentration of 20 mg/mL into DMSO. CB5/DMSO was diluted into sterile PBS and sonicated in a water-bath type

sonicator for 15 minutes at 30°C to form a stable suspension. (Sonication was performed before injections each day). Concentrations used were 10, 20, 40 and 80 µL of CB5/DMSO per mL for the doses of 2, 4, 8, and 16 mg/kg/day, respectively. Two 8-week old female NOD/SCID mice were obtained from the Johns Hopkins University Sidney Kimmel Comprehensive Cancer Center Office of Research Services Animal Resource. Each mouse received increasing doses of CB5 via a 200 µL intraperitoneal injection once daily. They received 2 mg/kg for 2 days, 4 mg/kg for 2 days, 8 mg/kg for 6 days, and 16 mg/kg for 2 days. Animals were observed for 30 minutes following each injection to determine any acute side effects of CB5.

Toxicity was also assessed using Kolliphor HS 15 (Millipore Sigma) as a vehicle. A 30% solution (w/v) was made of Kolliphor HS 15 in PBS. The solution was sterilized by filtration. CB5 was dissolved directly into the Kolliphor solution. Two 12-week old female NOD/SCID mice received the following doses of CB5 in a daily 200 µL injection: 2, 4, 8, 16, 32, and 64 mg/kg. Each dose was given for two days, and the final 64 mg/kg dose was given for 5 days. Animals were observed for several minutes after injections to determine any acute side effects.

U87 xenografts: WT U87 cells were harvested via trypsin and counted. 4,000,000 cells in 50 µL sterile PBS were injected subcutaneously into both hind flanks of 6 8-week old female NOD/SCID mice. Tumors were allowed to grow and measured every 2-3 day using calipers. Tumor volume was approximated using the following formula: volume = (length x width²)/2. Once average tumor size was approximately 100 mm³, daily drug injection began. CB5 was dissolved at a concentration of 20 mg/mL into DMSO, and then 10 µL CB5/DMSO was diluted into 1 mL sterile PBS and sonicated in a water-bath

type sonicator for 15 minutes at 30°C to form a stable suspension. 2 mg/kg CB5 was given to 3 mice via intraperitoneal injection once daily. The other 3 mice received equivalent volume of DMSO in PBS (vehicle). Mice receiving vehicle were sacrificed on Day 22, when average tumor volume exceeded 1 cm³. Mice receiving CB5 were sacrificed on Day 25 when a large outlier tumor volume exceeded 1 cm³. Tumors were excised and weighed after sacrifice.

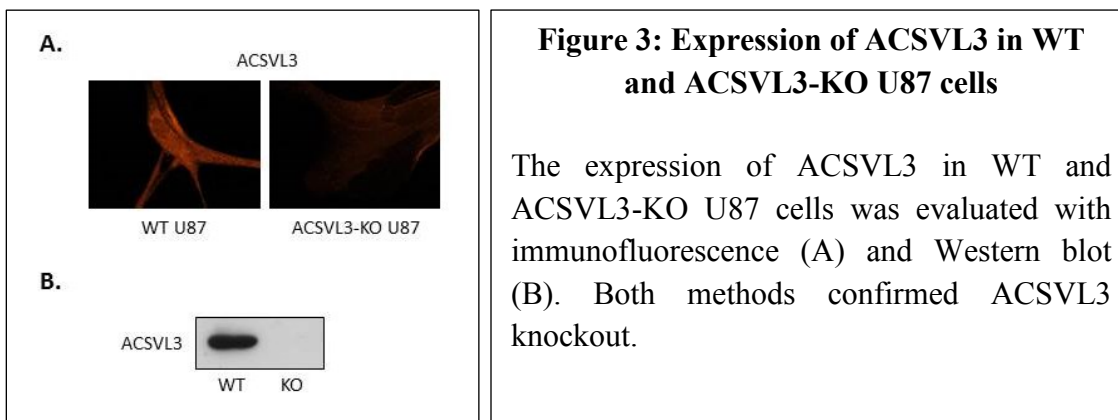
Mayo 22 xenografts: Mayo 22 cells were derived from a primary glioblastoma and are maintained by serial passage as subcutaneous xenografts. To implant new xenograft tumors, 500 mg was measured out from the previous generation's subcutaneous xenograft. This tumor section was finely chopped, suspended in 5 mL of sterile PBS, and passed 6 times through a 16-gauge needle using a 10 mL syringe. The suspension was centrifuged, aspirated, and resuspended in 2 mL of PBS. 100 µL of this suspension was implanted to form each new tumor. (The passage protocol was adapted from Carlson and Sarkaria, 2011).

Mayo 22 cells were implanted by subcutaneous injection into both hind flanks of 8-week old female NOD/SCID mice. CB5 was dissolved at a concentration of 20 mg/mL into DMSO, and then 40 µL CB5/DMSO was diluted into 1 mL sterile PBS and sonicated in a water-bath type sonicator for 15 minutes at 30°C to form a stable suspension. Drug injection began on Day 9, when average tumor was approximately 100 mm³. 8 mg/kg CB5 was given to half of the mice while the others received equivalent DMSO in PBS via intraperitoneal injection once daily. Mice were sacrificed on Day 23 once some tumor volumes exceeded 1 cm³. Tumors were excised and weighed.

Results

Validation of ACSVL3-KO U87 cell line

ACSVL3 expression in WT and ACSVL3-KO U87 cells was assessed with both immunofluorescence and western blotting. Both showed knockout of ACSVL3 (Figure 3).



ACSVL3 preferentially activates stearic and behenic acid

As a member of the very-long chain synthetase family, it was expected that ACSVL3 would activate long and very long chain fatty acids. To test its specificity, the thioesterification of radiolabeled fatty acids to their CoA derivatives was measured *in vitro* using pelleted WT and ACSVL3-KO U87 cells. The KO cells showed reduced conversion of all fatty acids tested: palmitic, stearic, behenic, and lignoceric (Figure 4). However, the reduction of conversion of stearic and behenic acid was more consistent and statistically significant than the other two. This implies that stearic and behenic acid are preferred substrates of ACSVL3. Because stearic acid is thioesterified to CoA at a

much higher rate than behenic acid, it was chosen for use in later experiments searching for ACSVL3 inhibitors.

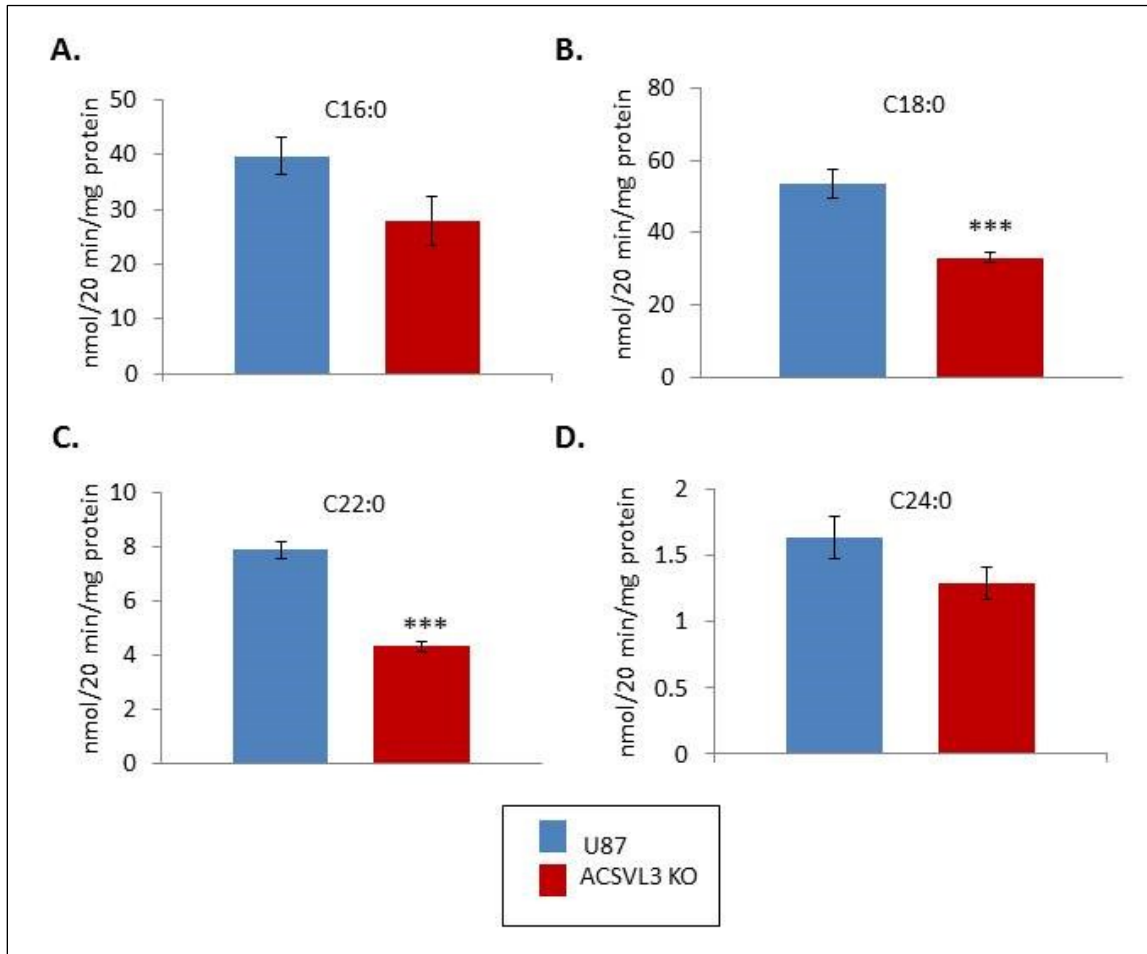


Figure 4: Total activation of long- and very-long chain fatty acids in WT and ACSVL3-KO U87 cells

Protein from WT and ACSVL3-KO U87 cells were assayed for conversion of [1-¹⁴C]-labeled fatty acids to their CoA derivatives. A total of 4 samples were assayed for each fatty acid. C16:0/palmitic acid (A) and C18:0/stearic acid (B) are considered long-chain fatty acids, and C22:0/behenic acid (C) and C24:0/lignoceric acid (D) are considered very long-chain fatty acids. There was a slight decrease in the activation of C16:0 and C24:0 in protein from ACSVL3-KO U87 cells, but the difference was not statistically significant. Activation of C18:0 and C22:0 was statistically decreased ($p < 0.001$) in protein from ACSVL3-KO U87 cells.

ACSVL1 inhibitors also inhibit ACSVL3

Several known inhibitors of ACSVL1 were screened for inhibition of ACSVL3. Inhibitors tested were the approved drugs triflupromazine, phenazopyridine, chlorpromazine, emodin, and perphenazine, and molecules from the ChemBridge Corporation compound library referred to as CB2, CB5, CB6, and CB16.2. The conversion of stearate to stearyl-CoA was again measured in WT and ACSVL3-KO U87 cells. Either 80 μ M of a known ACSVL1 inhibitor or the equivalent volume of DMSO (control) was added to the assay. Most of the inhibitors of ACSVL1 inhibited conversion of stearate to stearyl-CoA in WT U87 cells (Figure 5). However, this assay measures the total activity of all acyl-CoA synthetases in the cell pellet, not just ACSVL3. For this reason, synthetase activity on WT and KO U87 cells was compared. Figure 5a shows the fraction of conversion in the presence of inhibitors compared to DMSO, while Figure 5b shows the difference in total conversion of stearate to stearyl CoA in the presence of the inhibitors. An inhibitor is likely somewhat specific if it lowers total conversion of stearate to stearyl-CoA more in WT than ACSVL3-KO cells by one of these two measures. All of the ACSVL1 inhibitors except CB6 and CB16.2 lowered total conversion of stearate by a larger margin in WT compared to ACSVL3-KO U87 cells. The following inhibitors showed a greater percent decrease in WT versus ACSVL3-KO U87 cells: phenazopyridine, chlorpromazine, emodin, CB2, CB5, and CB16.2.

Since CB5 and CB16.2 were very inhibitory of conversion of stearate at 80 μ M, assays were repeated with lower doses of these two molecules. Again, the difference in inhibition in WT and ACSVL3-KO U87 cells was compared (Figure 5c and d). The inhibitory effect of CB16.2 was greatly decreased at these lower concentrations. CB5 still

inhibited most ACS activity when added to the assay at 10 μM , but not when added at 1 μM or 0.1 μM . As CB5 appears to be the most inhibitory molecule studied, it was selected to study its effect on live U87 cells.

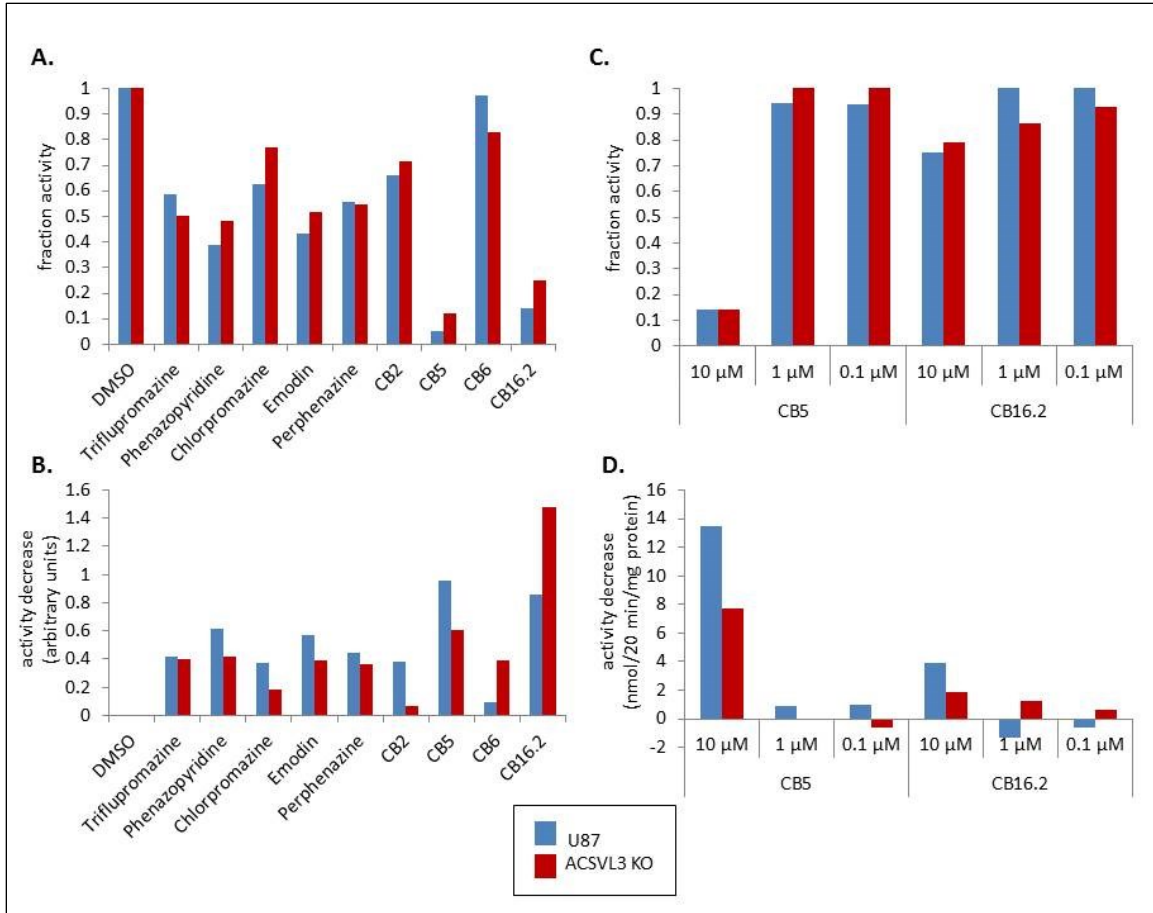


Figure 5: Inhibition of C18:0 activation by ACSVL1 inhibitors in WT and ACSVL3-KO U87 cells

80 μ M of various ACSVL1 inhibitors was added to assays assessing the conversion of [1- 14 C]-labeled C18:0 to its CoA derivative in protein from both WT and ACSVL3-KO U87 cells. For each drug or compound, the fraction of activity compared to assays containing DMSO (negative control) is shown (A). The total decrease in ACS activity, normalized to the DMSO control in each assay, is also shown (B). An inhibitor that is somewhat specific for ACSVL3 should exhibit either a higher fraction of activity in KO vs. WT, or a larger total difference in ACS activity in KO vs. WT. CB5 and CB16.2 were determined to be the most robust inhibitors and were added to ACS assays in smaller concentrations. Again, the fraction of activity (C) and the total decrease in ACS activity (D) are shown. 10 μ M CB5 inhibited ACS activity robustly, 10 μ M CB16.2 inhibited ACS activity partially (but less robustly than CB5), and lower concentrations of both drugs did not inhibit ACS activity.

Characterization of a domain-swapped ACSVL1/3 hybrid

To couple the ability to uptake the fluorescent fatty acid analog, C₁-BODIPY-C₁₂, with the enzymatic activity of ACSVL3, a hybrid was generated comprised of the regulatory, N-terminal domain of ACSVL1 and the enzymatic C-terminal domain of ACSVL3 (illustrated in Figure 6a). The construct was cloned into the plasmid pcDNA3 and transfected into Cos-1 cells. ACSVL1 and ACSVL3 were also each cloned into pcDNA3, and these constructs, as well as the empty vector, were each expressed in Cos-1 cells for comparison.

Fluorescence microscopy and a quantitative, fluorescence-based plate-reader assay were used to compare the uptake of C₁-BODIPY-C₁₂ by Cos-1 cells expressing ACSVL1, ACSVL3, the hybrid ACSVL1/3, and the empty vector pcDNA3. By microscopy, cells expressing ACSVL3 and pcDNA3 do not uptake C₁-BODIPY-C₁₂ while ACSVL1 and ACSVL1/3 both uptake C₁-BODIPY-C₁₂ at similar levels (Figure 6b). By the plate-reader assay, cells expressing ACSVL3 and pcDNA3 again show similar, lower levels of C₁-BODIPY-C₁₂ uptake, while cells expressing ACSVL1 and ACSVL1/3 exhibit similar, higher levels of uptake (Figure 6c).

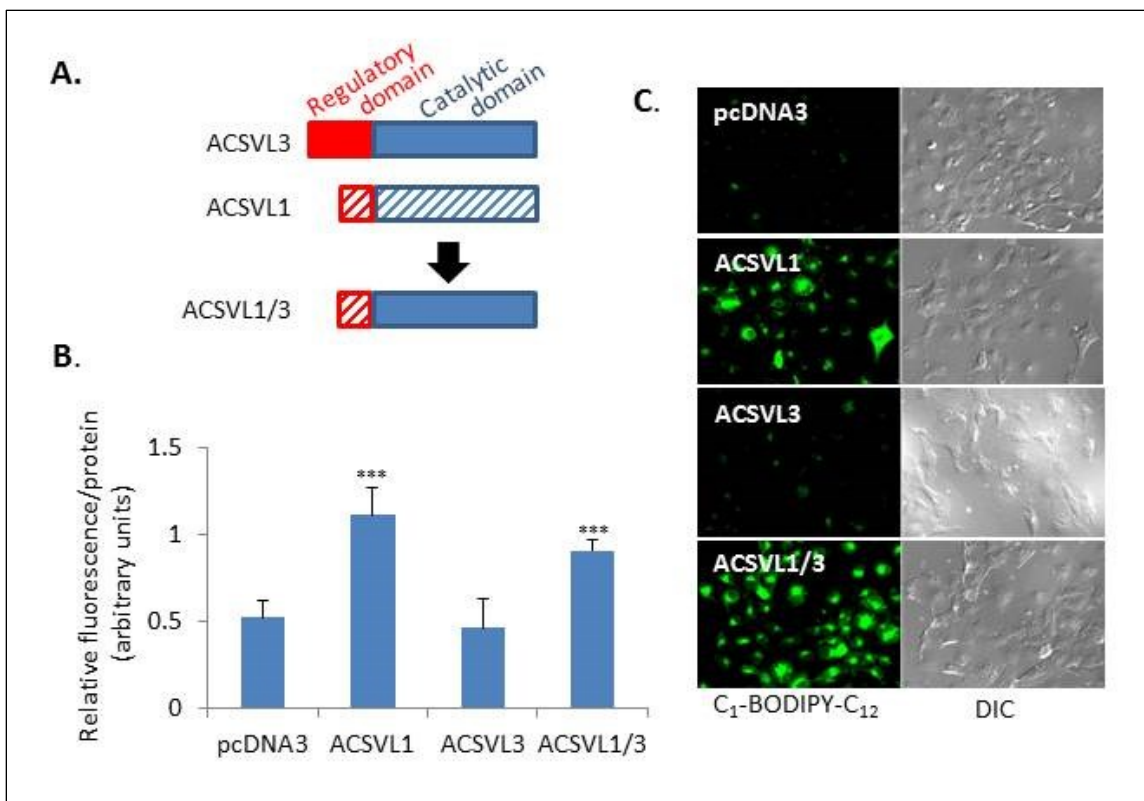


Figure 6: Characterization of the ACSVL1/3 hybrid enzyme

A. The domain swapped hybrid is illustrated. Cos-1 cells were transfected with the empty vector (pcDNA3) or a plasmid containing ACSVL1, ACSVL3 or the hybrid ACSVL1/3. These cells were evaluated for their ability to uptake C₁-BODIPY-C₁₂ by quantification of fluorescence in a plate reader (B) or immunofluorescence (C). For quantification of fluorescence, triplicates of Cos-1 cells expressing each construct were evaluated. ACSVL1 and ACSVL1/3 both showed increased uptake of C₁-BODIPY-C₁₂ compared to pcDNA 3 ($p < 0.001$), demonstrating that the domain swap conferred the ability to uptake C₁-BODIPY-C₁₂ to the catalytic domain of ACSVL3.

Most ACSVL1 inhibitors also inhibit uptake of C₁-BODIPY-C₁₂ and the acyl-CoA synthetase activity of ACSVL1/3

The same set of ACSVL1 inhibitors that were screened in the ACS activity assay were tested to see if they would inhibit uptake of C₁-BODIPY-C₁₂ in Cos-1 cells expressing ACSVL1/3. Each was added in multiple concentrations from 0.1 to 5 μ M in duplicate wells in a 96-well plate. Many of the inhibitors showed a dose-dependent

inhibition of C₁-BODIPY-C₁₂ uptake (Figure 7a). Again, the compounds CB5 and CB16.2 were found to be the most potent.

CB5 and CB16.2 were added to acyl-CoA synthetase assays measuring the conversion of radiolabeled stearic acid to stearyl-CoA to assess if they would have a similar inhibitory effect on ACSVL1/3 as they did on ACSVL3. Both drugs were tested at concentrations of 10 μM and 1 μM. Pellets from Cos-1 cells overexpressing all constructs (ACSVL1, ACSVL3, ACSVL1/3, and pcDNA3) were assayed. While 10 μM and 1 μM CB16.2 as well as 1 μM CB5 had minor inhibitory effects, 10 μM CB5 inhibited stearate conversion in all constructs (Figure 7b and 7c). (The inhibition seen in cells expressing pcDNA3 can be attributed to inhibition of long- and very long-chain ACSs naturally expressed by Cos-1 cells.)

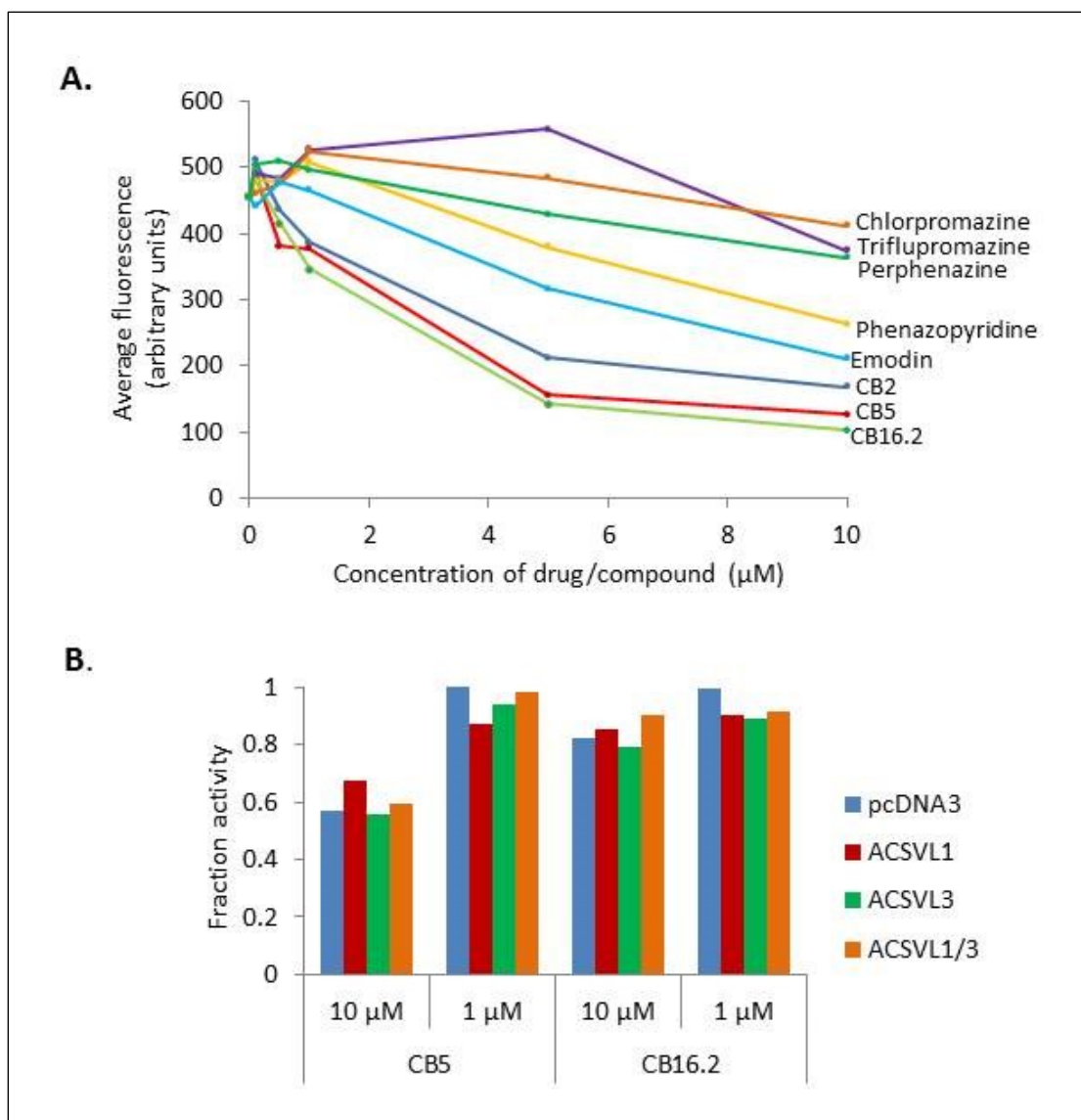


Figure 7: Inhibition of ACSVL1/3 by ACSVL1 inhibitors

A. Cos-1 cells expressing ACSVL1/3 were treated with various concentrations of ACSVL1 inhibitors, then assayed for the ability to uptake C₁-BODIPY-C₁₂. Fluorescence was quantified. Most drugs and compounds inhibited C₁-BODIPY-C₁₂ uptake in a dose-dependent manner. B. CB5 and CB16.2 were added to assays assessing the conversion of [1-¹⁴C]-labeled C18:0 to its CoA derivative in protein from Cos-1 cells expressing ACSVL1, ACSVL3, ACSVL1/3, or the empty vector pcDNA3. The fraction of activity compared to a DMSO control is shown. 10 μM CB5 inhibited Cos-1 cells containing each vector, including empty vector pcDNA3, most likely due to inhibition of ACS enzymes naturally expressed by Cos-1 cells.

CB5 slows the growth rate of U87 cells in culture

Due to its dramatic effects on acyl-CoA synthetase activity, the effects of CB5 on cells in culture were characterized. First, 10 μM CB5 was added to media of U87 cells in culture. This appeared to be toxic to the cells; many cells detached over the course of several days or gained a rounded, sick-looking morphology. Next 3 μM CB5 was added to U87 cells in culture, which were counted every 3 days. CB5 appeared to have no negative effects on cell adherence and mortality. However, it did significantly slow the growth rate of the U87s (Figure 8a). U87 cells grown in 3 μM CB5 grew slower than not only WT U87 cells treated with DMSO but also ACSVL3-KO U87 cells. 3 μM CB5 appeared to be somewhat toxic to ACSVL3-KO cells, as the number of cells began to decrease slightly after 9 days of treatment.

WT U87 cells were then treated for 12 days with varying concentrations of CB5. The cells were collected and counted. Growth was found to be inhibited by CB5 in a dose-dependent manner (Figure 8b). The usable range of CB5 is very narrow; 1 μM CB5 has no effect on growth, while 10 μM is toxic to U87 cells in culture.

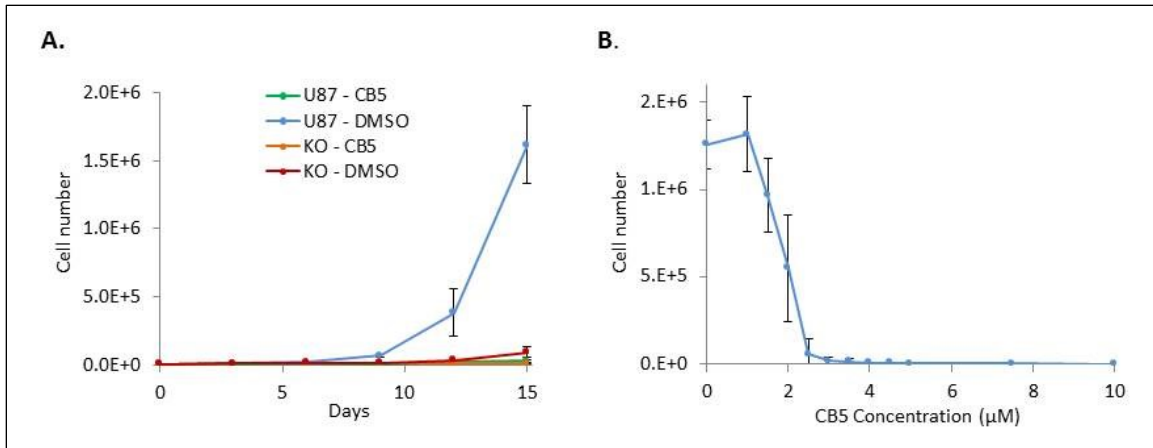


Figure 8: Inhibition of U87 proliferation by CB5

A. WT and ACSVL3-KO U87 cells were treated with either 3 μM CB5 or DMSO. 5000 cells were seeded in 6-well plates on Day 0. Cells from triplicate wells were counted every 3 days for 15 days. CB5 dramatically decreased the growth rate of both cell lines. Notably, the rate of proliferation of CB5-treated WT U87 cells was lower than the rate of untreated ACSVL3-KO U87 cells. B. Various concentrations of CB5 were given to WT U87 cells for 12 days, after which cells were counted. The therapeutic range of CB5 on U87 cells *in vitro* is narrow; 1 μM or less has no effect on proliferation rate, while 10 μM or more is toxic. 3 μM CB5, the dose used for other *in vitro* experiments using U87 cells, is near the lower point of inflection of the S-shaped dose response curve.

CB5 changes the morphology of U87 cells in culture

WT U87 cells treated with 3 μM CB5 grew larger and grew longer projections compared to U87 cells treated with DMSO over several days of treatment (Figure 9). This morphology is different from the morphology of ACSVL3-KO cells, which is also distinct from WT U87 morphology and is characterized by larger cells. The morphology induced by CB5 contributed to the hypothesis that CB5 may induce differentiation of WT U87 cells.

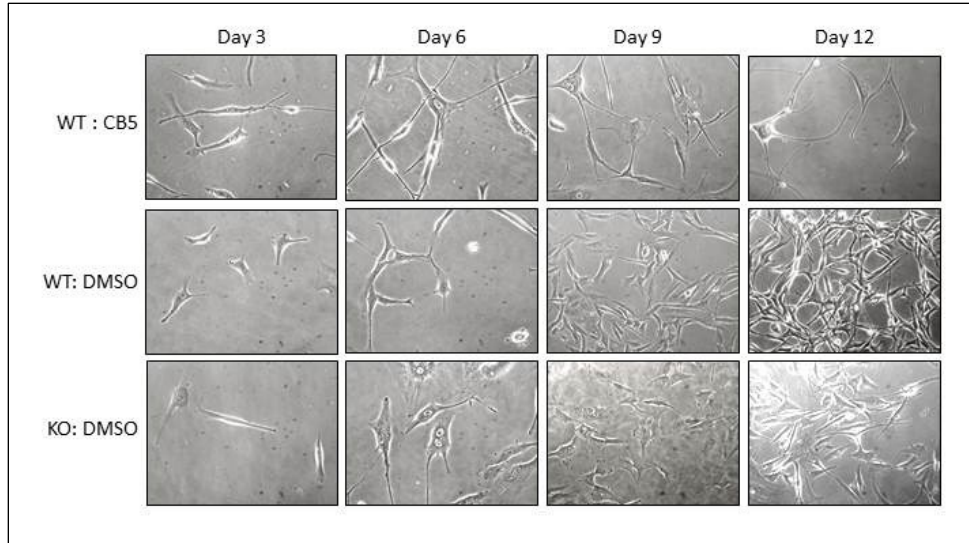


Figure 9: Morphology of U87 cells treated with CB5

WT U87 cells were treated with 3 μ M CB5 for 12 days. CB5 treatment induced a unique morphology in U87 cells. The cells grew larger and grew long projections. The morphology of ACSVL3-KO U87 cells is shown for comparison. ACSVL3-KO cells also have a morphology distinct from WT U87 morphology, and it is also dissimilar to the morphology induced by CB5.

When CB5 is removed from cells in culture, the growth rate reverts after several days

WT U87 cells were treated for 9 days with CB5. Media containing CB5 was removed from half of the groups of cells and replaced with media containing equivalent DMSO. The growth rate of the U87s from which CB5 was removed continued to grow slowly for several days, but the rate eventually increased to an exponential rate (as seen in WT U87 cells treated with DMSO) around Day 21, or 12 days after CB5 was removed (Figure 10).

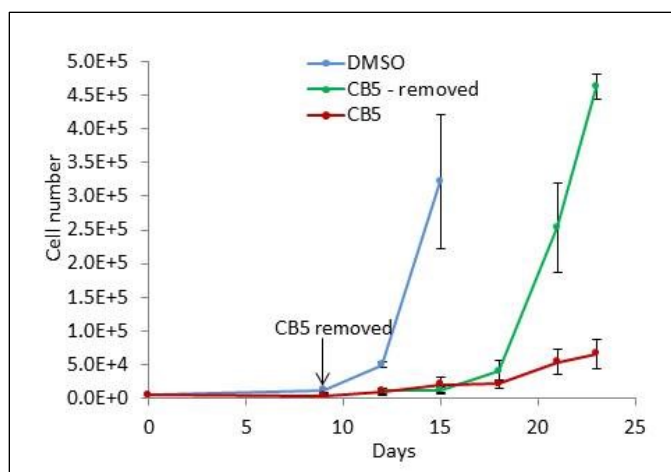


Figure 10: Reversion of growth rate in U87 treated with CB5 after drug removal

WT U87 cells were treated with DMSO or 3 μ M CB5 for 9 days, then CB5 was removed from half of the treated cells and replaced with DMSO. Cells were counted every 3 days. Several days after removal, U87 cells that had been previously treated with CB5 resumed the untreated growth rate. A statistical difference was seen in previously treated cells and continuously treated cells 12 days after removal of CB5.

CB5 does not affect cell growth or morphology of human fibroblasts

To test the effect of CB5 on a non-cancerous cell line, human fibroblasts in culture were treated with various concentrations of CB5 for 5 days. At all concentrations tested, CB5 did not appear to have an obvious effect on cell growth or morphology (Figure 11), even at concentrations that were toxic to WT U87 cells.

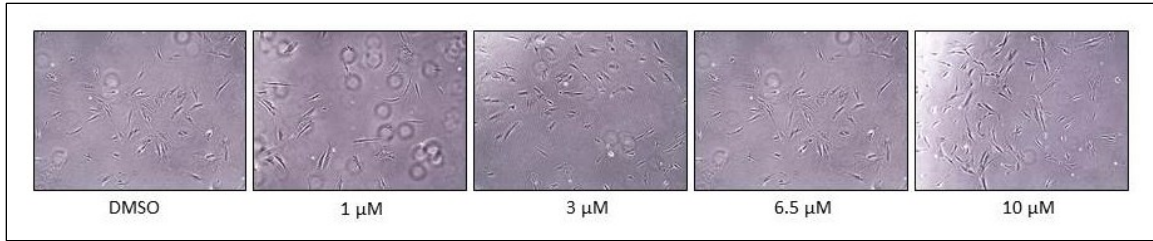


Figure 11: Treatment of human fibroblasts with CB5

Human skin fibroblasts were treated with varying concentrations of CB5 and observed for 5 days. None of the concentrations tested, including 10 μM CB5, which was found to be toxic to U87 cells, had an effect on number or morphology of the fibroblasts.

CB5 decreases invasiveness of U87 cells as measured by the scratch-wound assay

The scratch-wound assay was used to compare the invasiveness of WT U87 cells treated with 3 μM CB5 to WT and ACSVL3-KO U87 cells. For each condition, a layer of cells growing in culture was scratched, and the ability of the cells to close the scratch was assessed. After 48 hours, the scratch in the cells treated with CB5 remained visible, while the scratch in the DMSO-treated WT U87 cells had closed (Figure 12a). Quantification of the scratch size reveals that DMSO-treated WT U87 cells closed the scratch the quickest, followed by DMSO treated ACSVL3-KO U87s, and CB5-treated WT U87 cells closed the scratch the slowest (Figure 12b). While this assay does not demonstrate whether cell migration or cell division is a bigger factor in closing the scratch, it does suggest that CB5-treated U87 cells are less invasive than both WT and ACSVL3-KO U87 cells treated with DMSO.

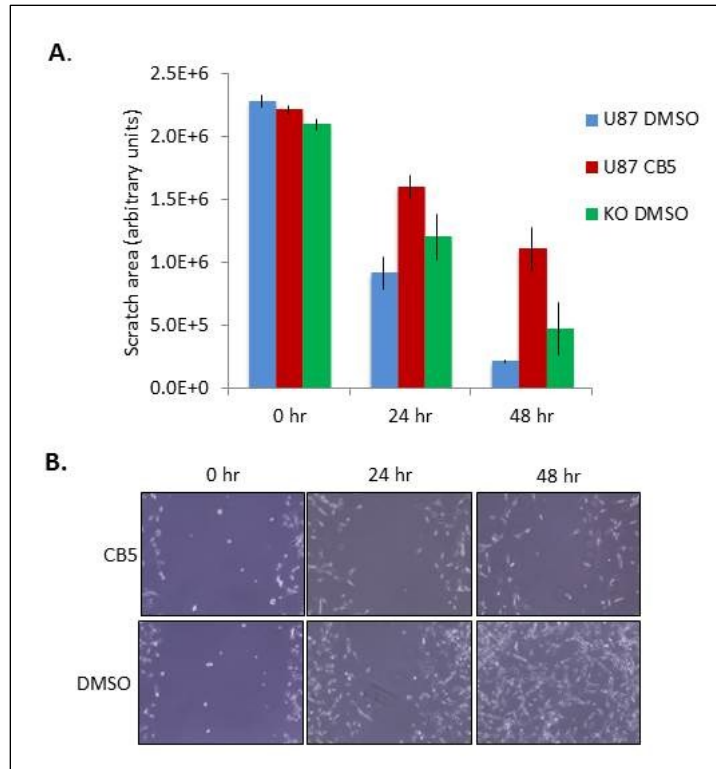


Figure 12: Scratch-wound assay of CB5-treated U87 cells

The scratch-wound assay was used to assess invasion of WT U87 cells treated with either 3 μ M CB5 or DMSO. ACSVL3-KO cells treated with DMSO were also compared. Quantification of the scratch sizes in each condition (A) and images of the scratches in CB5- and DMSO-treated U87 cells (B) are shown. In CB5-treated U87 cells, the scratch closed more slowly than in either WT or ACSVL3-KO cells. Scratch sizes were quantified using ImageJ (Schindelin *et al.*, 2015).

CB5 decreases β -oxidation of long-chain fatty acids in U87 cells

To determine whether CB5 affects the degradation of long- and very long-chain fatty acids, various radiolabeled fatty acids were given to WT U87 cells in culture. The U87 cells were treated with either 3 μ M CB5 or DMSO for 1.5 hour prior to the 2 hour incubation with a fatty acid. Fatty acids tested were palmitic, stearic, oleic, behenic, and lignoceric acids. After incubation, water soluble products were extracted to assess the breakdown of the fatty acids.

β -oxidation of palmitic, stearic, and oleic acids was reduced in the presence of CB5 (Figure 13). β -oxidation of behenic acid appeared to be only slightly reduced. The background was very high in the lignoceric acid assay, but β -oxidation again appeared to be reduced. Due to lower amounts of very-long chain fatty acids, and therefore lower utilization in WT cells, it is difficult to study β -oxidation of these fatty acids because of low signal-to-noise ratios.

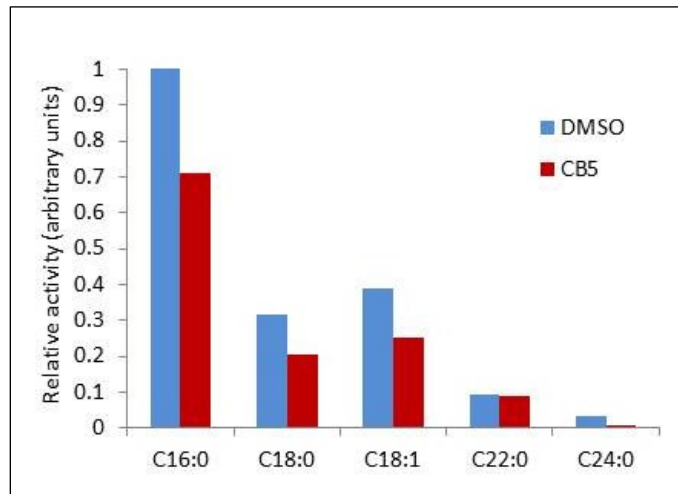


Figure 13: β -oxidation of long- and very long-chain fatty acids in U87 cells

The conversion of [$1\text{-}^{14}\text{C}$]-labeled fatty acids to their water soluble β -oxidation products over a 2 hr period was assayed in U87 cells treated with either 3 μM CB5 or DMSO. Cells were treated with CB5 for approximate 1.5 hr prior to the addition of labeled fatty acids. CB5 decreased the rate of β -oxidation of each fatty acid, especially the long-chain fatty acids C16:0, C18:0, and C18:1.

CB5 induces differentiation of U87 cells

To determine whether CB5 induces differentiation of U87 cells, expression of the astrocyte-specific marker glial fibrillary acidic protein (GFAP) was assessed by immunofluorescence and western blot. CB5-treated cells showed higher levels of GFAP

in U87 cells treated for 9 days with 3 μ M CB5 compared to cells treated with DMSO (Figure K). While RNAi knock-down of ACSVL3 led to an increase of GFAP in U87s (Sun *et al.*, 2014), the ACSVL3-KO U87 line did not exhibit this phenotype by immunofluorescence.

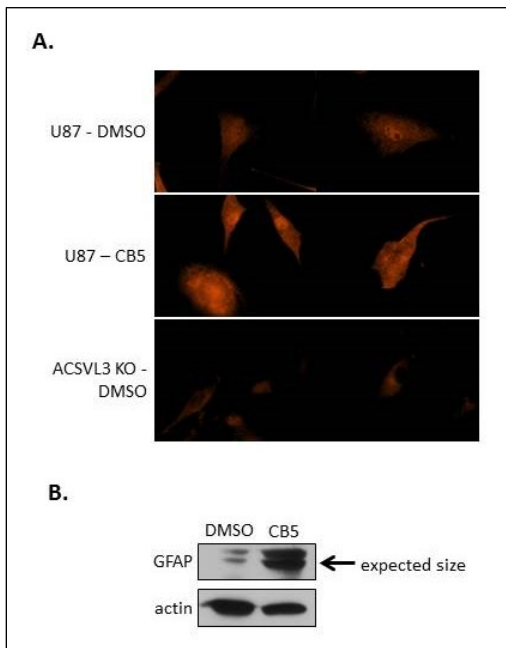


Figure 14: Expression of GFAP in U87 cells

Expression of the astrocyte-specific protein GFAP was evaluated in WT U87 cells treated with 3 μ M CB5 or DMSO for 9 days and ACSVL3-KO U87 cells. GFAP, a marker of differentiation, was detected using immunofluorescence (A) and Western blotting (B). GFAP was much more abundant in CB5-treated U87 cells than either WT or ACSCL3-KO U87 cells.

CB5 is well tolerated by mice

CB16.2 was toxic to mice in doses larger than 2 mg/kg when given by intraperitoneal injection; mice became immobile for several minutes after dosing (C. DiRusso, University of Nebraska-Lincoln, personal communication). To avoid potential toxicity of CB5, initial treatments of mice bearing xenografts used the same concentration, 2 mg/kg, of CB5 injected once per day. CB5 was dissolved in DMSO, which was then diluted into PBS to form a stable suspension. CB5 seemed to be better tolerated than CB16.2. NOD/SCID mice were treated with 2 mg/kg/day for 2 days, then 4 mg/kg/day for 2 days, 8 mg/kg/day for 6 days, and finally 16 mg/kg/day for 2 days. At no

point did the mice exhibit any obvious side effects, including the CNS side effects reported with larger doses of CB16.2.

Next, NOD/SCID mice were treated with CB5 dissolved in Kolliphor HS 15, which allowed CB5 to go into solution rather than the suspension of DMSO/PBS. This vehicle was tried in case CB5 was more bioavailable in solution rather than suspension. NOD/SCID mice were treated with the following doses for 2 days each: 2, 4, 8, 16, and 32 mg/kg. At all of these concentrations, CB5 was entirely dissolved in solution. Finally, the mice were treated for 5 days with the highest dose tested, 64mg/kg/day. This concentration did not go fully into solution but did form a stable solution. The mice did not exhibit obvious side effects from any doses. While the purpose of this study was to determine a toxic dose of CB5, no higher doses were given due to the limitations of getting CB5 into solution/suspension.

CB5 slows tumor growth in mice bearing U87 xenograft tumors but not Mayo-22 xenograft tumors

NOD/SCID mice were injected subcutaneously on both hind flanks with U87 cells to form xenograft tumors. Once the tumors had grown to an approximate average volume of 100 mm³, half of the mice began to receive a daily injection of CB5 (2mg/kg/day) while the other half received equivalent DMSO. Tumors were measured every 2-3 days. After 7 days of treatment (15 days post-xenograft implantation), tumors in the mice treated with DMSO began to grow more rapidly than those treated with CB5 (Figure 15a). After 12 days of treatment (20 days post-implantation), tumors in the mice treated with CB5 began, on average, to decrease in size. The tumor sizes exhibited by the

CB5-treated mice (except for one outlier, where $z = 2.0$ for final tumor weight) then stagnated. DMSO-treated mice were sacrificed on post-injection day 22 and CB5-treated mice on day 25. Despite this, harvested tumors from CB5-treated mice were on average much smaller than tumors from DMSO-treated mice (Figure 15b). Of the 6 total tumors from mice treated with CB5, one was an outlier; it grew at a similar rate to the tumors from the DMSO-treated mice. (The tumor on the mouse's other flank responded similarly to the other tumors from CB5-treated mice.)

Next, another cohort of NOD/SCID mice were injected subcutaneously with Mayo 22 cells and allowed to grow to approximately 100 mm^3 . Half of the mice then began receiving daily injections of CB5, this time at a higher dose of 8 mg/kg while the other half received equivalent DMSO. Tumors were measured every 2-3 days. Tumor growth was very variable within both the group of mice receiving CB5 and the group receiving DMSO. Furthermore, there was no statistical difference in estimated tumor volume or final weigh (Figure 15c and 15d).

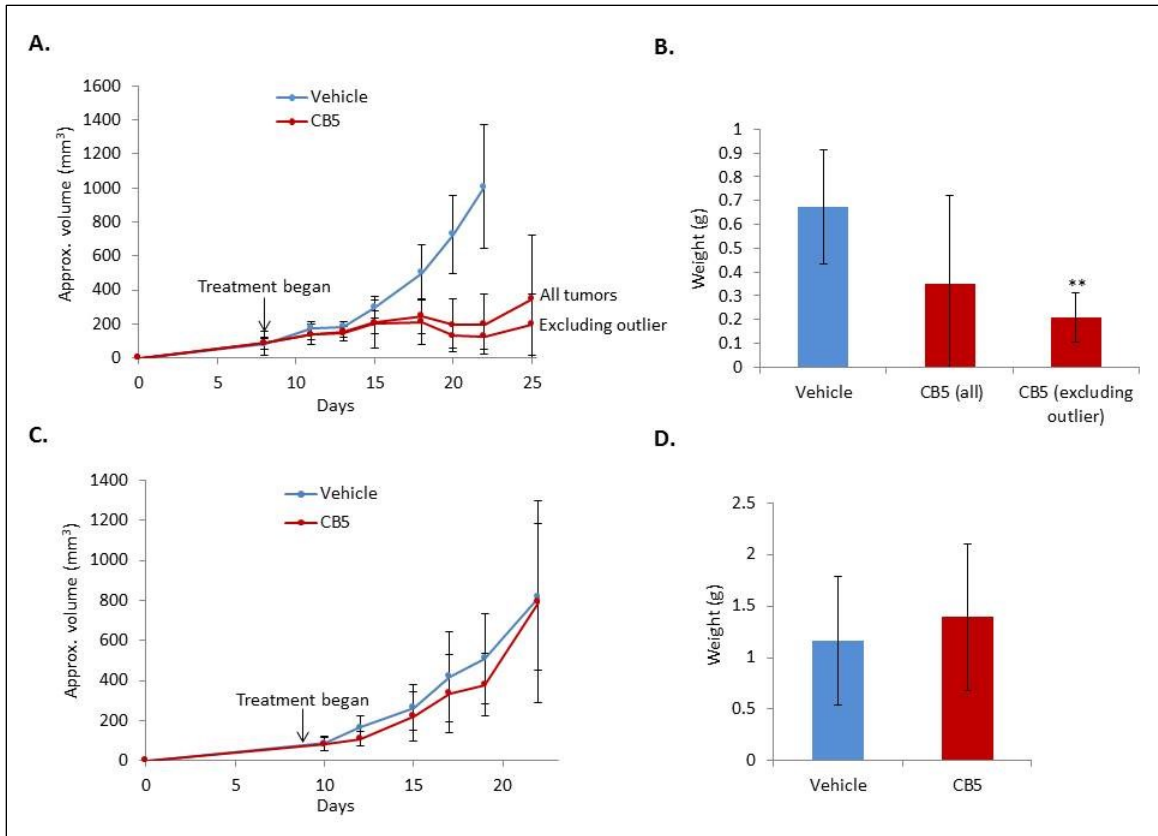


Figure 15: Treatment of mice bearing glioblastoma xenograft tumors with CB5

A. Mice bearing subcutaneous xenograft tumors formed from U87 cells were treated with 2 mg/kg/day CB5 or equivalent DMSO beginning 8 days after tumor implantation. Tumor size was approximated every 2-3 days by measuring with calipers. Vehicle-treated mice were sacrificed 22 days after xenograft implantation, and CB5-treated mice were sacrificed 25 days after injection. Except for one outlier, the tumors on the CB5-treated mice grew slower and even decreased in volume over the course of treatment. Final tumor weight after sacrifice is shown (B) although animals were sacrificed on different days (n= 6 for each condition, p < 0.01 if outlier is excluded). C. Mice bearing tumors formed from Mayo-22 cells were treated with 8 mg/kg/day CB5 beginning 9 days after tumor implantation. Approximate tumor size is shown. Mice were sacrificed 22 days after tumor implantation. There was no significant difference in approximate tumor size at any time point or final tumor weight after sacrifice (D).

Discussion

There are two main reasons to find an ACSVL3 inhibitor. First, a good inhibitor can be used to help understand the biology of ACSVL3 and tumorigenesis, and second, an inhibitor could have therapeutic potential in patients suffering from glioma. These experiments have identified inhibitors of ACSVL3 activity, and the most robust one, CB5, shows potential for both purposes.

A difficulty in finding inhibitors of acyl-CoA synthetases is that these enzymes overlap in function. U87 cells contain other long-chain and very-long chain ACS family members that likely activate stearic acid to stearyl-CoA, making it difficult to create a screen for inhibition of ACSVL3 activity alone. We have combated that by comparing ACS activity in WT U87 cellular protein to ACSVL3-KO U87 protein. If the inhibitors screened are somewhat specific for ACSVL3, they are expected to inhibit stearic acid activation more robustly in WT than in ACSVL3-KO U87 cellular protein. An ideal inhibitor (one that displayed no cross-reactivity with other ACS family members) would inhibit stearic acid activation in WT U87 cellular protein and would not affect activation in ACSVL3-KO protein. However, due to the high homology of the enzymatic regions of ACS enzymes, it is unlikely that a completely specific inhibitor will be found.

However, for therapeutic uses of identified inhibitors, specificity is not critical. The most important consideration is that the inhibitor combats cancerous phenotypes. For studying the biochemistry of ACSVL3 in glioma, a highly specific inhibitor would be most ideal. The ACSVL3-KO line has been very useful in characterizing the role that ACSVL3 plays in lipid metabolism in glioma, and halting ACSVL3 activity with an

inhibitor would in theory produce the same phenotypes exhibited in the KO line. However, my experiments demonstrate that this is not always the case. For example, CB5-treated U87 cells show an increase in GFAP over DMSO-treated U87 cells by immunofluorescence, while ACSVL3-KO cells did not show an increase. Many of the differences in ACSVL3-KO U87 cells versus CB5-treated U87 cells can be attributed to compensatory changes that arise in the KO line to combat the loss of ACSVL3. We know by proteomics that many proteins are upregulated or downregulated in the ACSVL3-KO line compared to WT U87s (Kolar, 2016), and while some of these changes are likely induced by CB5, using an inhibitor allows us to study the mechanism of ACSVL3 in glioma without worrying about as many compensatory changes that arise over time.

The small molecule CB5 was identified as a robust inhibitor of ACSVL3. We used two metrics to characterize potential inhibitors. First was the inhibition of the thioesterification of stearic acid to stearyl-CoA. Stearic acid was chosen above other long- and very long-chain fatty acids because it is activated preferentially by ACSVL3 at a relatively high rate. The second metric was the inhibition of uptake of C₁-BODIPY-C₁₂ in Cos-1 cells expressing the chimeric protein ACSVL1/3. By both metrics, CB5 was the most robust inhibitor of ACSVL3 activity. Therefore, it was chosen for further study to determine if it had therapeutic potential in glioma cells.

As a robust inhibitor of ACSVL1 (Sandoval *et al.*, 2010), it was expected that CB16.2 would be a good inhibitor of CB5 as well. However, results were mixed. CB16.2 inhibited uptake of BODIPY in Cos-1 cells expressing ACSVL1/3 approximately as well as CB5. At a concentration of 80 μ M, CB16.2 inhibited conversion of stearate to stearyl-CoA less robustly than CB5 but better than any other inhibitor, but at 10 μ M, CB5

significantly outperformed CB16.2. These inconsistencies may be due to the fact that CB16.2 appeared to be less soluble than the other inhibitors, including CB5, in the solvents used. It seemed more likely to precipitate out of DMSO, and when the stock DMSO solution was added to the aqueous assays, it appeared to only go into suspension, which may or may not have been stable. CB16.2 may have been a better inhibitor by our metrics if it was solubilized in a different solvent.

The chimera ACSVL1/3 was created to couple the ability to uptake C₁-BODIPY-C₁₂ to the enzymatic activity of ACSVL3. Here a fluorescence-based assay was used to compare several potential ACSVL3 inhibitors at multiple concentrations at once. This setup will also be used to screen chemical libraries to find other inhibitors of ACSVL3. A library of approved drugs and natural products and the ChemBridge CNS-Set library will be screened for reduction of C₁-BODIPY-C₁₂ uptake by measuring intracellular fluorescence using a plate reader. Positive hits will be defined as drugs or compounds that lower total fluorescence by at least 3 standard deviations from the mean of the control (no drug added) signal. A secondary screen will be performed to rule out decreases in fluorescence due to C₁-BODIPY-C₁₂ signal quenching, toxicity, or cellular membrane disruption. Identified drugs and compounds will be tested for inhibition of ACSVL3 synthetase activity in stably transfected COS-1 cells and U87 cells, with the ultimate goal to find multiple highly specific ACSVL3 inhibitors.

The effects of CB5 treatment of U87 cells in culture support its potential as an anti-tumorigenic drug. First and foremost, CB5 treatment greatly slowed the rate of proliferation of WT U87 cells. Since rapid, under-regulated cellular proliferation is a hallmark of tumorigenesis, this was an encouraging finding. Furthermore, treatment with

CB5 significantly decreased the rate at which a scratch-wound healed, a common measurement of invasiveness.

Toxicity was a concern since CB5 treatment led to some cellular death after several days in the ACSVL3-KO U87 cell line. However, treatment at high concentrations had no obvious effect on human fibroblasts, a non-cancerous cell line. This suggested that the drug may target tumor cells without affecting healthy cells, which is ideal for cancer therapeutic agents.

Interestingly, CB5 had a narrow range of effectiveness. 1 μM CB5 had no effect on cell proliferation compared to DMSO, while 10 μM was toxic to WT U87 cells. The effect of CB5 on proliferation was found to form an S-curve when cell number was plotted against CB5 concentration. The concentration 3 μM , which was used for most of the experiments performed on U87 cells in culture, was found to be at the lower point of inflection on this S-curve. This suggests that it may be an ideal dose to use on cells in culture, balancing toxicity with effectiveness.

Another effect of CB5 on U87 cells was an altered morphology. The large size and long projections induced by CB5 caused us to question whether CB5 was inducing differentiation in these cells. Increased GFAP in CB5-treated U87 cells as seen by both immunofluorescence and western blotting compared to DMSO-treated cells supported this hypothesis.

If WT U87 cells that were previously treated with 3 μM CB5 are switched to DMSO treatment, the rate of cell growth eventually, after several days, reverts to the growth rate exhibited by U87 cells that were never treated with CB5. This raised the question of how this occurs, given that CB5 seems to induce differentiation of U87 cells.

A hypothesis is that this increased proliferation stems from a smaller, sub-population of CB5-treated cells, explaining why it takes several days to revert to the untreated rate. After several days of treatment with CB5, there were a few WT U87 cells that did not have the altered morphology induced by CB5, and when GFAP expression was evaluated via immunofluorescence, occasional cells were found that exhibited less GFAP. This hypothesis could also explain the outlier xenograft U87 tumor that did not respond to CB5 treatment. Future experiments will aim to characterize this heterogeneity in treated cells.

The rate of β -oxidation of long-chain fatty acids decreased in WT U87 cells treated with CB5. While many of the changes exhibited by CB5-treated U87 cells appear over time, such as the altered morphology and expression of differentiation markers, this was an acute change, as cells were treated for only 1.5 hour prior to the assay. This makes sense, since fatty acids must be converted to acyl-CoA prior to β -oxidation. Because rapidly proliferating tumor cells need to generate a lot of energy, impairing β -oxidation may be one of the ways that CB5 slows proliferation of U87 cells.

CB5 was well tolerated by mice and did not appear to cause any side effects at the IP doses tested, up to 16mg/kg/day in DMSO/PBS and 64 mg/kg/day in 30% Kolliphor HS-15. CB5 reduced the rate of growth of U87-based subcutaneous xenograft tumors treated with 2 mg/kg/day of CB5 but not in Mayo 22-based xenografts treated with 8 mg/kg/day. The different responses could be explained by physiological differences between the two types of tumors, such as vascularization. Another possibility is that CB5 is inhibiting tumor growth in U87 xenografts not by inhibition of ACSVL3 but by targeting another pathway. CB5 is also a known inhibitor of ADP-ribosylation factor 6

(Arf6), a GTP-binding protein that regulates endocytic recycling and cytoskeleton remodeling (World Patent No. 2015183989). It is possible that CB5 could be inhibiting Arf6 in U87-based xenografts but not in Mayo 22-based xenografts. Future directions include evaluating the level of Arf6 in both U87 and Mayo 22 cells.

Another concern with CB5 treatment is the short half-life of the drug. CB5 has a half-life of 151.7 minutes in blood when given intravenously (C. DiRusso, University of Nebraska-Lincoln, personal communication). While IP injection likely leads to a longer half-life, better results may be achieved with multiple injections per day or a continuously-injecting, implanted micro-pump. Using a vehicle such as Kolliphor HS-15 (Millipore Sigma), which was used to characterize CB16.2 in mice, may affect the potency of the drug as well. Future experiments will test different delivery systems and higher concentrations of CB5 on Mayo 22-based xenografts.

It is not yet known if CB5 will cross the blood-brain barrier, which would be ideal for treating gliomas. A future experiment will be to treat mice bearing intracranial xenografts with CB5 and determine if the drug is still effective at reducing tumor growth rate.

Chapter 2: GPI-anchored proteins in WT and ACSVL3-KO

U87 cells

Introduction

Glycosyl phosphatidylinositol (GPI) anchors are lipid-based, post-translational modifications found in all eukaryotes that attach proteins to the cell surface. The core structure of a GPI anchor is phosphatidyl inositol (PI) that is partially inserted into the cell's plasma membrane, a central glycan core, and an ethanolamine phosphate sourced from phosphatidylethanolamine (PE) that is amide-bonded to the C-terminus of the GPI-anchored protein. In mammals, the PI moiety is a 1-alkyl 2-acyl phosphatidylinositol (Kinoshita and Takeda, 1994). The glycan core is comprised of one non-acetylated glucosamine and three mannose residues, and often there are glycan-based or side-branches or an additional linked PE moiety (Figure 16). GPI anchors are synthesized in the endoplasmic reticulum in a stepwise series of reactions catalyzed by GPI-GlcNAc transferase (GPI-T), then the anchor is transferred to the C-terminus of a protein by GPI transamidase (Kinoshita and Fujita, 2016). GPI anchors can be cleaved by phosphoinositide phospholipase C (PI-PLC), which hydrolyzes the phosphodiester bond of the PI molecule. After cleavage, the remaining GPI anchor has an exposed inositol cyclic-1,2-phosphate, referred to as the cross-reacting determinant (CRD). The CRD can be detected with an antibody, making the cleavage of GPI anchors and the subsequent

detection of the CRD a good method to identify GPI-anchored proteins (Jäger *et al.*, 1990).

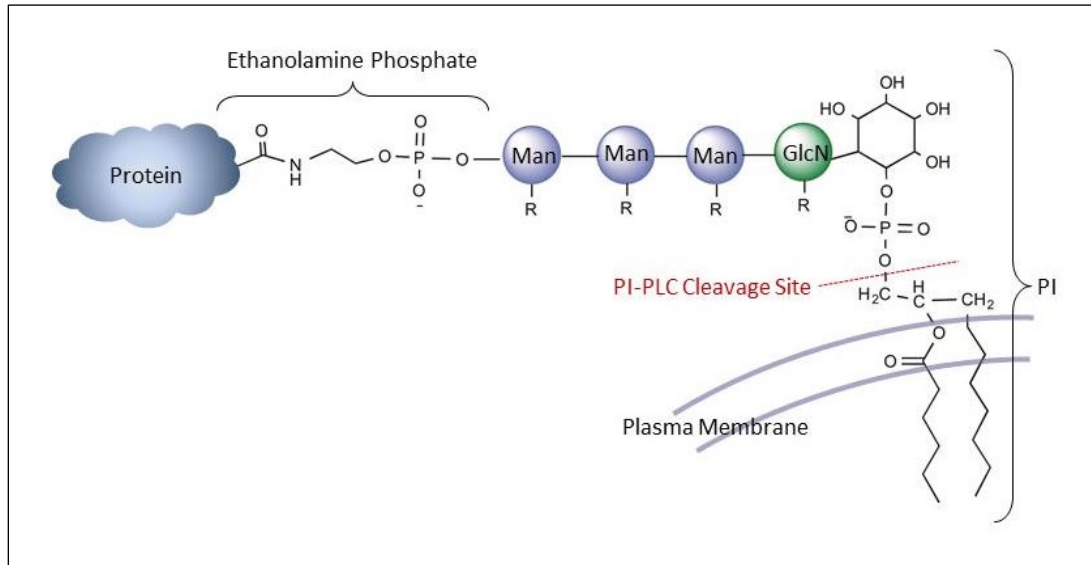


Figure 16: Diagram of a human GPI-anchored protein

A human GPI anchor is comprised of a 1-alkyl 2-acyl phosphatidylinositol moiety (PI), a non-acetylated glucosamine (GlcN), three mannose residues (Man), and an ethanolamine phosphate group that is amide-bonded to the C-terminus of the protein. The alkyl and acyl chains of the PI moiety are inserted into the plasma membrane, anchoring the protein. The saccharides can be modified with side chains. The site of cleavage by the enzyme PI-PLC, which releases the protein from the membrane and exposes the CRD, is indicated.

We have demonstrated that knockdown of ACSVL3 in U87 cells leads to decreased PI and PE synthesis in WT U87 cells (unpublished data). Since these are the two lipids required for GPI anchor synthesis, we hypothesized that ACSVL3-KO U87 cells would have lower levels of GPI-anchored proteins than WT U87 cells. Also supporting this hypothesis is the known role of GPI-anchored proteins in a range of cancers. Several subunits of GPI-T have been identified as oncogenes in various forms of

cancer, and many GPI-anchored proteins themselves are oncogenes or biomarkers of cancer (Gamage and Hendrickson, 2013).

We selected several common GPI-anchored proteins and tested for their expression in WT and ACSVL3-KO U87 cells: acetylcholinesterase (AChE), decay accelerating factor (DAF), 5'-Nucleotidase Ecto (NT5E), Alkaline Phosphatase, tissue nonspecific isoform (ALPL), and Thy-1 Cell Surface Antigen (Thy1). AChE aids cell proliferation, and increased AChE activity has been found in brain tumors (Barbosa *et al.*, 2001). NT5E is overexpressed in glioma, where it aids cell adhesion and interaction with the extracellular matrix (Cappellari *et al.*, 2012). DAF, a complement system regulator, has variable expression in primary and immortalized glioma cells (Mäenpää *et al.*, 1996). Thy-1 is often expressed in neural and glial cell lines as well as in neuroma tissue (Kenshead *et al.*, 1982). In gliomas, Thy-1 has been identified as a good biomarker for cancer stem cells (Parry and Engh, 2012). ALPL is a stem cell marker, and its presence in gliomas is associated with necrosis and poor patient outcomes (Iwadate *et al.*, 2016).

In this study, we use PCR to assess expression levels of GPI-anchored proteins in WT and ACSVL3-KO U87 cells. PI-PLC was isolated from *E. coli*, assayed for activity, and used to cleave GPI anchors in both cell lines, which can then be detected by their CRDs. We demonstrate that while several GPI-anchored proteins are found in U87 cells, levels of GPI-anchored proteins do not vary significantly between WT and ACSVL3-KO U87 cells. Thus, GPI-anchored proteins likely do not contribute to the tumorigenic phenotype associated with ACSVL3 expression in glial cells.

Materials and methods

PCR

RNA was extracted from WT and ACSVL3-KO cells using TRIzol reagent (Thermo Fisher Scientific) and concentration was measured with a NanoDrop ND-1000 spectrophotometer. 3 µg of RNA per sample was used to synthesize cDNA using the SuperScript III Reverse Transcriptase kit (Thermo Fisher Scientific).

Conventional PCR: Conventional PCR reactions were performed using the Invitrogen Platinum *Taq* DNA Polymerase kit (Thermo Fisher). The temperatures and times used in the reactions were as follows: initial melting temperature of 95°C for 45 seconds, melting temperature of 95°C for 23 seconds for each cycle, annealing temperature of 55°C for 15 seconds for each cycle, extension temperature of 68°C of 15 seconds for each cycle, and final temperature of 68°C for 5 minutes. Forty cycles were performed. The following table lists primers used:

Table 2: Primer sequences used to detect transcripts encoding for common GPI-anchored proteins

Gene	Forward primer sequence	Reverse primer sequence
Acetylcholinesterase (AchE)	GGGGCTCAGCAGTACGTTAG	TTCCAGTGCACCATGTAGGA
Decay Accelerating Factor (DAF)	TTCACCATGATTGGAGAGCA	CTGAACTGTTGGTGGGACCT
5'-Nucleotidase Ecto (NT5E)	GCCGCTTTAGAGAATGCAAC	CAGGTTTTCGGGAAAGATCA
Alkaline Phosphatase, tissue nonspecific isoform (ALPL)	CCTCCTCGGAAGACACTCTG	GCAGTGAAGGGCTTCTTGTC
Thy-1 Cell Surface Antigen (Thy1)	GGACTGAGATCCCAGAACCA	ACGAAGGCTCTGGTCCACTA
Glyceraldehyde 3-phosphate Dehydrogenase (GAPDH)	TGTGAGGGAGATGCTCAGTG	ACCCAGAAGACTGTGGATGG

Quantitative PCR (qPCR): Each qPCR reaction was comprised of 7.5 μ L of SYBR Green Master Mix (Thermo Fisher Scientific), 1 μ L each of forward and reverse primers, 5 μ L cDNA, and 0.5 μ L H₂O. The reactions were carried out in a Bio-Rad CFX96 Real Time PCR Detection System. The same temperatures, times, and primers used for conventional PCR were used again for qPCR, and 35 cycles were performed. GAPDH was used as a control to normalize results.

Purification of PI-PLC

Induction of PI-PLC expression in *E. coli*: LB plates bearing streaks of *E. coli* expressing an inducible plasmid containing PI-PLC were obtained from Dr. Charles Barlowe (Geisel School of Medicine at Dartmouth). 5 mL cultures were grown in LB at 37°C for 8 hours, then 40 mL cultures were grown overnight.

Bacteria from the overnight culture were added to a new 200 mL culture so that the optical density at 600 nm (OD₆₀₀) was 0.125. This new culture was grown at 37°C to an OD₆₀₀ of 0.5, then 1 mM Isopropyl β-D-1-thiogalactopyranoside (IPTG) was added to induce PI-PLC expression. (A small sample was removed prior to the addition of IPTG as an uninduced control.) The culture was grown in the presence of IPTG at 37°C for 3 hrs. The culture was centrifuged at 7969g for 30 min. Media was decanted from the bacterial pellet, and the pellet was frozen at -80°C overnight.

Bacterial Lysis: The pellet was thawed on ice and suspended in 3X its weight in a lysis buffer (50 mM Tris pH 8.0, 25 mM NaCl, 2 mM EDTA, and 0.1% Triton X-100). 1 mg/mL of lysozyme (dissolved into 10 mM Tris-Cl pH 8.0 at 10 mg/mL) and protease inhibitor (Calbiochem) were added to the suspension. The suspension was then incubated at 37°C in a water bath shaker for 30 minutes. The suspension was frozen at -80°C, thawed, and then incubated again at 37°C in a water bath shaker for 15 minutes. Next, DNase I was added at a concentration of 0.1 mg/mL (dissolved at 1 mg/mL into 10 mM Tris-CL pH 7.5 containing 150 mM NaCl and 1 mM MgCl₂), then 0.1 M MgCl₂ was added. The suspension was incubated at 37°C in a water bath shaker until the suspension was no longer viscous from DNA, approximately 15-30 min. The suspension was centrifuged at 12,000g for 15 min at 4°C, then decanted. The supernatant (referred to as “Supernatant 1”) was saved, and the pellet was resuspended into a stronger lysis buffer (50 mM Tris pH 8.0, 25 mM NaCl, 10 mM EDTA, and 0.5% Triton X-100). This suspension was incubated at 37°C in a water bath shaker for 15 minutes, centrifuged at 12,000g for 15 min at 4°C, and again decanted. The pellet and the supernatant (referred to as “Supernatant 2”) were saved. Both supernatants and the pellet were loaded on a 10%

acrylamide gel, and proteins were separated by SDS-PAGE. The gel was stained with Coomassie Blue to determine which fraction contained the most PI-PLC.

PI-PLC Purification: The purification procedure was adapted from Baldassare *et al.* (1989). All steps were performed at 4°C. A 1-cm diameter column was filled with 3.5 cm Q Sepharose Fast Flow resin (GE Healthcare Life Sciences). The column was equilibrated with with 20 mM Tris pH 8.0. Since most PI-PLC was located in Supernatant 1, this supernatant was added to the column next. The column was then washed twice with 5 mL 20 mM Tris pH 8.0. A gradient salt buffer was used to elute PI-PLC from the column. The buffer was 20 mM Tris pH 8.0 containing from 0 to 0.35 M NaCl. The total gradient elution volume was 50 mL, and ~2 mL fractions were collected. A sample from each fraction was loaded on a 10% acrylamide gel, and proteins were separated by SDS-PAGE to determine which fractions were enriched in PI-PLC. These fractions were pooled and concentrated using an Amicon Ultra 15 mL Centrifugal Filter Device (10 kDa MWCO; Millipore Sigma). To stabilize the enzyme, the final concentrated product was stored in 50% glycerol and 1 mM EDTA.

PI-PLC activity assay

To assess the activity of the purified PI-PLC, the activity of acetylcholinesterase released from erythrocyte membranes by PI-PLC was measured. This protocol was adapted from Ellman *et al.* (1961).

Erythrocyte membrane preparation: This preparation protocol was adapted from Hanahan and Ekholm (1974). Expired packed red blood cells (American Red Cross) were obtained. The cells were thawed and diluted 50% into 0.172 M Tris pH 7.5 for a total

volume of approximately 1 mL. The suspension was mixed for 1 min. 6 mL of 11 mM Tris pH 7.5 was added 1 mL at a time while vortexing. The suspension was then left on ice for 5 min. The suspension was centrifuged at 20,000g for 40 min at 4°C. The supernatant was decanted, and the pellet was resuspended in 6 mL of 11 mM Tris pH 7.5. The entire wash process (suspension in 11 mM Tris pH 7.5, resting on ice, centrifugation, and decanting) was repeated 3 times for a total of 4 washes. After the final decantation, the pellet contained a hard red lower pellet (a clot) and a looser, light colored upper pellet (the membranes). 2 mL of 11 mM Tris pH 7.5 was added gently to resuspend the membranes but not the clot. The membrane preparation was stored at 4°C.

Modified Ellman assay: For assays without prior PI-PLC treatment, the membrane preparation was diluted (3, 30, or 300 times) into phosphate buffer pH 8.0. 1 mL was added to a 1 mL cuvette.

For assays following PI-PLC treatment, the membrane preparation was diluted 30 times into phosphate buffer pH 8.0. 33 μ L of Supernatant 1 from the induction of PI-PLC expression, or 33 μ L from a fraction from the Q sepharose column that had a high amount of purified PI-PLC, was mixed into the diluted membrane preparation. This suspension was placed on a shaker at 37°C for 2 hours. An Ultrafree-MC 0.45 μ m filter unit (Millipore Sigma) was used to remove membranes from the suspension, and the remaining solution was transferred to a 1 mL cuvette.

For all assays, 8.33 μ L of 0.01 M 5,5'-dithio-bis-(2-nitrobenzoic acid) (DNTB) in phosphate buffer pH 7.0 was mixed into the cuvette. The spectrophotometer (Thermo Scientific Spectronic Genesys 5) was set to 412 nM and adjusted to zero. 6.66 μ L of 0.075 M acetylthiocholine iodide was mixed into the cuvette. Absorbance was recorded

every 10 seconds. Relative rates of AchE activity were determined by calculating the ratios of the slopes exhibited by the total absorbance plotted against time.

GPI anchor digestion by PI-PLC

This method was adapted from the protocol of Englund (1988). WT and ACSVL3-KO U87 cells were cultured as described in Chapter 1. Cells were collected by aspirating and rinsing culture plates, then adding PBS without calcium and magnesium and allowing cells to detach. Cells were pelleted and washed twice with PBS containing a protease inhibitor cocktail (Calbiochem). Protein concentration was determined via the Pierce 660 nm Protein Assay. Equal amounts of protein were loaded on a 10% acrylamide gel and separated by SDS-PAGE, and proteins were transferred from the gel to PVDF as described in Chapter 1. The membranes were incubated at 37°C in buffer containing 10 mM Tris pH 7.3, 150 mM NaCl, 2% Triton X-100, protease inhibitors, and purified PI-PLC. (10-, 50-, and 500-fold dilutions of PI-PLC were all performed.) A replicate membrane was incubated in buffer without PI-PLC as a negative control.

After PI-PLC digestion, immunoblotting was performed as described in Chapter 1. The primary antibody used was α -CRD (3 μ L antibody solution per 1 mL milk solution) and the secondary was goat α -rabbit IgG-HRP (1:8000 dilution in milk solution; Santa Cruz Biotechnology).

Results

WT and ACSVL3-KO U87 cells express several GPI-anchored proteins commonly found in cancer cells

As shown by conventional PCR, both WT and ACSVL3-KO U87 cells express mRNA for all five commonly GPI-anchored proteins that were tested (Figure 17a). While this is a diagnostic and not a quantitative PCR, the difference in brightness of some bands between WT and ACSVL3-KO warranted qPCR to compare expression levels. qPCR showed similar mRNA expression of all genes except for ALPL in WT and ACSVL3-KO U87 cells (Figure 17b). ALPL mRNA expression in ACSVL3-KO cells was about 17% of its expression in WT U87 cells.

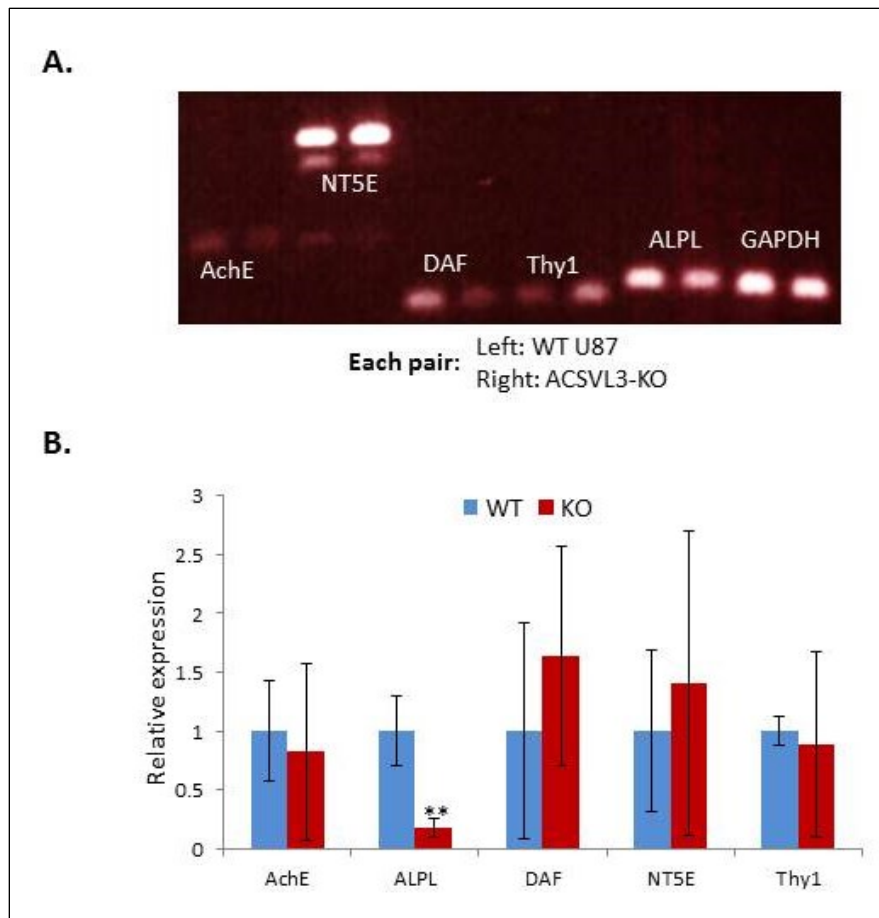


Figure 17: Expression of GPI-anchored proteins in WT and ACSVL3-KO U87 cells

A. PCR was performed using cDNA derived from mRNA extracted from WT and ACSVL3-KO U87 cells. Transcripts of GPI-anchored proteins commonly found in cancer were detected in both cell lines. B. Expression levels of mRNA transcripts of GPI-anchored proteins were compared between WT and ACSVL3-KO U87 cells. Levels were determined to be the same in all proteins except ALPL. Expression of ALPL transcripts in ACSVL3-KO U87 cells was approximately 17% of expression in WT U87 cells (n = 3 for each cell line, p < 0.01).

Characterization of PI-PLC purification

Figure 18a shows the results of the induction of PI-PLC in transformed *E. coli*. The most prominent band in the IPTG-induced total protein lane is approximately the expected size of PI-PLC (29 kDa) and thus is most likely induced PI-PLC. When the

bacteria were lysed to release the expressed protein, PI-PLC was located in Supernatant 1. Therefore, Supernatant 1 was purified using anion-exchange column chromatography. Bound protein was eluted with a salt gradient.

Figure 18b shows the input and output of the column. The first wash has a large band at the expected size for PI-PLC, meaning the column may have been overloaded and not able to trap all of the PI-PLC. However, it appears that significant PI-PLC was retained by the column, since it eluted later in several of the collected fractions. Some PI-PLC was visible via Coomassie Blue staining in fractions 5-16. The fractions with the most PI-PLC, 9-13, were pooled, concentrated, and used for the digestion of GPI anchors.

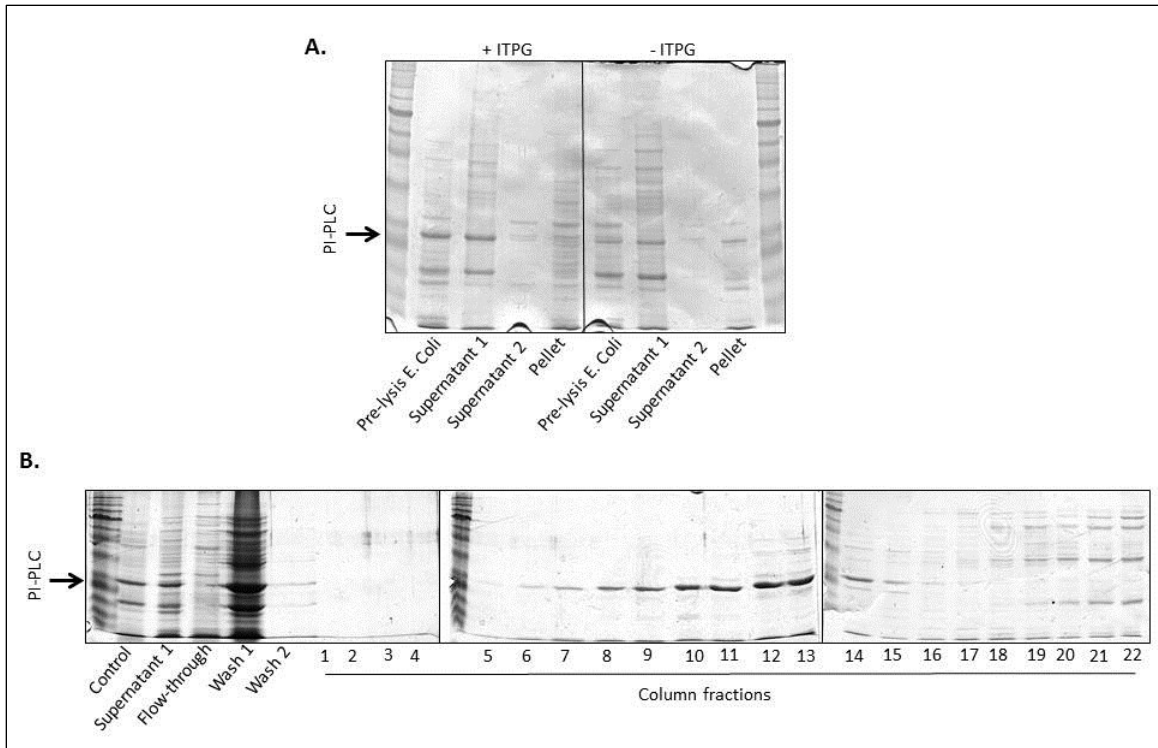


Figure 18: Expression and purification of PI-PLC from *E. coli*

A. *E. coli* expressing an inducible plasmid containing PI-PLC were grown in LB medium. PI-PLC expression was induced in one of the cultures with IPTG. Bacteria were lysed, and proteins were separated with SDS-PAGE and stained with Coomassie Blue. Induction of PI-PLC expression was successful. PI-PLC was found mainly in Supernatant 1 of the lysis procedure. B. PI-PLC was purified from Supernatant 1 using anion-exchange chromatography. Samples from the input, flow through, column washes, and collected fractions are shown. Proteins were again separated with SDS-PAGE and stained with Coomassie Blue. Although some PI-PLC was lost during the column wash, much of it bound to the column and eluted in fractions 9-14.

Purified PI-PLC is enzymatically active

In order to determine if the purified PI-PLC is enzymatically active, release of the abundant GPI-anchored protein acetylcholinesterase (AChE) from erythrocyte membranes was measured. The rationale is that PI-PLC purified from *E. coli* will release AChE from erythrocyte membranes, and then after the membranes are removed a modified Ellman assay can be performed to determine how much AChE was released, and thus how active

the PI-PLC is. The Ellman assay measures AchE activity by measuring the conversion of one of its substrates, acetylthiocholine, to thiocholine (Ellman *et al.*, 1961). Thiocholine reacts with DTNB in the assay to produce a yellow color that absorbs at 412 nm.

Erythrocyte membranes were prepared from frozen, centrifuged red blood cells. To determine the relative activity of AchE found on the blood cell membranes, varying amounts of membranes were added to Ellman assays (Figure 19a). A 3-fold dilution of the membrane preparation caused the increase in absorbance to level out quickly, indicating that the acetylthiocholine had all been quickly converted; this revealed the upper limit and thus the useful range of the Ellman assay. 30-fold and 300-fold dilutions of the membrane preparation in the Ellman assay provided the desired linear increase in absorbances. However, the 300-fold dilution provided a very slow increase, so the 30-fold dilution was selected to use in the modified Ellman assays coupled to PI-PLC activity.

Membrane dilutions were incubated with solutions that contain PI-PLC: Supernatant 1 from the *E. coli* lysis, Wash 1 from the purification column, and Fraction 13 from the purification column. Each of these was determined by Coomassie staining to have a high level of PI-PLC. Supernatant 1 and Wash 1 appeared to have more total PI-PLC, but Fraction 13 was more purified. After the membrane dilutions were incubated in the solutions containing PI-PLC, the membranes were filtered out of solution so that only AchE that had been cleaved off of the membranes remained. Next, acetylthiocholine and DTNB were added to the solutions, and absorbance was recorded. An Ellman assay containing the same amount of membranes was performed as a positive control of the maximum expected AchE activity. Of the solutions containing PI-PLC, Fraction 13

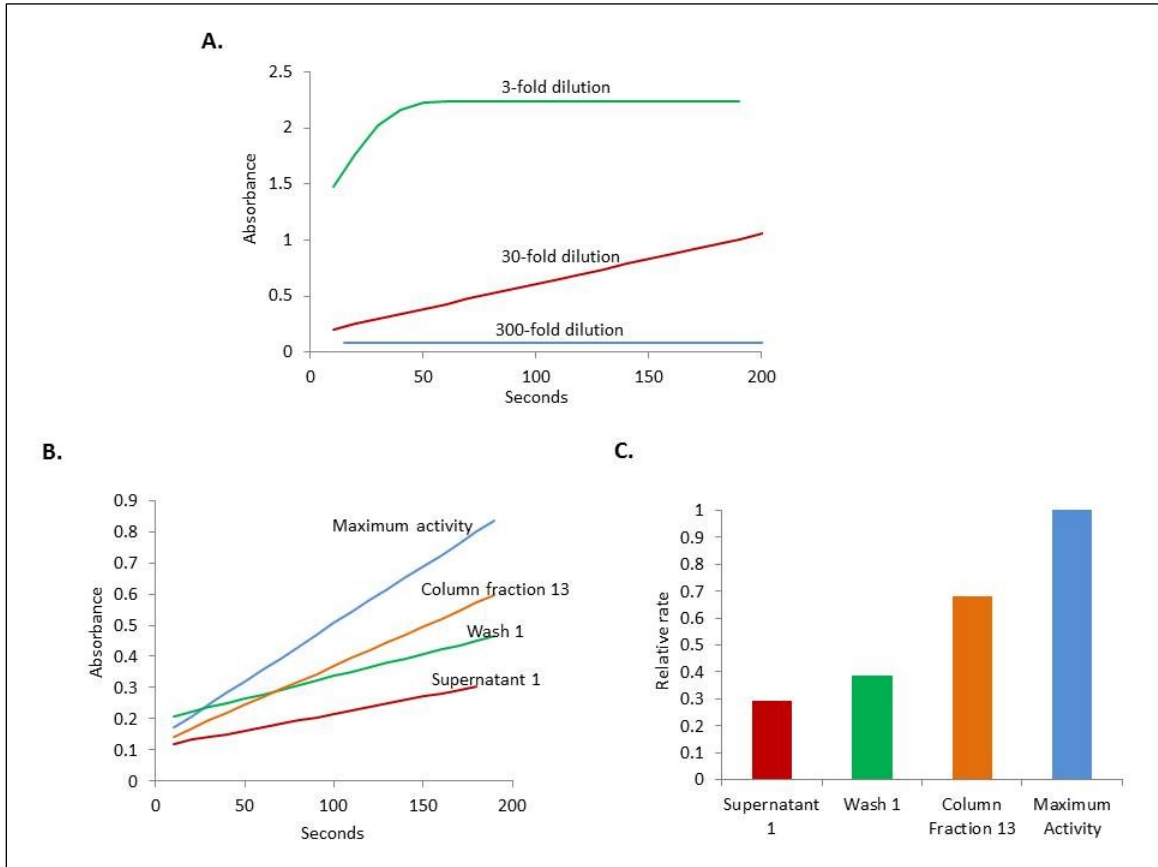
cleaved the most GPI anchors as determined by AchE activity (Figure 19b). However, all solutions exhibited AchE activity and are therefore inferred to have PI-PLC activity.

Figure 19c compares relative rates of AchE activity between the solutions.

Figure 19: Assessment of purified PI-PLC activity using the Ellman assay

A. Erythrocyte membranes were used as a source of AchE in Ellman assays, which measure the conversion of acetylthiocholine to thiocholine by AchE. Three different dilutions of an erythrocyte membrane preparation were compared in order to determine the ideal amount to use in the modified Ellman assays coupled to PI-PLC digestion. A 3-fold dilution quickly converted all the acetylthiocholine and revealed the upper limit of the Ellman assay. 30- and 300-fold dilutions provided the desired linear increase in absorbance, but the 300-fold dilution provided a very slow increase in absorbance. Thus, modified Ellman assays coupled to PI-PLC digestion used a 30-fold dilution of erythrocyte membranes. B. Modified Ellman assays were performed by using PI-PLC to cleave AchE from erythrocyte membranes, then removing membranes by filtration and using released AchE in an Ellman assay. Erythrocyte membranes were incubated with solutions from the purification process that were shown to contain PI-PLC by Coomassie staining: Supernatant 1 from the lysis process, Wash 1 of the anion-exchange column, and Fraction 13 from the column. Membranes were removed by filtration, and then aliquots from these solutions were added to Ellman assays. The slopes of the increases in absorbance represent the rate of conversion of acetylthiocholine, which is determined by the amount of AchE in the assay. In turn, the amount of AchE in the assay is determined by the amount cleaved by PI-PLC during the incubation with erythrocyte membranes. Therefore, the slopes of the increase in absorbance in the modified Ellman assay (shown in C) represent relative PI-PLC activity of the solutions incubated with erythrocyte membranes. Maximum activity was determined by including a traditional Ellman assay using the same amount of erythrocyte membranes, thus providing the maximum available AchE.

Figure 19



WT and ACSVL3-KO U87 cells have similar levels of proteins with GPI anchors

Total cellular protein from WT and ACSVL3-KO U87 cells was collected. Instead of collecting with trypsin, which could prematurely digest GPI-anchored proteins, cells were harvested by treating them with PBS containing no calcium or magnesium. Without these ions, the cells detached from the cell culture dishes while remaining intact. Total cellular proteins were separated by SDS-PAGE and were then transferred to PVDF membrane. PVDF membranes were incubated in purified PI-PLC. Following incubation, immunoblotting was performed with α -CRD primary antibody in order to detect cleaved GPI anchors. Several dilutions of PI-PLC were tested since the specific activity of the

purified, concentrated PI-PLC was unknown. A 1:50 dilution of PI-PLC was determined to be ideal, as incubation in this dilution resulted in several clear bands representing GPI-anchored proteins without excessive noise (Figure 20a). When several samples of WT and ACSVL3-KO U87 protein were ran simultaneously, there were no apparent differences between band patterns or intensities in the final Western blot (Figure 20b). Therefore, there do not appear to be differences in the amount of GPI-anchored proteins between WT and ACSVL3-KO U87 cells.

Ellman assays were also attempted using lysed WT U87 cells rather than erythrocyte membranes. Since U87 cells also express AchE, it was thought that they would also provide an increase in absorbance due to the production of thiocholine in an Ellman assay. The relative rates of the increases in absorbance could be used to compare GPI-anchored AchE levels between WT and ACSVL3-KO U87 cells. However, no recordable increase in absorbance occurred (data not shown).

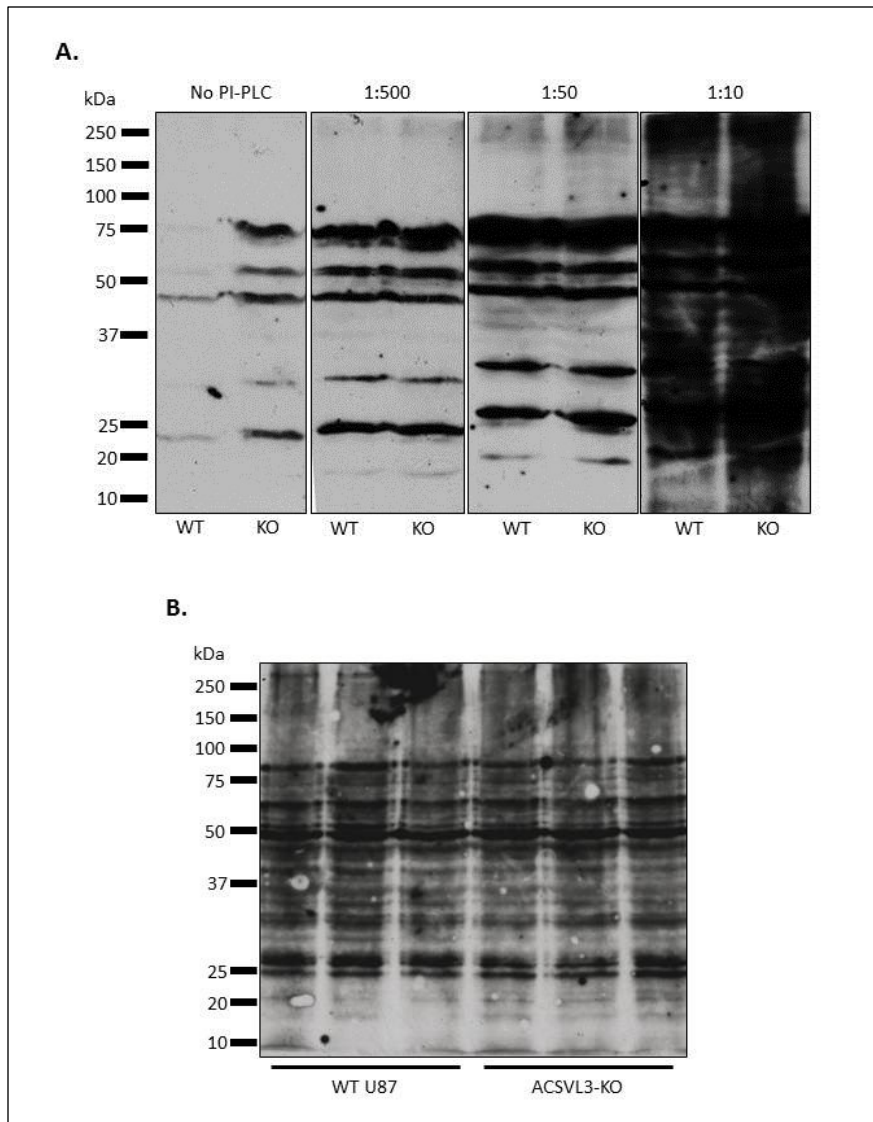


Figure 20: Detection of GPI-anchored proteins in WT and ACSVL3-KO U87 cells

A. Proteins from WT and ACSVL3-KO U87 cells were collected, separated by SDS-page, and transferred to PVDF. PVDF membranes were incubated in various dilutions of purified PI-PLC to cleave GPI anchors from proteins, revealing the CRD. CRDs were detected using Western blotting. A 1:50 dilution of PI-PLC was chosen to use in future on-membrane digestions. B. CRDs from proteins from triplicate WT and ACSVL3-KO cell samples were detected using Western blotting. No differences were seen between CRDs of WT and ACSVL3-KO U87 cells, indicating that there are likely not difference in levels of GPI-anchored proteins between the two cell lines.

Discussion

U87 cells express several GPI-anchored proteins commonly found in cancer cells. Since GPI anchors are synthesized from the phospholipids PI and PE, and both of these are synthesized at a lower rate in ACSVL3-KO U87 cells compared to WT U87 cells, we hypothesized that GPI anchors would also be synthesized at a lower rate in ACSVL3-KO compared to WT U87 cells.

Expression of several GPI-anchored proteins was evaluated by using qPCR to compare levels of mRNA. For most of the proteins, mRNA levels were similar between WT and ACSVL3-KO U87 cells. It was important to compare mRNA expression for two reasons: first, to determine if GPI anchors were likely to be found in U87 cells, and second, to ensure that differences in GPI anchor levels between WT and ACSVL3-KO U87 cells was not due to different gene expression between the cell lines. It would also be important to ensure that differences between GPI anchor levels were not due to differences in protein expression. Western blotting or immunofluorescence could be used to compare protein expression levels, and immunofluorescence could also be used to determine if the proteins were localized to the plasma membrane, as would be expected with GPI-anchored proteins. Since no differences were found between GPI anchor levels in WT and ACSVL3-KO U87 cells, these experiments were not performed.

The one commonly GPI-anchored protein that had a difference in mRNA expression between WT and ACSVL3-KO U87 cells was ALPL, which was about 5 times more abundant in WT U87 cells. Consistent with this finding, recent research shows that ALPL is upregulated in some aggressive, treatment-resistant glioblastomas

(Iwadate *et al.*, 2017). ACSVL3-KO cells are, by many measures, less tumorigenic than their WT counterparts, and the lower level of ALPL reflects this phenotype. ALPL is the tissue nonspecific (also called liver/bone/kidney) isoform of alkaline phosphatase, but there are two other isoforms: intestinal (ALPI) and placental (ALPP). Future directions include comparing mRNA levels of these isoforms as well.

Purified PI-PLC is commercially available. However, it is sold in small quantities and seemed to quickly diminish in activity, so we decided to express, purify, and use fresh PI-PLC. The enzyme was expressed in *E. coli*, released by lysis of the bacteria, and purified using anion-exchange chromatography on Q-sepharose. PI-PLC expression was assessed at several points of the purification process using Coomassie Blue staining, and enzyme activity was assessed using a modified Ellman assay. This assay uses PI-PLC to cleave the GPI anchors of AchE expressed on erythrocyte membranes, releasing AchE into solution. Next, this solution is added to the colorimetric Ellman assay, which measures AchE activity. More active PI-PLC will release more AchE, which will lead to a higher rate of activity in the Ellman assay.

The fractions from the purification process that contained putative PI-PLC protein by molecular size on gels were found to be enzymatically active in the modified Ellman assay. The first supernatant from the bacterial lysis, the first wash of the column, and a fraction from the column that was enriched in a 29 kDa protein were each tested. The supernatant and column wash had more total PI-PLC than the column fraction, but the column fraction had the most PI-PLC activity. This may have been because other proteins in the supernatant and wash interfered with PI-PLC or AchE activity, and purification removed most of the natural inhibitors.

The Ellman assays were attempted with WT U87 cells rather than erythrocyte membranes. No increase in absorbance was recorded, indicating that the level of AchE in U87 cells is too low to be detected by this assay. This is consistent with the relatively low levels of AchE detected in U87 cells via PCR.

The purification of active PI-PLC was successful, and this enzyme was used to digest GPI anchors on protein collected from WT and ACSVL3-KO U87 cells. Total cell protein was collected by treating cells with PBS without calcium and magnesium rather than trypsin to preserve the GPI-anchored proteins. Protein was transferred to PVDF, which was treated with our purified PI-PLC to digest GPI anchors. Finally, the digested anchors were detected with α -CRD antibody. There were no apparent differences between levels of GPI anchors in WT and ACSVL3-KO U87 cells. This was surprising, since two lipid components required to synthesize GPI anchors, PI and PE, were synthesized at a lower rate in ACSVL3-KO U87 cells compared to WT U87 cells. This may be because GPI anchors occur at a relatively low abundance compared to other post-translational modifications. Even with the lower rates of lipid synthesis, cells may be able to compensate easily. Furthermore, while turnover of GPI anchors occurs by a variety of mechanisms and at varying rates, some GPI-anchored proteins, such as Thy-1, turnover very slowly (Censullo and Davitz, 1994). In the cases of proteins with very slow rates of turnover, the lower rates of lipid synthesis would probably matter little.

Chapter 3: Protein Acylation in WT and ACSVL3-KO U87

cells

Introduction

The covalent attachment of fatty acids to proteins, or acylation, is a post-translational modification that serves many purposes, including regulating trafficking and subcellular location, allowing binding to lipid membranes, and facilitating protein-protein interactions. While acylation can occur with fatty acids from 8 to 20 carbons long, the long-chain fatty acids myristic and palmitic acids are the most commonly attached fatty acids (Resh, 2016). Both the mechanism of acylation and the properties conferred to the acylated protein are unique to each fatty acid.

Palmitoylation is most commonly the thioesterification of palmitic acid to the side chain of cysteine, although occasionally it is an amidation of palmitic acid to the side chain of lysine (Resh, 2012). This process required palmitoyl-CoA and is a reversible modification. Several hundred proteins are known to be palmitoylated (Resh, 2016). The enzyme family that attaches the palmitoyl-CoA to the protein is called the DHHC (Asp-His-His-Cys) family, a group of acyltransferases named after their shared sequence (Greaves and Chamberlain, 2010). Palmitoylation has been shown to be critical for protein trafficking, membrane anchoring, and lipid raft association. Abnormalities in several of the 23 human DHHC proteins have been associated with tumorigenesis, with members acting as either tumor suppressors or oncogenes (Yeste-Velasco *et al.*, 2015).

We chose to study palmitoylation in WT and ACSVL3-KO U87 cells because of its abundance and links to tumorigenesis. However, we also chose to study a much less well understood form of acylation, stearoylation, since stearate is preferentially and robustly activated by ACSVL3 (Chapter 1). Like palmitate, stearate is also attached to cysteine via a thioester linkage (Liang *et al.*, 2002) and is hypothesized to also be attached by DHHC enzymes (Resh, 2016). A recent study showed that stearoylation of transferrin receptor 1 induces mitochondrial fusion, and providing cells with palmitate instead of stearate did not lead to mitochondrial fusion (Senyilmaz *et al.*, 2015). This suggests that stearoylation is not simply a substitute for palmitoylation, but confers its own distinct properties to proteins to which it is attached.

A new tool to study protein acylation is click chemistry. Click chemistry is the name given to the copper-catalyzed cycloaddition of an azide group to a terminal alkyne, allowing two molecules bearing these groups to be covalently linked (Rostovtsev *et al.*, 2002). Click chemistry-compatible probes have been developed to study fatty acylation (Hannoush, 2011). These are fatty acids have the same number of carbons and saturation as their naturally-occurring counterparts, except for a ω -alkyne bond. These probes can be added to cell culture media, where they are taken up by cells and used in protein acylation. After harvesting protein from cells, acylated proteins can be detected by using the click reaction. Biotin azide can be used to detect acylated proteins on a membrane using streptavidin-HRP, or rhodamine azide can be used to detect acylated proteins via in-gel fluorescence. In this study, we used ω -alkynyl-palmitate and ω -alkynyl-stearate to study palmitoylation and stearoylation in WT and ACSVL3-KO U87 cells.

Knockdown of ACSVL3 disrupts Akt signaling in glioma cells (Pei *et al.*, 2009). Less phosphorylated Akt was detected in response to HGF stimulation when ACSVL3 was knocked down in U87 cells. These cells also grew more slowly and were less tumorigenic, which correlates with the knowledge that Akt signaling promotes cell proliferation and survival. One of the kinases inhibited downstream by Akt signaling, glycogen synthase kinase 3 (GSK3), promotes degradation of sterol regulatory element-binding proteins (SREBPs). SREBPs promote fatty acid uptake and biosynthesis, so Akt signaling has a positive effect on lipid production (Sundqvist *et al.*, 2005). Our lab has demonstrated that ACSVL3 knockdown in U87 cells leads to reduced production of some sterols and phospholipids (Kolar, 2016). We hypothesized that Akt signaling might also have a positive effect on protein acylation, and that knock out of ACSVL3 would diminish any positive effects induced by Akt.

In this study, we demonstrated that knockout of ACSVL3 in U87 cells has little effect on palmitoylation but does affect stearoylation. We used mass spectrometry to characterize some of the changes in stearoylation induced by ACSVL3 knockout. Finally, we used EGF to stimulate Akt in WT and ACSVL3-KO U87 cells, and showed that, at least over a short time period, this had no effect on protein stearoylation.

Materials and Methods

Immunoblot-like analysis of protein acylation using ω -alkynyl fatty acid probes

This procedure was modified from the protocols of Rami Hannoush (2011).

Preparation of click chemistry probes: 50 mM stock solutions were made of each ω -alkynyl-fatty acid probe in DMSO. The stocks were aliquoted and frozen at -80°C until used.

Cell culture: WT and ACSVL3-KO U87 cells were cultured as described in Chapter 1. Cells were seeded into 6-well plates in duplicate or triplicate wells and allowed to grow to confluence.

Preparation of cell culture media with click chemistry probes: Serum-free DMEM containing 5% fatty acid free BSA was prepared. The media was sonicated at 37°C in a water bath type sonicator until all BSA was dissolved and filtered for sterilization. Click chemistry probes were diluted to $100\ \mu\text{M}$ in DMEM + 5% BSA. (The equivalent volume of DMSO was diluted into media as a negative control.) The media containing probes was sonicated for 15 minutes at 37°C in a water bath type sonicator and then allowed to rest at room temperature for 15 minutes.

Treatment of U87 cells with click chemistry probes: Culture media was aspirated from the cells. The cells were washed once with PBS and then treated with 1 mL of media containing click chemistry probes per well. Cells were incubated for 24 hours.

Collection of total cellular protein: Probe-containing media was aspirated from cells. Cells were washed three times with ice-cold PBS containing calcium and magnesium. Each well was then treated with $400\ \mu\text{L}$ of ice-cold lysis buffer comprised of 100 mM sodium phosphate, 150 mM NaCl, and 1 % Nonidet-P40, as well as fresh protease and phosphatase cocktails (Calbiochem). The wells were scraped with sterile cell scrapers, cell lysate was transferred to microcentrifuge tubes, and the lysates were incubated on a gentle shaker at 4°C for 1 hour. Next, the lysates were centrifuged at

16,000g for 10 minutes at 4°C. The supernatant was removed from the pellet (debris) and moved to Amicon Ultra 0.5 mL centrifugal filter units (30 kDa NMWL; Millipore Sigma). The filter units were centrifuged according to the manual instructions until the lysate volume was approximately 100 µL. Protein concentration was determined using the Pierce 660 nm Protein Assay (Thermo Fisher Scientific).

Cycloaddition/click reaction: An aliquot containing 20 µg of protein was placed in a microcentrifuge tube and lysis buffer was added to yield a total volume of 23 µL per sample. To each sample, the following reagents were added in the following order: 0.5 µL of 5 mM biotin-azide (BN₃), 0.5 µL of 50 mM freshly prepared tris(2-carboxyethyl)phosphine hydrochloride (TCEP) in H₂O, and 0.5 µL of 10 mM tris[(1-benzyl-1H-1,2,3-triazol-4-yl)methyl]amine (TBTA) in DMSO/t-butanol (1:4, v:v). The samples were vortexed for 5 seconds. Next, 0.5 µL of freshly prepared 50 mM CuSO₄ in PBS was added to each sample. Samples were vortexed again for 5 seconds, then incubated in the dark for 1 hour.

The reaction was stopped by adding 250 µL of ice cold acetone to each sample and vortexing. Samples were then left at -20°C for at least 2 hours to allow protein to precipitate. Finally, the samples were centrifuged at 16,000g for 10 minutes to form a protein pellet. The acetone was aspirated and the pellets were left to air dry (approximately 10 minutes).

Blotting: Pellets were resuspended in with agitation in 24 µL of lysis buffer and 6 µL of 5X SDS gel running buffer (described in Chapter 1, “Western blotting”). Samples were boiled for 5 minutes then separated using SDS-PAGE. Proteins were transferred to PVDF membrane as described in Chapter 1. The membrane was incubated for 1 hour in

10% milk in TBST to block, rinsed 3 times with TBST, and washed 5 times for 10 minutes in TBST. Next, the membrane was incubated in streptavidin-horseradish peroxidase (HRP) diluted 1:80,000 in TBST. Again the membrane was rinsed 3 times with TBST and washed 5 times for 10 minutes in TBST. Finally, the membrane was incubated in SuperSignal West Pico Chemiluminescent Substrate (Thermo Fisher Scientific) according to the reagent manual's instructions and exposed to film to detect signal.

Treatment of U87 cells with EGF

EGF treatment time course: WT and ACSVL3-KO U87 cells were seeded into 6-cm dishes and allowed to grow to confluency. Cell media was aspirated and replaced with media containing 0.1% FBS (low serum media) overnight to serum starve the cells prior to EGF treatment. Cells were then treated with low serum media with 0.2 mM epidermal growth factor (EGF) for 0, 0.5, 1, 2, or 24 hours. Cells were lysed with 150 μ L ice-cold radioimmunoprecipitation assay (RIPA) buffer (25 mM Tris-HCl pH 7.6, 150 mM NaCl, 1% NP-40, 1% sodium deoxycholate, and 0.1% SDS) with protease inhibitors (Calbiochem) and scraped to collect. Protein concentration was measured using the assay described by Lowry *et al.* (1951). 30 μ g of total protein from each sample was separated using SDS-PAGE. Western blotting was performed as described in Chapter 1 with the primary antibodies α -Akt, α -phospho-Akt (Ser473), and α -phospho-S6 (Ser240/244; all from Cell Signaling Technology). All antibodies are rabbit polyclonal antibodies diluted 1:1000 in milk solution. The secondary antibody was goat α -rabbit IgG-HRP (1:8000 dilution in milk solution).

Concurrent treatment of U87 cells with EGF and ω -alkynyl-stearic acid probe:

WT and ACSVL3-KO U87 cells were cultured and seeded into 6-well plates as described in the previous section. Once confluent, cells were serum-starved with low serum media for 1 hour. Next, this media was aspirated and replaced with DMEM containing 5% BSA, 100 μ M stearic acid probe, and 0.2 mM EGF. Cells were incubated for 2 hours. Cells were lysed, protein was collected, and the click reaction and blotting were performed as described in the previous section.

Mass spectrometry of stearylated proteins

Preparation of stearylated protein: Cells were seeded into 6-well plates and cultured as described previously. 5 wells each of WT and ACSVL3-KO U87 cells were set up, 4 replicates and one negative control for both cell lines. (The negative control cells were treated with media that did not contain the ω -alkynyl fatty acid probe). The cells were treated and collected as described previously. The click reaction was performed with 3 times the previously used volumes of all reagents (75 μ L instead of 25 μ L total), amounting to 43 μ g of protein per sample. Instead of stopping the reaction with acetone, the lysis buffer was exchanged to remove unreacted reagents. This was done by transferring the reaction volume to an Amicon Ultra 0.5 mL centrifugal filter unit (30 kDa NMWL; Millipore Sigma) and adding 250 μ L of lysis buffer. The filter units were centrifuged at 14,000g for approximately 5 minutes, or until the total volume in the unit was approximately 100 μ L. Next, 250 μ L of lysis buffer was again added to the column, and the column was again centrifuged at 14,000g until approximately 100 μ L remained. This process was repeated a total of 5 times.

Precipitation and washing: After the buffer exchange, the lysates were moved from the filter units to microcentrifuge tubes. 200 μL of lysis buffer was added to each sample for a total volume of approximately 300 μL . 15 μL of streptavidin agarose resin slurry (Thermo Fisher Scientific) was added to each lysate. The samples were turned end-over-end for 1 hour at room temperature in order for the streptavidin beads to bind with biotinylated proteins. Afterwards, the beads and lysate were transferred to Ultrafree-MC 0.45 μm filter units (Millipore Sigma). The tubes were centrifuged at 12,000g to separate lysate from the beads. 300 μL of 100 mM sodium phosphate with 150 mM NaCl (the same composition as lysis buffer without detergent) was added to the beads to wash away unbound proteins. The filter units were agitated gently to mix, and then centrifuged at 12,000g for 1 minute. This process was repeated for 5 total washes. After the final wash, the beads were resuspended in 200 μL 100 mM sodium phosphate/150 mM NaCl and transferred to microcentrifuge tubes. The tubes were centrifuged for 1 minute and excess buffer was aspirated. Just enough buffer was left so the beads would not dry out. The samples were frozen at -80°C until mass spectrometry analysis.

Preparation of peptides for mass spectrometry: Beads were prepared, proteins were digested, and mass spectrometry was performed by the Johns Hopkins Mass Spectrometry and Proteomics Core directed by Robert N. Cole, PhD. The pH of the beads in buffer was adjusted by adding 2 μL 500mM triethylammonium bicarbonate (TEAB) to each sample. Proteins were reduced by treating each sample with 2 μL of iTRAQ TCEP (SCIEX) and incubating at 60°C for 1 hour, then alkylated by incubating each sample with 1 μL of methyl methanethiosulfonate for 15 min at room temperature. To remove any proteins pulled down due to protein-protein interactions from the beads,

the following wash was performed to each set of beads 3 times: 40 μ L of 50 mM TEAB was added to each sample, the beads were centrifuged briefly, and supernatant was discarded. To digest proteins remaining on the beads, beads were incubated overnight at 37°C with 800 ng of trypsin in 50mM TEAB. Peptides were collected by washing each set of beads 3 times with 100 μ L of 50% acetonitrile/0.1% trifluoroacetic acid (TFA), saving and combining the supernatants from each wash. Each sample was dried down and then reconstituted in 30 μ L TEAB. Each sample was labeled with 2.5 μ L of Tandem Mass Tag (TMT) 10-plex (Thermo Fisher Scientific), split into 2 aliquots, and dried. One aliquot from each sample was fractionated using basic reversed-phase peptide fractionation using Oasis PRiME HLB 96-well plates (Waters). To perform this fractionation, the samples were resolubilized 3 times in 150 μ L 0.1% TFA and loaded onto the plates, then eluted with 10mM TEAB containing the following increasing percentages of acetonitrile: 5%, 15%, 20%, 30%, 75%. The fractions were split into two, and one half of each fraction was dried and reconstituted in 20 μ L 2% acetonitrile/0.1 % TFA. 5 μ L of each reconstituted fraction was used for liquid chromatography-tandem mass spectrometry (LC-MS/MS) analysis.

Liquid chromatography-tandem mass spectrometry (LC-MS/MS) analysis:

Samples were analyzed by tandem MS using a nano-LC-Orbitrap-Fusion in FTFT (Thermo Fisher Scientific) interfaced with Easy-LC system (Waters). The LC component used reversed-phase chromatography (2%-90% acetonitrile/0.1% FA gradient over 105 min at 300 nl/min) on 75 μ m x 150 mm ProntoSIL C18-EPS (particle size 5 μ m) columns (BISCHOFF). Eluted proteins were sprayed into the mass spectrometer through a 1 μ m emitter tip (New Objective) at 2.0 kV. Survey scans were acquired on the Orbitrap from

380-1700 Da m/z using data-dependent acquisition with a Top15 method with a dynamic exclusion time of 30 seconds. Precursor ions were individually isolated with 1.0 Dalton window, then fragmented using higher-energy collisional dissociation (HCD) fragmentation using a normalized collision energy of 35%. Precursor and HCD fragmentation ions were analyzed at resolution settings of 60,000 and 120,000. The AGC target value was set to 3×10^6 at a maximum ion accumulation time of 50 ms.

Data analysis: Spectra were processed in Proteome Discoverer version 2.2 (Thermo Fisher Scientific) using 2Nodes by both common processing and Xtract. When using Xtract, spectra are extracted, charge state deconvoluted, and deisotoped at a resolution of 85K at 400 Da. MS/MS spectra from 2Nodes were analyzed with Mascot Server version 2.5.1. (Matrix Science) using 2015RefSeq_72r_human_plus (with added enzyme and BSA for quality control) with the following specifications: all species, trypsin as the enzyme, 2 allowed missed cleavage sites, precursor mass tolerance of 10 ppm, fragment mass tolerance of 0.02 Da, methylthio groups attached to cysteine, TMT 6-plex attached to N-termini, and the variable modifications of oxidation of methionine, deamidation of N and Q, and TMT 6-plex attached to lysine. Peptide identifications from Mascot searches were processed within Proteome Discoverer version 2.2 using Target Decoy Peptide-Spectrum Match Validator both to identify peptides with a confidence threshold 1% False Discovery Rate based on a concatenated decoy database search and to calculate the protein and peptide ratios. The following settings were used in the Reporter Ions Quantifier Node: the normalization mode “Total Peptide Amount”, the scaling mode “On All Average”, the ratio calculation “Summed Abundance Based”, and the ANOVA hypothesis test (individual proteins).

Results

Protein palmitoylation is similar between WT and ACSVL3-KO U87 cells, but stearoylation is reduced in ACSVL3-KO U87 cells

The products of the acyl-CoA synthetase reaction catalyzed by ACSVL3 can generate substrates such as palmitoyl-CoA and stearoyl-CoA that can potentially acylate proteins. To assess this possibility, we examined the differences in protein palmitoylation and protein stearoylation in WT U87 glioma cells and cells lacking ACSVL3. Terminal-alkyne palmitate and stearate were added to cell media and allowed to incorporate into WT and ACSVL3-KO U87 cells. Cell protein was collected and was used in a “click” reaction, which is a copper-catalyzed cycloaddition of azide- and alkyne-bearing molecules. In this case, the terminal-alkyne fatty acids reacted with biotin azide so that following the reaction, palmitoylated or stearoylated proteins are then biotinylated. After the reaction, proteins were separated by SDS-PAGE and transferred to PVDF. To detect acylated proteins, a technique similar to a Western blot was used. Instead of antibodies, PVDF membranes were incubated in a solution containing streptavidin-HRP. The streptavidin bound to the biotinylated (and therefore acylated) proteins, and HRP catalyzed a chemiluminescent signal used to visualize acylated protein bands. This process is illustrated in Figure 21a.

Using this technique, the palmitoylation profiles of WT and ACSVL3-KO U87 cells appear very similar (Figure 21b). However, the stearoylation profiles of the 2 cell lines are different. In general, protein stearoylation appears reduced in ACSVL3-KO U87 cells

compared to WT U87 cells (Figure 21c). However, when comparing proteins band-by-band, some appear to have increased intensity and some appear to have decreased intensity, suggesting that stearylation changes in ACSVL3-KO U87 cells compared to WT U87 cells are complex and vary from protein-to-protein.

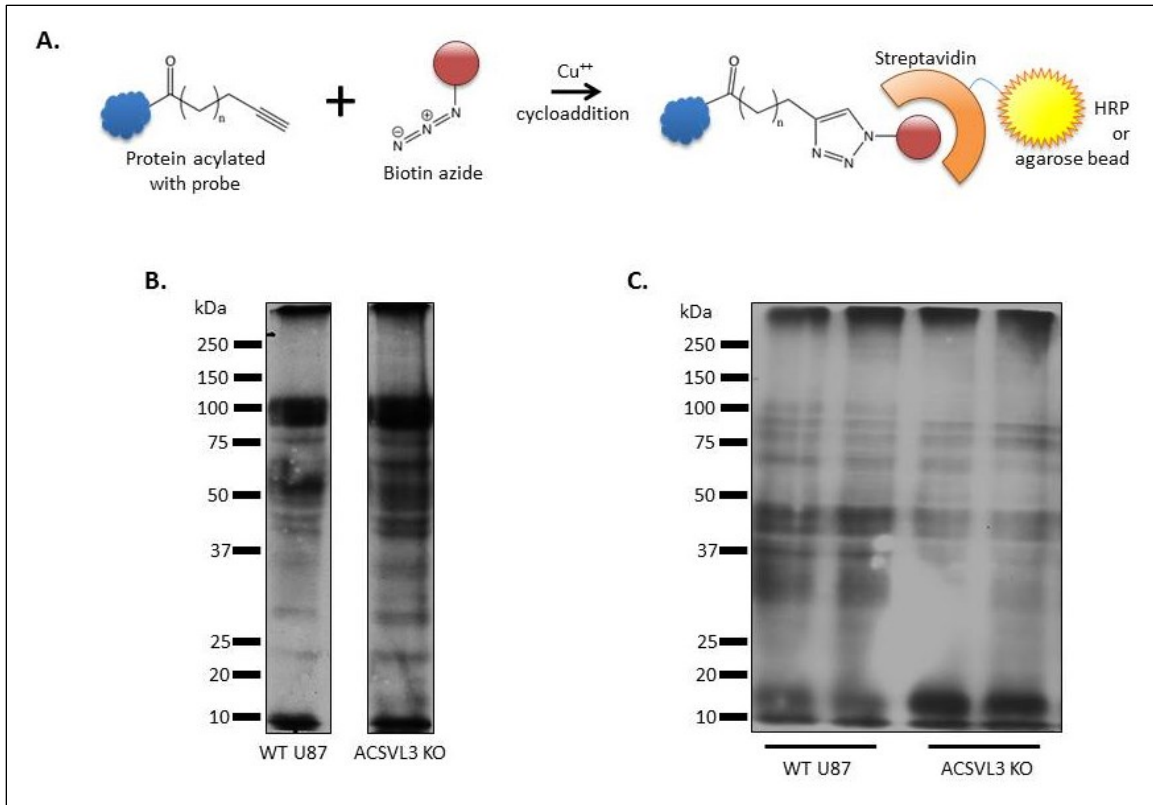


Figure 21: Detection of acylated proteins in WT and ACSVL3-KO U87 cells

A. Illustration of the click chemistry reaction. Cellular proteins are acylated by culturing cells in the presence of terminal alkyne probes (ω -alkynyl-fatty acids). Cells are lysed and protein is collected and used in the click reaction with biotin azide. The azide group in biotin azide reacts with the terminal alkyne of acylated proteins through a cycloaddition, thus linking biotin to acylated proteins. These proteins can be detected on a membrane using streptavidin-HRP or pulled down using streptavidin-linked agarose beads. B. Palmitoylation of proteins from WT and ACSVL3-KO U87 cells was detected with streptavidin-HRP. The palmitoylation pattern appears very similar between the cell lines. C. Stearoylation of proteins from WT and ACSVL3-KO U87 cells were detected in the same manner. There appear to be many differences between the two cell lines. Overall, stearoylation appears decreased in ACSVL3-KO cells, but stearoylation of some proteins appear increased and others decreased between the cell lines.

Akt signaling in WT U87 cells responds similarly to EGF as to HGF

Previously published data showed that when U87 cells were treated with HGF, phospho-Akt (pAkt) levels rose over the next few hours, peaking around 2 hours, and

remained elevated after 24 hours (Pei *et al.*, 2009). Total Akt varied slightly, but not as dramatically, over the same time frame. To determine if EGF would have similar effects on WT U87 cells, cells were treated for most of the same time points, and pAkt and total Akt levels were assessed by Western blots. The blots revealed a similar rise in pAkt levels over the course of 2 hours (Figure 22). At 24 hours, the pAkt level had dropped from its level at the 2-hour time point, but remained elevated over its initial, pre-EGF treatment level. (In fact, the pAkt level prior to EGF treatment was undetectable on this Western blot.) Total Akt also rose somewhat over the first 2 hours of EGF treatment, and appeared to have returned to its pre-EGF treatment level by 24 hours. In general, EGF had a similar, excitatory effect on WT U87 cells as HGF.

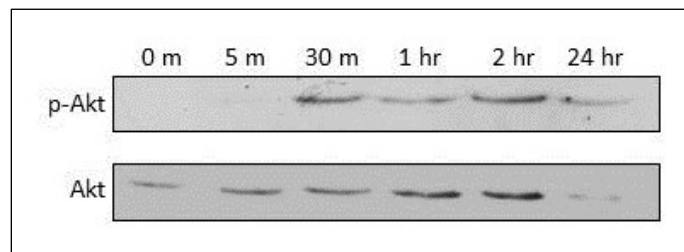


Figure 22: Activation of Akt by EGF in U87 cells

Phosphorylation of Akt (p-Akt) was seen after the addition of EGF to U87 cells, peaking 2 hours after EGF treatment, and remaining slightly elevated after 24 hours. Total Akt also rose, but not as dramatically. Akt signaling in U87 cells responds similarly to EGF treatment as it does to HGF treatment.

Akt signaling in response to EGF is disrupted in ACSVL3-KO cells

When ACSVL3 was knocked down using RNAi, pAkt did not increase in response to HGF. It decreased over 2 hours and then returned to approximately initial levels by 24 hours (Pei *et al.*, 2009). To determine if ACSVL3-KO U87 cells respond similarly to EGF treatment, both WT and ACSVL3-KO cells were treated with EGF.

Cells were collected at 3 time point: 0, 0.5, and 2 hours. As expected, pAkt rose over the time points in WT U87 cells. (Figure 23) Although there is high background on the Western blot, pAkt did not appear to rise over the time points in ACSVL3-KO U87 cells. This indicates that, as expected, the knockout of ACSVL3 disrupts EGF-incited Akt signaling in U87 cells.

Since S6K is activated in response to Akt signaling in glioblastomas (Riemenschneider *et al.*, 2006), phosphorylated S6 was also detected in WT and ACSVL3-KO U87 cells using Western blotting. Its level rose over the time points in both cell lines, although it appeared to rise more dramatically in WT U87 cells than in ACSVL3-KO cells.

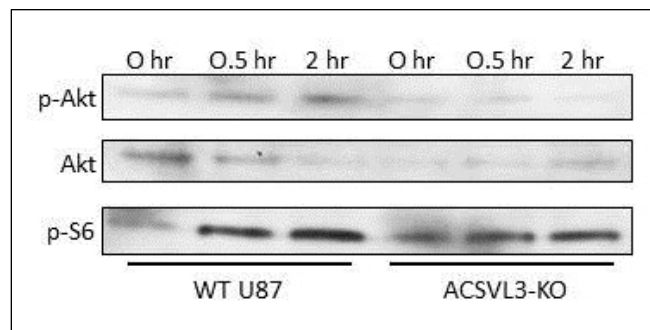


Figure 23: Comparison of activation of Akt by EGF in WT and ACSVL3-KO U87 cells

Phosphorylation of Akt (p-Akt) rose over 2 hours after EGF treatment in WT U87 cells, but not in ACSVL3-KO U87 cells. Phosphorylation of S6 (p-S6), a downstream target of the Akt signaling pathway, rose more dramatically in WT U87 cells than in ACSVL3-KO U87 cells. This data indicates that knockout of ACSVL3 disrupts EGF-induced Akt signaling.

EGF does not affect short-term protein stearylation in WT or ACSVL3-KO U87 cells

To determine if stearylation changed in response to Akt signaling, and to determine if stearylation would respond differently to Akt signaling in WT and

ACSVL3-KO U87 cells, both cell lines were treated concurrently with EGF and ω -alkynyl-stearate. Cells were collected after 2 hours, and stearylated proteins were detected using the streptavidin-HRP based, Western blot-like technique described earlier. Stearoylation did not appear to change in response to EGF in either WT or ACSVL3-KO U87 cells (Figure 24). Furthermore, there was no apparent difference in stearoylation between WT and ACSVL3-KO U87 cells that were not treated with EGF at this time point.

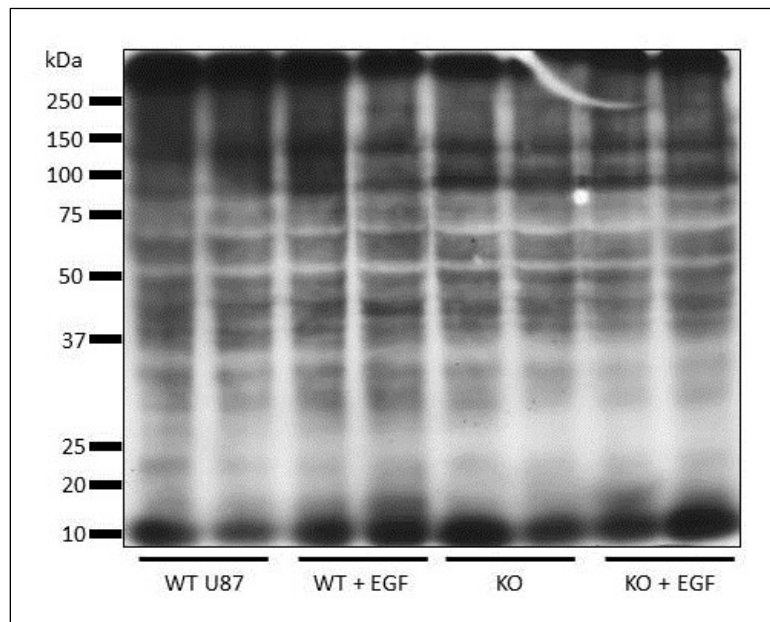


Figure 24: Stearoylation of proteins in WT and ACSVL3-KO U87 cells stimulated with EGF

WT and ACSVL3-KO U87 cells were treated simultaneously with ω -alkynyl-stearate and EGF for two hours. Stearoylation was evaluated by submitting proteins from each cell sample to the click reaction, separating proteins by SDS-PAGE, and detecting stearylated proteins with streptavidin-HRP. EGF did not appear to affect stearoylation of proteins in either cell line. Furthermore, stearoylation did not appear to differ between WT and ACSVL3-KO U87 cells in this experiment, indicating that the differences in stearoylation between the two cell lines arise between 2 and 24 hours of incubation with ω -alkynyl-stearate.

Upregulated and downregulated stearylation of proteins identified by mass spectrometry

Because of the complex variation of protein stearylation between WT and ACSVL3-KO U87 cells, mass spectrometry was used to identify specific stearylated proteins and quantify their amounts in both cell lines. WT and ACSVL3-KO U87 cells were treated with terminal-alkyne stearic acid. Protein was collected and used in click reactions to biotinylate stearylated proteins. These proteins were then pulled down using streptavidin agarose resin, then digested and subjected to mass spectrometry.

Nine stearylated proteins were identified as significantly more abundant in WT U87 cells than in ACSVL3-KO U87 cells ($p < 0.05$). Despite global stearylation appearing to be down regulated in ACSVL3-KO U87 cells compared to WT U87 cells, 37 stearylated proteins were identified as significantly more abundant in ACSVL3-KO U87 cells compared to WT U87 cells ($p < 0.05$). These proteins are listed in the tables below. Of all the proteins identified (over 1200), approximately the same number of proteins were upregulated and downregulated in ACSVL3-KO U87 cells compared to WT U87 cells if. A number of stearylated proteins were detected only in WT U87 cells and so relative abundance could not be calculated. However, these proteins may be of interest because they may be stearylated only in WT U87 cells.

In each of the tables below, proteins in bold were assigned high confidence by Mascot analysis. The second column lists the ratios of the abundances of stearylated proteins in WT vs ACSVL3-KO U87 cells. Mass spectrometry of stearylated proteins was cross-referenced with a total proteomic analysis described by Kolar (2016). The ratios of the abundances of total WT and ACSVL3-KO U87 proteins are listed in the

third column. Ratios in red represent ratios that showed upregulation in stearylolation, but downregulation in total protein. “ND” refers to proteins not detected in MS analysis.

Table 3 expresses the ratios as WT/KO, and Table 4 expresses the ratios as KO/WT.

Table 3: Stearoylated proteins more abundant in WT U87 cells vs. ACSVL3-KO U87 cells

Protein name (Symbol)	Abundance ratio: Stearoylated protein, WT/KO	Abundance ratio: Total protein, WT/KO
immortalization up-regulated protein (IMUP)	2.4	ND
plastin-3 isoform X1 (PLS3)	2.4	ND
heat shock 70 kDa protein 1A/1B (HSPA1A; HSPA1B)	2.1	0.7
14-3-3 protein zeta/delta isoform X1 (YWHAZ)	1.8	0.6
moesin isoform X1 (MSN)	1.8	ND
plasminogen activator inhibitor 2 (SERPINB2)	1.8	0.2
14-3-3 protein epsilon (YWHAE)	1.7	0.5
glutathione S-transferase P (GSTP1)	1.6	0.4
platelet-activating factor acetylhydrolase IB subunit beta isoform a (PAFAH1B2)	1.4	0.5

Table 4: Stearoylated proteins more abundant in ACSVL3-KO U87 cells vs. WT U87 cells

Protein name (Symbol)	Abundance ratio: Stearoylated protein, KO/WT	Abundance ratio: Total protein, KO/WT
CD81 antigen isoform 1 (CD81)	5.2	ND
transmembrane 4 L6 family member 1 (TM4SF1)	4.1	ND
CD9 antigen (CD9)	4.0	1.2
alpha-2-macroglobulin isoform X1 (A2M)	3.8	ND
CD59 glycoprotein preproprotein (CD59)	3.4	0.2
dnaJ homolog subfamily C member 5 isoform X1 (DNAJC5)	3.4	ND
poliovirus receptor isoform alpha precursor (PVR)	3.4	ND
SH3 domain-binding glutamic acid-rich-like protein 3 (SH3BGRL3)	3.4	2.1
7,8-dihydro-8-oxoguanine triphosphatase isoform p22 (NUDT1)	3.2	ND
tetraspanin-4 isoform X3 (TSPAN4)	3.1	0.5
5'-nucleotidase isoform 1 preproprotein (NT5E)	3.0	0.9
CD151 antigen (CD151)	3.0	0.4
integrin alpha-2 precursor (ITGA2)	3.0	1.3
reticulon-3 isoform X1 (RTN3)	2.9	ND
transgelin-2 isoform a (TAGLN2)	2.8	ND
nicastrin isoform 1 precursor (NCSTN)	2.7	ND
glycolipid transfer protein (GLTP)	2.7	ND
adenine phosphoribosyltransferase isoform a (APRT)	2.5	ND
bcl-2-like protein 1 isoform X1 (BCL2L1)	2.5	ND
transmembrane protein 109 precursor (TMEM109)	2.4	0.7

phospholipase D3 isoform X1 (PLD3)	2.3	1.9
B-cell receptor-associated protein 31 isoform a (BCAP31)	2.3	ND
transaldolase (TALDO1)	2.3	4.6
protein kish-A precursor (TMEM167A)	2.2	ND
astrocytic phosphoprotein PEA-15 isoform a (PEA15)	2.2	ND
ATP synthase subunit g, mitochondrial (ATP5L)	2.2	0.9
transmembrane protein 14C (TMEM14C)	2.1	0.8
ATP synthase F0 subunit 6, mitochondrial (ATP6)	2.1	0.6
ras-related protein Rab-14 (RAB14)	2.1	0.7
FUN14 domain-containing protein 2 (FUNDC2)	2.0	1.5
CAAX prenyl protease 1 homolog (ZMPSTE24)	1.9	1.1
voltage-dependent anion-selective channel protein 3 isoform 2 (VDAC3)	1.9	ND
p53 apoptosis effector related to PMP-22 (PERP)	1.9	ND
aspartate aminotransferase, cytoplasmic (GOT1)	1.8	2.9
cytosol aminopeptidase (LAP3)	1.8	1.2
ATP synthase subunit d, mitochondrial isoform a (ATP5H)	1.7	0.6
serpin A12 isoform X1 (SERPINA12)	1.5	ND

Discussion

The purpose of this study was to determine if ACSVL3 is involved in the acylation of proteins, as this approach might identify novel cancer targets. Because acylation requires the fatty acids to be activated by an acyl-CoA synthetase, we hypothesized that acylation of long-chain fatty acids would be reduced in ACSVL3-KO U87 cells compared to WT U87 cells. Furthermore, many of the DHHC enzymes, which catalyze the transfer of palmitoyl-CoA and likely stearoyl-CoA to cysteine residues within proteins, are implicated in tumorigenesis (Yeste-Velasco *et al.*, 2015). We hypothesized that changes in long chain acyl-CoA levels caused by upregulated ACSVL3 in tumor cells are tumor-promoting as well.

To study acylation in cell cultures, we used click chemistry-compatible probes: fatty acids identical to palmitic and stearic acid except for a terminal alkyne bond between the final two carbons (a ω -alkynyl bond). Using an alkyne group preserved the neutral, hydrophobic nature of the fatty acids and hopefully allowed them to be trafficked normal within the cells. However, the alkyne group also conferred reactivity to the fatty acids. After protein was collected, the click reaction, a cycloaddition of biotin azide and the alkyne group at the end of the fatty acids. This reaction biotinylated proteins that had been acylated in the cells, allowing them to be detected with streptavidin-HRP on a membrane or pulled down from a whole cell lysate using streptavidin beads.

First, we used a Western blot-like analysis to compare palmitoylation and stearoylation in WT and ACSVL3-KO U87 cells. Palmitoylation was not significantly changed, but stearoylation was. Overall, stearoylation was decreased in ACSVL3-KO

U87 cells compared to WT U87 cells, but it appeared that some proteins had increased stearoylation and others had decreased stearoylation when ACSVL3 was knocked out. The general trends aligned with our findings of the preferred substrates of ACSVL3, discussed in Chapter 1. Like palmitoylation, the activation of palmitic acid was not significantly reduced in ACSVL3-KO U87 cells, and like stearoylation, activation of stearic acid was reduced in ACSVL3-KO cells compared to WT U87 cells. The variation of protein stearoylation between WT and ACSVL3-KO U87 cells led us to use mass spectrometry to identify stearoylated proteins and determine which are upregulated and downregulated in response to ACSVL3 knock-out.

Consistent with the immunoblot-like data, some proteins appeared to have increased stearoylation and others appeared to have decreased stearoylation in ACSVL3-KO U87 cells compared to WT U87 cells as detected by mass spectrometry. However, while the immunoblot-like data suggested a global decline in stearoylation with ACSVL3 knockout, MS data revealed approximately equal numbers of upregulated and downregulated stearoylated proteins, and more statistically significant downregulated stearoylated proteins. As expected, many of the proteins identified that showed up- or down-regulated stearoylation also exhibited up- or down-regulation of total protein. However, a few proteins exhibited upregulated stearoylation with ACSVL3 knockout but a decrease in total protein, or, conversely, an increase in total protein but a decrease in stearoylation with ACSVL3 knockout. These proteins are targets of interest for future experiments. One interesting takeaway from the MS data is that three subunits of ATP synthase were stearoylated, and stearoylation of each was increased in ACSVL3-KO cells. Our lab has shown that knockout of ACSVL3 disrupts mitochondrial function, and

that ACSVL3-KO U87 cells have less ATP synthase than WT U87 cells (Kolar, 2016). Perhaps stearoylation is a negative regulator of ATP synthase, or somehow regulates its function.

We wanted to determine if Akt stimulation via EGF would affect stearoylation, but first we had to determine if EGF-stimulated Akt signaling was disrupted by ACSVL3 knockout. Previously, it was shown that Akt signaling through another receptor tyrosine kinase, c-Met, was disrupted with RNAi knockdown of ACSVL3 (Pei *et al.*, 2009). In those studies, Akt signaling was stimulated by the c-Met ligand, hepatocyte growth factor (HGF), so we demonstrated that EGF stimulation elicited a similar response in WT U87 cells. Next, we demonstrated that knockout of ACSVL3 had a similar effect on Akt signaling as stable knockdown of ACSVL3. The highest level of pAkt in WT U87 cells, and the biggest difference in pAkt levels between WT and ACSVL3-KO U87 cells, occurred at 2 hours after the addition of EGF. Based on this finding, we added stearate probes and EGF simultaneously and collected cell protein after 2 hours, and then used blotting to compare stearoylation of proteins from WT and ACSVL3-KO U87 cells both with and without EGF treatment. EGF treatment did not lead to differences in stearoylation in either cell line. However, this is not sufficient to conclude that EGF does not affect stearoylation. While Akt phosphorylation peaks at 2 hours after EGF treatment, protein acylation could peak later. Also, as discussed earlier, Akt upregulates *de novo* synthesis of lipids, and newly-synthesized fatty acids were used in acylation; the detection of click-compatible probes would not reflect this. Surprisingly, no differences in stearoylation were seen in the control (no EGF treatment) WT and ACSVL3-KO U87 cells after 2 hours. Since differences in stearoylation occurred after 24 hours of treatment,

a time course will be done to see when these differences arise. This will help determine the ideal length of treatment with EGF in future experiments.

A shortcoming of using blotting and mass spectrometry to assess levels of acylation is that changes in band intensity between samples could reflect not only changes in acylation, but also changes in protein level. While the same total amount of protein was loaded onto gels used for blotting, there is no way to control for individual protein levels. We know from independently obtained proteomic data that several proteins exhibit different expression levels between WT and ACSVL3-KO U87 cells (Kolar, 2016; unpublished data). When individual proteins are identified to have different levels of acylation between the two cell lines, protein level will be assessed as well, either by cross-referencing to proteomic data or by western blotting. However, acylation could affect protein level either positively (eg. by promoting stability) or negatively (eg. by targeting the protein for endocytosis and degradation). Therefore, the purpose of acylation of individual proteins must be studied as well, making this a very interesting and fruitful future direction.

References

- Allen, M., Bjerke, M., Edlund, H., Nelander, S., & Westermark, B. (2016). Origin of the U87MG glioma cell line: Good news and bad news. *Science Translational Medicine*, 8(354), 354re3-354re3. doi:10.1126/scitranslmed.aaf6853
- Baldassare, J. J., Henderson, P. A., & Fisher, G. J. (1989). Isolation and characterization of one soluble and two membrane-associated forms of phosphoinositide-specific phospholipase C from human platelets. *Biochemistry*, 28(14), 6010-6016. doi:10.1021/bi00440a043
- Barbosa, M., Rios, O., Velásquez, M., Villalobos, J., & Ehrmanns, J. (2001). Acetylcholinesterase and butyrylcholinesterase histochemical activities and tumor cell growth in several brain tumors. *Surgical Neurology*, 55(2), 106-112. doi:10.1016/s0090-3019(01)00351-2
- Berg, P. (1956). Acyl adenylates; an enzymatic mechanism of acetate activation. *Journal of Biological Chemistry*, 222(2), 991-1013. Retrieved from <http://www.jbc.org/>
- Black, P. B., DiRusso, C. C. (2006). U.S. Patent No. 7,070,944. Washington, DC: U.S. Patent and Trademark Office.
- Black, P. N., Zhang, Q., Weimar, J. D., & DiRusso, C. C. (1997). Mutational analysis of a fatty acyl-coenzyme A synthetase signature motif identifies seven amino acid residues that modulate fatty acid substrate specificity. *Journal of Biological Chemistry*, 272(8), 4896-4903. doi:10.1074/jbc.272.8.4896

Camarda, R., Zhou, A. Y., Kohnz, R. A., Balakrishnan, S., Mahieu, C., Anderton, B., ... Goga, A. (2016). Inhibition of fatty acid oxidation as a therapy for MYC-overexpressing triple-negative breast cancer. *Nature Medicine*, 22(4), 427-432. doi:10.1038/nm.4055

Cappellari, A. R., Vasques, G. J., Bavaresco, L., Braganhol, E., & Battastini, A. M. (2011). Involvement of ecto-5'-nucleotidase/CD73 in U138MG glioma cell adhesion. *Molecular and Cellular Biochemistry*, 359(1-2), 315-322. doi:10.1007/s11010-011-1025-9

Carlson, B. L., Pokorny, J. L., Schroeder, M. A., & Sarkaria, J. N. (2011). Establishment, Maintenance, and In Vitro and In Vivo Applications of Primary Human Glioblastoma Multiforme (GBM) Xenograft Models for Translational Biology Studies and Drug Discovery. *Current Protocols in Pharmacology*. doi:10.1002/0471141755.ph1416s2

Censullo, P., & Davitz, M. A. (1994). How GPI-anchored proteins turnover: or where do they go after arrival at the plasma membrane. *Seminars in Immunology*, 6(2), 81-88. doi:10.1006/smim.1994.1012

Cheng, M., Bhujwalla, Z. M., & Glunde, K. (2016). Targeting phospholipid metabolism in cancer. *Frontiers in Oncology*, 6. doi:10.3389/fonc.2016.00266

Coleman, D. T., Soung, Y. H., Surh, Y., Cardelli, J. A., & Chung, J. (2015). Curcumin prevents palmitoylation of integrin β 4 in breast cancer cells. *PLOS ONE*, 10(5), e0125399. doi:10.1371/journal.pone.0125399

Cui, M., Wang, Y., Sun, B., Xiao, Z., Ye, L., & Zhang, X. (2014). MiR-205 modulates abnormal lipid metabolism of hepatoma cells via targeting acyl-CoA synthetase long-

chain family member 1 (ACSL1) mRNA. *Biochemical and Biophysical Research Communications*, 444(2), 270-275. doi:10.1016/j.bbrc.2014.01.051

Dole, V. P. (1956). A relation between non-esterified fatty acids in plasma and the metabolism of glucose. *Journal of Clinical Investigation*, 35(2), 150-154.
doi:10.1172/jci103259

Durante, S., Orienti, I., Teti, G., Salvatore, V., Focaroli, S., Tesei, A., ... Falconi, M. (2014). Anti-tumor activity of fenretinide complexed with human serum albumin in lung cancer xenograft mouse model. *Oncotarget*, 5(13), 4811-4820.
doi:10.18632/oncotarget.2038

Eberlé, D., Hegarty, B., Bossard, P., Ferré, P., & Foufelle, F. (2004). SREBP transcription factors: master regulators of lipid homeostasis. *Biochimie*, 86(11), 839-848.
doi:10.1016/j.biochi.2004.09.018

Ellman, G. L., Courtney, K., Andres, V., & Featherstone, R. M. (1961). A new and rapid colorimetric determination of acetylcholinesterase activity. *Biochemical Pharmacology*, 7(2), 88-95. doi:10.1016/0006-2952(61)90145-9

Englund, P. T. (1988). PI-PLC assay on nitrocellulose filter immobilized proteins. In U. Brodbeck & C. Bordier (Eds.), *Post-translational modifications of proteins by lipids: A laboratory manual*. Berlin, Germany: Springer-Verlag.

Falcon, A., Doege, H., Fluitt, A., Tsang, B., Watson, N., Kay, M. A., & Stahl, A. (2010). FATP2 is a hepatic fatty acid transporter and peroxisomal very long-chain acyl-CoA

synthetase.AJP: Endocrinology and Metabolism, 299(3), E384-E393.

doi:10.1152/ajpendo.00226.2010

Folch, J., Lees, M., & Sloane Stanley, G. H. (1957). A simple method for the isolation and purification of total lipides from animal tissues. *Journal of Biological Chemistry*, 226(1), 497-509. Retrieved from <http://www.jbc.org/>

Fresno Vara, J. Á., Casado, E., De Castro, J., Cejas, P., Belda-Iniesta, C., & González-Barón, M. (2004). PI3K/Akt signalling pathway and cancer. *Cancer Treatment Reviews*, 30(2), 193-204. doi:10.1016/j.ctrv.2003.07.007

Gamage, D. G., & Hendrickson, T. L. (2013). GPI transamidase and GPI anchored proteins: Oncogenes and biomarkers for cancer. *Critical Reviews in Biochemistry and Molecular Biology*, 48(5), 446-464. doi:10.3109/10409238.2013.831024

Gassler, N., Schneider, A., Kopitz, J., Schnölzer, M., Obermüller, N., Kartenbeck, J., ... Autschbach, F. (2003). Impaired expression of Acyl-CoA-synthetase 5 in epithelial tumors of the small intestine. *Human Pathology*, 34(10), 1048-1052. doi:10.1053/s0046-8177(03)00431-3

Goujon, M., McWilliam, H., Li, W., Valentin, F., Squizzato, S., Paern, J., & Lopez, R. (2010). A new bioinformatics analysis tools framework at EMBL-EBI. *Nucleic Acids Research*, 38(Web Server), W695-W699. doi:10.1093/nar/gkq313

Greaves, J., & Chamberlain, L. (2010). S-acylation by the DHHC protein family. *Biochemical Society Transactions*, 38(2), 522-524. doi:10.1042/bst0380522

Hanahan, D. J., & Ekelund, J. E. (1974). The preparation of red cell ghosts (membranes). *Methods in Enzymology*, 168-172. doi:10.1016/0076-6879(74)31018-x

Hannoush, R. N. (2011). Development of chemical probes for biochemical detection and cellular imaging of myristoylated and palmitoylated proteins. *Current Protocols in Chemical Biology*. doi:10.1002/9780470559277.ch100143

Hu, C., Chen, L., Jiang, Y., Li, Y., & Wang, S. (2008). The effect of fatty acid-CoA ligase 4 on the growth of hepatic cancer cells. *Cancer Biology & Therapy*, 7(1), 131-134. doi:10.4161/cbt.7.1.5198

Iwadate, Y., Matsutani, T., Hirono, S., Shinozaki, N., & Saeki, N. (2016). Transforming growth factor- β and stem cell markers are highly expressed around necrotic areas in glioblastoma. *Journal of Neuro-Oncology*, 129(1), 101-107. doi:10.1007/s11060-016-2145-6

Iwadate, Y., Suganami, A., Tamura, Y., Matsutani, T., Hirono, S., Shinozaki, N., ... Saeki, N. (2017). The pluripotent stem-cell marker alkaline phosphatase is highly expressed in refractory glioblastoma with DNA hypomethylation. *Neurosurgery*, 80(2), 248-256. doi:10.1093/neuros/nyw026

Janardhan, S., Srivani, P., & Sastry, G. (2006). Choline kinase: an important target for cancer. *Current Medicinal Chemistry*, 13(10), 1169-1186. doi:10.2174/092986706776360923

- Jia, Z., Pei, Z., Maignel, D., Toomer, C. J., & Watkins, P. A. (2007). The fatty acid transport protein (FATP) family: very long chain acyl-CoA synthetases or solute carriers? *Journal of Molecular Neuroscience*, 33(1), 25-31. doi:10.1007/s12031-007-0038-z
- Jäger, K., Meyer, P., Stieger, S., & Brodbeck, U. (1990). Production and characterization of antibodies against the cross-reacting determinant of glycosyl-phosphatidylinositol-anchored acetylcholinesterase. *Biochimica et Biophysica Acta (BBA) - Protein Structure and Molecular Enzymology*, 1039(3), 367-373. doi:10.1016/0167-4838(90)90272-h
- Kapoor, G. S., & O'Rourke, D. M. (2003). Receptor tyrosine kinase signaling in gliomagenesis: pathobiology and therapeutic approaches. *Cancer Biology & Therapy*, 2(4), 330-342. doi:10.4161/cbt.2.4.507
- Kemshead, J. T., Ritter, M. A., Cotmore, S. F., & Greaves, M. F. (1982). Human Thy-1: expression on the cell surface of neuronal and glial cells. *Brain Research*, 236(2), 451-461. doi:10.1016/0006-8993(82)90727-2
- Kinoshita, T., & Fujita, M. (2015). Biosynthesis of GPI-anchored proteins: special emphasis on GPI lipid remodeling. *Journal of Lipid Research*, 57(1), 6-24. doi:10.1194/jlr.r063313
- Kinoshita, T., & Takeda, J. (1994). GPI-anchor synthesis. *Parasitology Today*, 10(4), 139-143. doi:10.1016/0169-4758(94)90261-5
- Koizume, S., & Miyagi, Y. (2016). Lipid droplets: a key cellular organelle associated with cancer cell survival under normoxia and hypoxia. *International Journal of Molecular Sciences*, 17(9), 1430. doi:10.3390/ijms17091430

- Kolar, E. A. (2016). Effects of ACSVL3 knockout on lipid and glucose metabolism in malignant glioma cells (Doctoral dissertation). Retrieved from <https://jscholarship.library.jhu.edu/bitstream/handle/1774.2/39716/KOLAR-DISSERTATION-2016.pdf>
- Kuzu, O. F., Noory, M. A., & Robertson, G. P. (2016). The role of cholesterol in cancer. *Cancer Research*, 76(8), 2063-2070. doi:10.1158/0008-5472.can-15-2613
- Laemmli, U. K. (1970). Cleavage of structural proteins during the assembly of the head of bacteriophage T4. *Nature*, 227(5259), 680-685. doi:10.1038/227680a0
- Larkin, M. A., Blackshields, G., Brown, N. P., Chenna, R., McGettigan, P. A., McWilliam, H., ... Higgins, D. G. (2007). ClustalW and ClustalX version 2. *Bioinformatics*, 23(21), 2947-8. doi:10.1093/bioinformatics/btm404
- Letunic, I., & Bork, P. (2016). Interactive tree of life (iTOL) v3: an online tool for the display and annotation of phylogenetic and other trees. *Nucleic Acids Research*, 44(W1), W242-W245. doi:10.1093/nar/gkw290
- Liang, X. (2002). Mass spectrometric analysis of GAP-43/neuromodulin reveals the presence of a variety of fatty acylated species. *Journal of Biological Chemistry*, 277(36), 33032-33040. doi:10.1074/jbc.m204607200
- Li, H., Black, P. N., Chokshi, A., Sandoval-Alvarez, A., Vatsyayan, R., Sealls, W., & DiRusso, C. C. (2007). High-throughput screening for fatty acid uptake inhibitors in humanized yeast identifies atypical antipsychotic drugs that cause dyslipidemias. *Journal of Lipid Research*, 49(1), 230-244. doi:10.1194/jlr.d700015-jlr200

Li, M. Z., & Elledge, S. J. (2012). SLIC: a method for sequence- and ligation-independent cloning. *Methods in Molecular Biology*, 51-59. doi:10.1007/978-1-61779-564-0_5

Louis, D. N., Perry, A., Reifenberger, G., Von Deimling, A., Figarella-Branger, D., Cavenee, W. K., ... Ellison, D. W. (2016). The 2016 World Health Organization classification of tumors of the central nervous system: a summary. *Acta Neuropathologica*, 131(6), 803-820. doi:10.1007/s00401-016-1545-1

Lowry, O. H., Rosebrough, N. J., Farr, A. L., & Randall, R. J. (1951). Protein measurement with the Folin phenol reagent. *Journal of Biological Chemistry*, 193(1), 265-75. Retrieved from <http://www.jbc.org/>

Maekawa, M., Iwayama, Y., Ohnishi, T., Toyoshima, M., Shimamoto, C., Hisano, Y., ... Yoshikawa, T. (2015). Investigation of the fatty acid transporter-encoding genes SLC27A3 and SLC27A4 in autism. *Scientific Reports*, 5(1). doi:10.1038/srep16239

Mashima, T., Sato, S., Okabe, S., Miyata, S., Matsuura, M., Sugimoto, Y., ... Seimiya, H. (2009). Acyl-CoA synthetase as a cancer survival factor: its inhibition enhances the efficacy of etoposide. *Cancer Science*, 100(8), 1556-1562. doi:10.1111/j.1349-7006.2009.01203.x

McWilliam, H., Li, W., Uludag, M., Squizzato, S., Park, Y. M., Buso, N., ... Lopez, R. (2013). Analysis tool web services from the EMBL-EBI. *Nucleic Acids Research*, 41(W1), W597-W600. doi:10.1093/nar/gkt376

- Melton, E. M., Cerny, R. L., Watkins, P. A., DiRusso, C. C., & Black, P. N. (2011). Human fatty acid transport protein 2a/very long chain acyl-CoA synthetase 1 (FATP2a/Acsvl1) has a preference in mediating the channeling of exogenous n-3 fatty acids into phosphatidylinositol. *Journal of Biological Chemistry*, 286(35), 30670-30679. doi:10.1074/jbc.m111.226316
- Menendez, J. A., & Lupu, R. (2007). Fatty acid synthase and the lipogenic phenotype in cancer pathogenesis. *Nature Reviews Cancer*, 7(10), 763-777. doi:10.1038/nrc2222
- Mollinedo, F., & Gajate, C. (2015). Lipid rafts as major platforms for signaling regulation in cancer. *Advances in Biological Regulation*, 57, 130-146. doi:10.1016/j.jbior.2014.10.003
- Morad, S. A., & Cabot, M. C. (2012). Ceramide-orchestrated signalling in cancer cells. *Nature Reviews Cancer*, 13(1), 51-65. doi:10.1038/nrc3398
- Morgillo, F., & Lee, H. (2006). Lonafarnib in cancer therapy. *Expert Opinion on Investigational Drugs*, 15(6), 709-719. doi:10.1517/13543784.15.6.709
- Murata, S., Yanagisawa, K., Fukunaga, K., Oda, T., Kobayashi, A., Sasaki, R., & Ohkohchi, N. (2010). Fatty acid synthase inhibitor cerulenin suppresses liver metastasis of colon cancer in mice. *Cancer Science*, 101(8), 1861-1865. doi:10.1111/j.1349-7006.2010.01596.x
- Murphy, D. (2001). The biogenesis and functions of lipid bodies in animals, plants and microorganisms. *Progress in Lipid Research*, 40(5), 325-438. doi:10.1016/s0163-7827(01)00013-3

Mäenpää, A., Junnikkala, S., Hakulinen, J., Timonen, T., & Meri, S. (1996). Expression of complement membrane regulators membrane cofactor protein (CD46), decay accelerating factor (CD55), and protectin (CD59) in human malignant gliomas. *American Journal of Pathology*, 148(4), 1139-52. Retrieved from <http://ajp.amjpathol.org/>

Nieman, K. M., Kenny, H. A., Penicka, C. V., Ladanyi, A., Buell-Gutbrod, R., Zillhardt, M. R., ... Lengyel, E. (2011). Adipocytes promote ovarian cancer metastasis and provide energy for rapid tumor growth. *Nature Medicine*, 17(11), 1498-1503.
doi:10.1038/nm.2492

Novelli, G., & D'Apice, M. R. (2012). Protein farnesylation and disease. *Journal of Inherited Metabolic Disease*, 35(5), 917-926. doi:10.1007/s10545-011-9445-y

Ohkuni, A., Ohno, Y., & Kihara, A. (2013). Identification of acyl-CoA synthetases involved in the mammalian sphingosine 1-phosphate metabolic pathway. *Biochemical and Biophysical Research Communications*, 442(3-4), 195-201.
doi:10.1016/j.bbrc.2013.11.036

Ollila, S., Hyvönen, M. T., & Vattulainen, I. (2007). Polyunsaturation in lipid membranes: dynamic properties and lateral pressure profiles. *The Journal of Physical Chemistry B*, 111(12), 3139-3150. doi:10.1021/jp065424f

Ostanin, K., Shenderovich, M., Bajji, A., Cioffi, C. L., Moss, N., ... Li, D. (2015). World Patent No. WO/2015/183989. Geneva, Switzerland, World Intellectual Property Organization.

- Ostrom, Q. T., Gittleman, H., Xu, J., Kromer, C., Wolinsky, Y., Kruchko, C., & Barnholtz-Sloan, J. S. (2016). CBTRUS statistical report: primary brain and other central nervous system tumors diagnosed in the United States in 2009–2013. *Neuro-Oncology*, 18(suppl_5), v1-v75. doi:10.1093/neuonc/nov207
- Parry, P. V., & Engh, J. A. (2012). CD90 is identified as a marker for cancer stem cells in high-grade gliomas using tissue microarrays. *Neurosurgery*, 70(4), N23-N24. doi:10.1227/01.neu.0000413227.80467.92
- Pei, Z., Fraisl, P., Berger, J., Jia, Z., Forss-Petter, S., & Watkins, P. A. (2004). Mouse very long-chain Acyl-CoA synthetase 3/fatty acid transport protein 3 catalyzes fatty acid activation but not fatty acid transport in MA-10 cells. *Journal of Biological Chemistry*, 279(52), 54454-54462. doi:10.1074/jbc.m410091200
- Pei, Z., Fraisl, P., Shi, X., Gabrielson, E., Forss-Petter, S., Berger, J., & Watkins, P. A. (2013). Very long-chain acyl-CoA synthetase 3: overexpression and growth dependence in lung cancer. *PLoS ONE*, 8(7), e69392. doi:10.1371/journal.pone.0069392
- Pei, Z., Jia, Z., & Watkins, P. A. (2005). The second member of the human and murine "bubblegum" family is a testis- and brainstem-specific acyl-CoA synthetase. *Journal of Biological Chemistry*, 281(10), 6632-6641. doi:10.1074/jbc.m511558200
- Pei, Z., Oey, N. A., Zuidervaart, M. M., Jia, Z., Li, Y., Steinberg, S. J., ... Watkins, P. A. (2003). The acyl-CoA synthetase "bubblegum" (lipidosin): further characterization and role in neuronal fatty acid beta-oxidation. *Journal of Biological Chemistry*, 278(47), 47070-47078. doi:10.1074/jbc.m310075200

Pei, Z., Sun, P., Huang, P., Lal, B., Laterra, J., & Watkins, P. A. (2009). Acyl-CoA synthetase VL3 knockdown inhibits human glioma cell proliferation and tumorigenicity. *Cancer Research*, 69(24), 9175-9182. doi:10.1158/0008-5472.can-08-4689

Pike, L. S., Smift, A. L., Croteau, N. J., Ferrick, D. A., & Wu, M. (2011). Inhibition of fatty acid oxidation by etomoxir impairs NADPH production and increases reactive oxygen species resulting in ATP depletion and cell death in human glioblastoma cells. *Biochimica et Biophysica Acta (BBA) - Bioenergetics*, 1807(6), 726-734. doi:10.1016/j.bbabi.2010.10.022

Pisanti, S., Picardi, P., Ciaglia, E., D'Alessandro, A., & Bifulco, M. (2014). Novel prospects of statins as therapeutic agents in cancer. *Pharmacological Research*, 88, 84-98. doi:10.1016/j.phrs.2014.06.013

Pyne, N. J., Ohotski, J., Bittman, R., & Pyne, S. (2014). The role of sphingosine 1-phosphate in inflammation and cancer. *Advances in Biological Regulation*, 54, 121-129. doi:10.1016/j.jbior.2013.08.005

Resh, M. D. (2012). Targeting protein lipidation in disease. *Trends in Molecular Medicine*, 18(4), 206-214. doi:10.1016/j.molmed.2012.01.007

Resh, M. D. (2016). Fatty acylation of proteins: The long and the short of it. *Progress in Lipid Research*, 63, 120-131. doi:10.1016/j.plipres.2016.05.002

Riemenschneider, M. J., Betensky, R. A., Pasedag, S. M., & Louis, D. N. (2006). AKT activation in human glioblastomas enhances proliferation via TSC2 and S6 kinase signaling. *Cancer Research*, 66(11), 5618-5623. doi:10.1158/0008-5472.can-06-0364

Rostovtsev, V. V., Green, L. G., Fokin, V. V., & Sharpless, K. B. (2002). A stepwise Huisgen cycloaddition process: copper(I)-catalyzed regioselective “ligation” of azides and terminal alkynes. *Angewandte Chemie International Edition*, 41(14), 2596-2599. doi:10.1002/1521-3773(20020715)41:14<2596::aid-anie2596>3.0.co;2-4

Rowinsky, E. K., Windle, J. J., & Von Hoff, D. D. (1999). Ras protein farnesyltransferase: A strategic target for anticancer therapeutic development. *Journal of Clinical Oncology*, 17(11), 3631-3652. doi:10.1200/jco.1999.17.11.3631

Rysman, E., Brusselmans, K., Scheys, K., Timmermans, L., Derua, R., Munck, S., ... Swinnen, J. V. (2010). De novo lipogenesis protects cancer cells from free radicals and chemotherapeutics by promoting membrane lipid saturation. *Cancer Research*, 70(20), 8117-8126. doi:10.1158/0008-5472.can-09-3871

Saini, N., Black, P. N., Montefusco, D., & DiRusso, C. C. (2015). Fatty acid transport protein-2 inhibitor Grassofermata/CB5 protects cells against lipid accumulation and toxicity. *Biochemical and Biophysical Research Communications*, 465(3), 534-541. doi:10.1016/j.bbrc.2015.08.055

Samudio, I., Harmancey, R., Fiegl, M., Kantarjian, H., Konopleva, M., Korchin, B., ... Andreeff, M. (2010). Pharmacologic inhibition of fatty acid oxidation sensitizes human leukemia cells to apoptosis induction. *Journal of Clinical Investigation*, 120(1), 142-156. doi:10.1172/jci38942

- Sandoval, A., Chokshi, A., Jesch, E. D., Black, P. N., & DiRusso, C. C. (2010). Identification and characterization of small compound inhibitors of human FATP2. *Biochemical Pharmacology*, 79(7), 990-999. doi:10.1016/j.bcp.2009.11.008
- Schaffer, J. E., & Lodish, H. F. (1994). Expression cloning and characterization of a novel adipocyte long chain fatty acid transport protein. *Cell*, 79(3), 427-436. doi:10.1016/0092-8674(94)90252-6
- Schindelin, J., Rueden, C. T., Hiner, M. C., & Eliceiri, K. W. (2015). The ImageJ ecosystem: An open platform for biomedical image analysis. *Molecular Reproduction and Development*, 82(7-8), 518-529. doi:10.1002/mrd.22489
- Schug, Z., Peck, B., Jones, D., Zhang, Q., Alam, I., Witney, T., ... Gottlieb, E. (2014). Acetyl-coA synthetase 2 promotes acetate utilization and maintains cell growth under metabolic stress. *Cancer & Metabolism*, 2(Suppl 1), O9. doi:10.1186/2049-3002-2-s1-o9
- Selvakumar, P., Lakshmikuttyamma, A., Shrivastav, A., Das, S. B., Dimmock, J. R., & Sharma, R. K. (2007). Potential role of N-myristoyltransferase in cancer. *Progress in Lipid Research*, 46(1), 1-36. doi:10.1016/j.plipres.2006.05.002
- Senyilmaz, D., Virtue, S., Xu, X., Tan, C. Y., Griffin, J. L., Miller, A. K., ... Teleanu, A. A. (2015). Regulation of mitochondrial morphology and function by stearoylation of TFR1. *Nature*, 525(7567), 124-128. doi:10.1038/nature14601
- Shao, W., & Espenshade, P. (2012). Expanding roles for SREBP in metabolism. *Cell Metabolism*, 16(4), 414-419. doi:10.1016/j.cmet.2012.09.002

Steinberg, S. J., Morgenthaler, J., Heinzer, A. K., Smith, K. D., & Watkins, P. A. (2000). Very long-chain acyl-CoA synthetases. Human "bubblegum" represents a new family of proteins capable of activating very long-chain fatty acids. *Journal of Biological Chemistry*, 275(45), 35162-35169. doi:10.1074/jbc.m006403200

Steinberg, S. J., Wang, S. J., Kim, D. G., Mihalik, S. J., & Watkins, P. A. (1999). Human very-long-chain acyl-CoA synthetase: cloning, topography, and relevance to branched-chain fatty acid metabolism. *Biochemical and Biophysical Research Communications*, 257(2), 615-621. doi:10.1006/bbrc.1999.0510

Sundqvist, A., Bengoechea-Alonso, M. T., Ye, X., Lukiyanchuk, V., Jin, J., Harper, J. W., & Ericsson, J. (2005). Control of lipid metabolism by phosphorylation-dependent degradation of the SREBP family of transcription factors by SCF(Fbw7). *Cell Metabolism*, 1(6), 379-391. doi:10.1016/j.cmet.2005.04.010

Sun, P., Xia, S., Lal, B., Shi, X., Yang, K. S., Watkins, P. A., & Latterra, J. (2014). Lipid metabolism enzyme ACSVL3 supports glioblastoma stem cell maintenance and tumorigenicity. *BMC Cancer*, 14(1). doi:10.1186/1471-2407-14-401

Watkins, P. A. (1997). Fatty acid activation. *Progress in Lipid Research*, 36(1), 55-83. doi:10.1016/s0163-7827(97)00004-0

Watkins, P. A., Ferrell, E. V., Pedersen, J. I., & Hoefler, G. (1991). Peroxisomal fatty acid β -oxidation in HepG2 cells. *Archives of Biochemistry and Biophysics*, 289(2), 329-336. doi:10.1016/0003-9861(91)90419-j

Watkins, P. A., Howard, A. E., & Mihalik, S. J. (1994). Phytanic acid must be activated to phytanoyl-CoA prior to its α -oxidation in rat liver peroxisomes. *Biochimica et Biophysica Acta (BBA) - Lipids and Lipid Metabolism*, 1214(3), 288-294.

doi:10.1016/0005-2760(94)90075-2

Watkins, P. A., Maignel, D., Jia, Z., & Pevsner, J. (2007). Evidence for 26 distinct acyl-coenzyme A synthetase genes in the human genome. *Journal of Lipid Research*, 48(12), 2736-2750. doi:10.1194/jlr.m700378-jlr200

Wu, X., Li, Y., Wang, J., Wen, X., Marcus, M. T., Daniels, G., ... Monaco, M. E. (2013). Long chain fatty Acyl-CoA synthetase 4 is a biomarker for and mediator of hormone resistance in human breast cancer. *PLoS ONE*, 8(10), e77060.

doi:10.1371/journal.pone.0077060

Yamashita, Y., Kumabe, T., Cho, Y., Watanabe, M., Kawagishi, J., Yoshimoto, T., ... Yamamoto, T. T. (2000). Fatty acid induced glioma cell growth is mediated by the acyl-CoA synthetase 5 gene located on chromosome 10q25.1-q25.2, a region frequently deleted in malignant gliomas. *Oncogene*, 19(51), 5919-5925. doi:10.1038/sj.onc.1203981

Yeste-Velasco, M., Linder, M. E., & Lu, Y. (2015). Protein S-palmitoylation and cancer. *Biochimica et Biophysica Acta (BBA) - Reviews on Cancer*, 1856(1), 107-120.

doi:10.1016/j.bbcan.2015.06.004

Yoshii, Y., Furukawa, T., Yoshii, H., Mori, T., Kiyono, Y., Waki, A., ... Fujibayashi, Y. (2009). Cytosolic acetyl-CoA synthetase affected tumor cell survival under hypoxia: the

possible function in tumor acetyl-CoA/acetate metabolism. *Cancer Science*, 100(5), 821-827. doi:10.1111/j.1349-7006.2009.01099.x

Zha, S., Ferdinandusse, S., Hicks, J. L., Denis, S., Dunn, T. A., Wanders, R. J., ... Isaacs, W. B. (2005). Peroxisomal branched chain fatty acid beta-oxidation pathway is upregulated in prostate cancer. *The Prostate*, 63(4), 316-323. doi:10.1002/pros.20177

Zhong, S., Zhang, X., Chen, L., Ma, T., Tang, J., & Zhao, J. (2015). Statin use and mortality in cancer patients: Systematic review and meta-analysis of observational studies. *Cancer Treatment Reviews*, 41(6), 554-567. doi:10.1016/j.ctrv.2015.04.005

Curriculum Vitae

Emily Clay

Born 7/14/1989, Greenwich, CT, U.S.A

EDUCATION

Johns Hopkins University School of Medicine

Ph.D. in Biochemistry, Cellular and Molecular Biology **Expected 2017**

Advisor: Paul Watkins, M.D., Ph.D.

Brigham Young University, Provo, UT

B.S. in Biochemistry **2010**

PUBLICATIONS

Emily M. Clay, Xiaohai Shi, Emily M. Clay, Concetta C. DiRusso, Paul N. Black, Paul A. Watkins. (In preparation) The small molecule CB5 inhibits tumor growth and induces differentiation in U87 glioma cells.

Emily M. Clay, Xiaohai Shi, Paul A. Watkins. (In preparation) Very long-chain acyl-CoA synthetase-3 (ACSVL3) knockout alters protein stearoylation in U87 glioma cells.

Haiyan Yang, Elizabeth A. Kolar, Xiaohai Shi, Emily M. Clay, Bachchu Lal, Shuli Xia, Raja Sekhar, Akhilesh X. Pandey, John Lattera, Zhengtong Pei, Paul A. Watkins. (In preparation) Very long-chain acyl-CoA synthetase-3 (ACSVL3) promotes the malignant growth behavior of U87 glioma cells via changes in cell cycle without affecting membrane phospholipid synthesis, apoptosis or autophagy.

RESEARCH PRESENTATIONS

Emily M. Clay, Xiaohai Shi, Yanqiu Liu, Concetta C. DiRusso, Paul N. Black, Paul A. Watkins. Identification of inhibitors of ACSVL3, a therapeutic target in glioma. Experimental Biology 2017, Chicago, IL, April 22-26, 2017 (Presenter, oral and poster presentations).

Paul A. Watkins, Zhengtong Pei, Elizabeth A. Kolar, Emily M. Clay, Xiaohai Shi, John Laterra. Lipid metabolism alterations in U87 glioma cells deficient in very long-chain acyl-CoA synthetase 3 are associated with a less malignant phenotype. Experimental Biology 2012, San Diego, CA, April 21 - 25, 2012.

AWARDS

- ASBMB Graduate Student Travel Award (2017): Awarded \$1,000 from the American Society of Biochemistry and Molecular Biology to travel to and present at the annual Experimental Biology conference in Chicago, IL.
- Johns Hopkins School of Medicine Core Coins in Proteomics grant: Received \$4,000 towards proteomic services to study protein stearoylation in malignant glioma cells

RESEARCH EXPERIENCE

Investigation of the mechanism of Acyl-CoA Synthetase Very Long Chain 3 (ACSVL3) in human glioma

- Helped to generate an ACSVL3 knock-out human glioblastoma cell line.
- Studied effect of EGF on Akt signaling and stearoylation in WT and ACSVL3-KO cells.
- Studied difference in total cellular acyl-CoA synthetase activity in WT and ACSVL3-KO cells.
- Studied expression of GPI-anchored proteins in WT and ACSVL3-KO cells.
- Studied differences in protein acylation (especially stearoylation) in wild-type and ACSVL3 knock-out glioma cells.

Search for and characterization of ACSVL3 inhibitors

- Tested known inhibitors of ACSVL1, a homologous enzyme, for inhibition of acyl-CoA synthetase activity in WT and ACSVL3-KO cells.
- Helped to develop a screen to identify new inhibitors of ACSVL3.
- Characterized the effects of a potent inhibitor, CB5, on cell growth rate and invasiveness of glioma cells.
- Studying the effect of CB5 on cell differentiation and tumor growth in cells in culture and mice bearing xenograft tumors.

Undergraduate Research Assistant, Laboratory of Steven Graves, Ph.D., Brigham Young University, Provo UT, 2009-2010

Search for plasma-based biomarkers of preeclampsia and preterm birth

- Analyzed mass spectrometry readings to find significant peptides associated with preeclampsia and preterm birth
- Analyzed data for significance and reported statistics for patent consideration
- Prepared samples for analysis on mass spectrometer

OTHER PROFESSIONAL EXPERIENCE

Undergraduate Intern, Spectrum Laboratories, Coeburn VA, 2008

- Performed thermogravimetric analysis, acid-base titrations, and constant volume calorimetry on hundreds of coal and soil samples
- Analyzed data
- Prepared report forms for over 50 clients
- Revised standard operating procedures and wrote a standard operating procedure for temperature regulation
- Became a licensed surface miner (coal) in the state of Virginia

SERVICE & LEADERSHIP

- Volunteer Team Leader for Thread, 2010-2017: mentored high school and college students in Baltimore, organized a team of volunteers working several students for 3 years, planned events, and recruited new volunteers

- Hopkins Marathon Team Captain, 2013-2015: Organized workouts and events for several dozen students at Johns Hopkins University as they trained for marathons and half marathons, applied for and managed all group funding, and served as an Organization Representative to the Johns Hopkins School of Medicine Graduate Student Organization
- Volunteer for Student Outreach Program, 2013-2014: Designed curriculum and taught weekly experiment-based science lessons to 3rd and 4th grade students enrolled in after school and summer enrichment programs